Computer vision profiling of neurite outgrowth morphodynamics reveals spatio-temporal modularity of Rho GTPase signaling

Inauguraldissertation

zur

Erlangung der Würde eines Doktors der Philosophie

vorgelegt der

Philosophisch- Naturwissenschaftlichen Fakultät

der Universität Basel

von

Ludovico Maria Fusco

aus Italien

Basel, 2016

Departement **Biomedizin** Basel

Genehmigt von der Philosophisch-Naturwissenschaftlichen Fakultät
auf Antrag von

Prof. P. Scheiffele, Prof. O. Pertz, Prof. G. Christofori

Basel, 24.6.14

Prof. Dr. Jörg Schibler

Contents

1. Abstract

Neurite outgrowth is essential to build the neuronal processes that produce axons and dendrites that connect the adult brain. In cultured cells, the neurite outgrowth process is highly dynamic, and consists of a series of repetitive morphogenetic sub-processes (MSPs), such as neurite initiation, elongation, branching, growth cone motility and collapse (da Silva and Dotti 2002). Neurons also actively migrate, which might in part reflect neuronal migration during brain development. Each of the different MSPs inherent to neurite outgrowth and cell migration is likely to be regulated by precise spatio-temporal signaling networks that control cytoskeletal dynamics, trafficking and adhesion events. These MSPs can occur on a range of time and length scales. For example, microtubule bundling in the neurite shaft can be maintained during hours, while growth cone filopodia dynamically explore their surrounding on time scales of seconds and length scales of single microns. This implies that a correct understanding of these processes will require analysis with an adequate spatio-temporal resolution.

The Rho family of GTPases are signaling switches that regulate a wide variety of cellular processes, such as actin and adhesion dynamics, gene transcription, and neuronal differentiation (Boguski and McCormick 1993). Rho GTPases are activated by guanine nucleotide exchange factors (GEFs), and are switched off by GTPase activating proteins (GAPs). Upon activation, Rho GTPases can associate with effectors to initiate a downstream response. Current models propose that Rac1 and Cdc42 regulate neurite extension, while RhoA controls growth cone collapse and neurite retraction (da Silva and Dotti 2002).

However, until now the effects of Rho GTPases on neurite outgrowth have mostly been assessed using protein mutants in steady-state experiments, most often at late differentiation stages, which do not provide any insight about the different MSPs during neurite outgrowth. However, our proteomic analysis of biochemically-purified neurites from N1E-115 neuronal-like cells (Pertz et al. 2008), has suggested the existence of an unexpectedly complex 220 proteins signaling network consisting of multiple GEFs, GAPs, Rho GTPases, effectors and additional interactors. This is inconsistent with the simplistic view that classical experiments have provided before.

In order to gain insight into the complexity of this Rho GTPase signaling network, we performed a siRNA screen that targets each of these 220 proteins individually. We hypothesized that specific spatio-temporal Rho GTPase signaling networks control different MSPs occurring during neurite outgrowth, and therefore designed an integrated approach to capture the whole morphodynamic continuum of this process. Perturbations of

4

candidates that lead to a similar phenotype might be part of a given spatio-temporal signaling network. This approach consisted of: 1) A high content microscopy platform that allowed us to produce 8000 timelapse movies of 660 siRNA perturbations; 2) A custom built, computer vision approach that allowed us to automatically segment and track neurite and soma morphodynamics in the timelapse movies (collaboration with the group of Pascal Fua, EPFL, Lausanne); 3) A sophisticated statistical analysis pipeline that allowed the extraction of morphological and morphodynamic signatures (MDSs) relevant to each siRNA perturbation (collaboration with the group of Francois Fleuret, IDIAP, Martigny).

Analysis of our dataset revealed that each siRNA perturbation led to a quantifiable phenotype, emphasizing the quality of our proteomic dataset. Hierarchical clustering of the MDSs revealed the existence of 24 phenoclusters that provide information about neurite length, branching, number of neurites, soma migration speed, and a panel of additional morphological and morphodynamic features that are more difficult to grasp using visual inspection. This complex phenotypic space can more easily be understood when classified according to the first 4 features. Our screen then suggests the existence of 4 major morphodynamic phenotypes that define distinct stages of the neurite outgrowth process. These consist of phenotypes with short neurites, multiple short neurites, long neurites, and long and branched neurites. Further subdivision using the other features provides more information, with cell migration features being very often affected. This implies a high overlap between the signaling machinery that regulates the neurite outgrowth and cell migration processes. The high phenotypical redundancy (24 clusters for 220 candidate genes) provides only limited information to deduce unambiguous signaling networks regulating distinct MSPs.

Further knowledge acquired from other approaches we used to study Rho GTPase signaling (FRET biosensors, and other live cell imaging techniques), made us realize that some morphodynamic phenotypes can only be understood when growth cone dynamics are inspected at a much higher resolution. For this purpose, we decided to further investigate a defined subset of genes using high resolution live cell imaging and a custom built growth cone segmentation and tracking pipeline for accurate quantification (collaboration with the group of Gaudenz Danuser, Harvard Medical School, Boston). These results shed light into how distinct cytoskeletal networks enabling growth cone advance can globally impact the neurite outgrowth process. A clear understanding of spatio-temporal Rho GTPase signaling will therefore require multi-scale approaches.

Our results provide the first insight into the complexity of spatio-temporal Rho GTPase signaling during neurite outgrowth. The technologies we devised and our initial results, pave the way for a systems biology understanding of these complex signaling systems.

2. Introduction

2.1 The cytoskeleton

The cytoskeleton is a complex network of protein filaments that allows eukaryotic cells to adopt a variety of shapes and to generate coordinated and directed movements. The cytoskeleton represents a crucial step in the evolution of eukaryotic cells, as it is directly involved in cell migration, embryonic development and muscle contraction.

Despite the plethora of activities in which it is involved, we recognize only three principal types of protein filaments that form the cytoskeleton: actin filaments, intermediate filaments and microtubules.

Each of these filaments is composed by monomeric units that, depending on the specific proteins they are associated with, can build a vast variety of structures.

2.1.1 Actin Filaments

Actin is one of the most abundant proteins in eukaryotic cells and usually in mammals it consists of six main isoforms, encoded by different genes. Despite the strong similarity in the amino acidic (aa) sequence, each of these isoforms has a cellular function. Four of these isoforms are found in different types of muscles, while two of them (β and γ) are present in non-muscular cell types.

The minimal component of the actin filaments is the monomeric actin, sometimes known as globular actin or G actin, which is formed by a single polypeptide of 374 aa and is associated with one molecule of ATP. The hydrolization of ATP is crucial for the formation of actin filaments and plays a crucial role in their dynamics (Korn 1982). In migrating cells, almost 50% of the actin content is in the monomeric state. This facilitates the rapid recruitment and assembly of new filaments.

The actin filaments have an important feature called polarity that allows the directional growth of the filament and generates cellular movements. This polarity is structural, and involves the kinetics of polymerisation at the two ends of the filaments. The barbed ends of the filament have an in vitro rate of growth which is estimate to be 5 to 10 times higher than at the pointed ends (Pollard and Mooseker 1981). The orientation of growth at the barbed end of a filament will determine the directionality of growth.

The Actin polymerisation always starts with a lag phase, in which three monomers must interact together in a specific geometric configuration. This phase called nucleation is normally very slow, but once it is achieved the addition of further actin monomers occurs quite rapidly allowing the rapid polymerisation of the filament at the barbed ends and slow depolymerisation at the pointed ends (Cooper et al. 1983). The actin polymerisation can reach a plateau, called critical concentration, in which the rate of monomers addition to the filament is the same as the rate of dissociation. At this stage, in vitro experiments have proven, that actin monomers associate predominantly at the barbed end and dissociate at the pointed end. This mechanism of dissociation/association of actin monomers is called treadmilling and requires energy (Neuhaus et al. 1983). This energy comes from the hydrolysis of the ATP molecules bond to the actin monomer. Shortly after the monomer is integrated at the barbed end, the bound ATP is hydrolyzed. This is accompanied by the dissociation of a monomer of actin at the pointed end. Treadmilling plays a crucial role in the generation of cell movements (Neuhaus et al. 1983) (Figure 1).

The polymerisation of the actin filaments is crucial for the formation of several components of eukaryotic cells such as the cell cortex, filopodia, lamellipodia, stress fibers and microvilli (Small 1981; Burridge et al. 1988; O'Connor and Bentley 1993), as well as in some cellular processes as cytokinesis (Pelham and Chang 2002) and gene transcription (Louvet and Percipalle 2009).

The phases of polymerisation and the different functions of the actin polymers in the cell are regulated by a class of proteins called actin binding proteins (ABP).

We can distinguish ABPs in different groups, depending on the specific phase of polymerisation, on the ends of the filament they interact with or on the structural order in which they interact with the actin filaments.

Nucleation is a phase of polymerisation, in which the ABPs create new filaments, and bypass the lag phase of the growth. A molecule known to nucleate new actin filaments is the seven-subunit actin-related protein 2/3 (Arp2/3) complex. The Arp2/3 complex has the ability to nucleate new filaments of actin from the side of an existing filament (Mullins et al. 1998). Normally Arp2 and 3 bind actin monomers creating a stable trimer that acts as a nucleus for the extension of the filament. In this case Arp2/3 acts as the pointed end, promoting then the polymerisation at the barbed end of the filament. The ability of the Arp2/3 complex to nucleate actin filaments can be enhanced by specific interacting proteins, as SCAR/WAVE or WASP (Machesky et al. 1999). Nucleation can also be driven by another family of proteins called formins. The characteristic FH2 domain of these

proteins enhances the addition of actin monomers to the barbed end of an actin filament (Pruyne et al. 2002). Nucleation can eventually be stopped to prevent spontaneous formation of filaments. Profilin is an actin binding protein that interacts in a one-to-one complex with the actin monomer, blocking nucleation (Pollard and Cooper 1986). However, it was recently demonstrated that profilin is crucial for formin activation, therefore this protein could act also as a specific promoter that facilitates new filament formation (Kovar et al. 2006).

After nucleation, the extension of the actin filament, as well as the balance between polymerisation and depolymerisation, also involves several ABPs.

Capping proteins normally act as inhibitors of actin polymerisation. Gelsolin (Sun et al. 1999) and tensin (Lo et al. 1994), for example, block the recruitment of actin monomers at the barbed end of the filament, causing an overall decrease of its length, while on the other hand actin depolymerizing factor (ADF)/Cofilin promotes the dissociation of the ADP-actin monomers from the pointed end of the filament, increasing the rate of depolymerisation (Carlier et al. 1997).

Conversely, the tropomyosin family acts as an inhibitor of the depolymerisation, protecting the actin filament from the activity of gelsolin and cofilin, while at the same time stabilizing the filament against spontaneous collapse (Bernstein and Bamburg 1982).

In order to regulate different processes in the cell, the actin filaments must be organized into networks. The role of these networks is to control mechanical properties of cells. In this case ABPs regulate the formation of either actin bundles or actin crosslinks, which determine the order and shape of a cell. Filamin (Wang and Singer 1977) and spectrin (Cohen et al. 1980) are responsible for the formation of the actin crosslinks, in which the actin filaments are assembled in a specific orthogonal matrix. On the other hand, actin bundles are organized in a matrix of parallel and antiparallel filaments of actin, which depending on the ability of ABPs to bind to one or more filaments at the same time, appear to be tight or loose. Tight bundles can be formed by a protein called fimbrin (Glenney et al. 1981), and are important for the formation of filopodia, while loose bundles can be found in association with another protein called α-actinin (Pelletier et al. 2003).

Finally actin filaments can also function as a structural scaffold to connect cellular elements together. In this context, proteins as dystrophin (Ervasti and Campbell 1993), utrophin (Winder et al. 1995) and talin (Calderwood and Ginsberg 2003), can connect the actin filaments to the cell adhesion receptors such as integrin or dystroglycan, creating an important connection between the cytoskeleton and the extracellular matrix (ECM).

Actin filaments are responsible for many types of cell movements. Myosin is an ATP-dependent motor protein, which binds actin filament contractile bundles in the cytoplasm. The interaction of actin filaments with myosin is crucial for muscle contraction (Rayment et al. 1993), as well as for a variety of movements of nonmuscle cells, including cell division (Hill et al. 1996). In nonmuscle cells, actin and myosin can interact to form contractile structures, an example of which is the stress fiber. The contraction of stress fibers produces tension across the cell, allowing the cell to pull on a substrate to which it is anchored, thereby facilitating cell movements (Hotulainen and Lappalainen 2006).
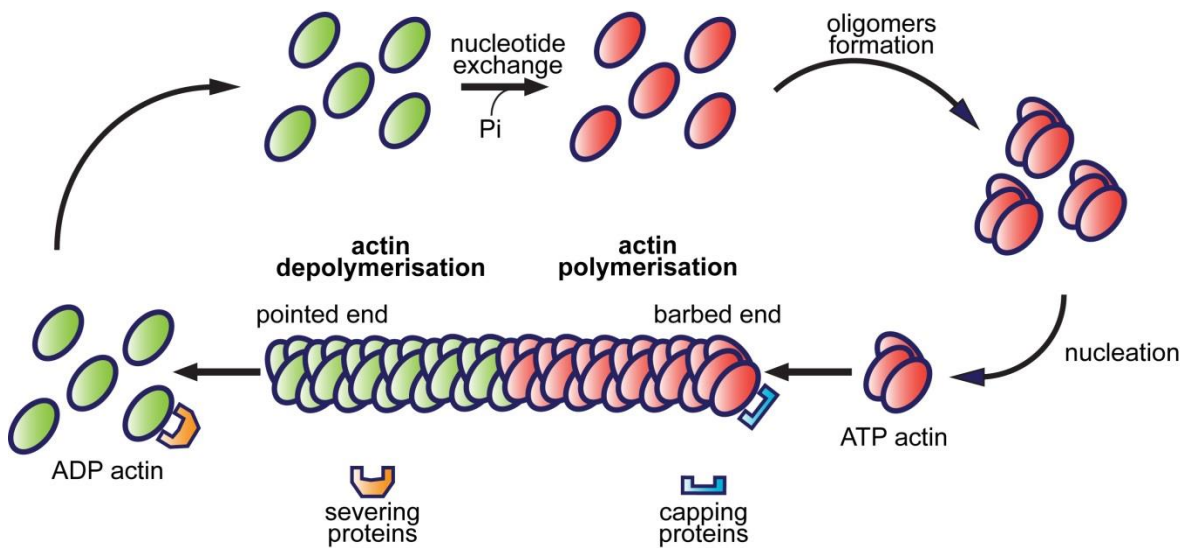
Figure1. Actin polymerisation. Individual subunits of ATP-bound globular actin (G-actin) are assembled into long polymers of filamentous actin (F-actin), creating a double helix structure. Hydrolysis of the ATP destabilizes the polymer, causing dissolution of F-actin polymers into G-actin monomers. The dissociation of the phosphate destabilizes the filament and renders it more susceptible to the action of severing proteins, such as members of the actin depolymerizing factor (ADF)/cofilin family. Capping proteins, such as gelsolin, can associate with the growing barbed end and inhibit filament elongation.

2.1.2 Microtubules

Microtubules are polymers, formed from heterodymeric molecules of tubulin, with a diameter of approximately 25 nm (Kirschner 1978; Mitchison and Kirschner 1984). These filaments are crucial to determine cell shape and movements, and at the same time, they have an important role in intracellular transport and mitosis. Tubulin molecules, normally consist of two globular subunits of 450 aa called α- and β-tubulin. In addition, three other

isoforms of tubulin are usually found in eukaryotic cells: γ-tubulin, which is important in the nucleation an orientation of microtubules, and δ and ε, which are involved in the formation of the mitotic spindle during mitosis (Burns 1991).

Tubulin molecules form protofilaments, upon the interaction of the β-tubulin unit of a molecule with the α-tubulin unit of another. The microtubules are finally formed by 13 protofilaments, arranged in a tubular shape, with a 14 nm width empty core (Evans et al. 1985). Since the protofilaments are parallel to each other, they have the same polarity, and similar to actin, the microtubules are also polar structures, with a plus (fast-growing) and a minus (slow-growing) end (Allen and Borisy 1974). The polarity of a microtubule allows, as for actin, a rapid assembly and disassembly of the filament. Both α- and β-tubulin bind GTP, which is involved in the control of polymerisation. During this phase, after a new heterodimer of tubulin is integrated in the filament, the GTP of the β-tubulin is rapidly hydrolyzed (David-Pfeuty et al. 1977). The hydrolysis of GTP weakens the binding affinity of tubulin molecules to the adjacent heterodimers, allowing the rapid depolymerisation of the microtubule (Weisenberg et al. 1976) (Figure 2). Microtubules, similar to actin undergo filament treadmilling. Through this mechanism, GDP bound tubulin molecules are constantly lost at the minus end, while GTP bound molecules are integrated at the plus end (Waterman-Storer and Salmon 1997). Another mechanism that involves the hydrolysis of GTP is called dynamic instability. In this case, while the rate of polymerisation is higher than depolymerisation, the microtubule retains a GTP cap at the plus end that allows the filament to grow. However, when the rate of depolymerisation is greater, the GTP cap at the plus end is hydrolyzed, resulting in the dissociation of this molecule and the rapid depolymerisation of the filaments. This mechanism is crucial to maintain a rapid turnover of the microtubule filaments in the cell, which represents an important clue for rapid remodeling of the cytoskeleton (Erickson and O'Brien 1992). In eukaryotic cells, tubulin is encoded by a family of genes which are closely related. This is common with actin and other cytoskeletal proteins, and reflects the evolutionary conservation and the structural constrains imposed by a large number of proteins that bind to these filaments. Specifically, eukaryotic cells express different types of microtubules associated proteins (MAPs), including motor proteins, structural proteins and enzymes (Maccioni and Cambiazo 1995). Generally, the MAPs can be clustered in two specific types.

Type I: this includes the Map1 family, known for its ability to bind to the microtubule sides and stabilize the structure.

Type II: includes the Map2/Tau family, which also binds to the microtubule sides and increases filament rigidity and bundles formation.

The Map1 family includes three proteins, MAP1A, MAP1B and MAP1S, all encoded by different genes. Upon post-translational modifications, each of these proteins is characterized by a heavy chain (300-350 KDa) and a light chain (30-25 KDa), both with the ability to bind microtubules. Once they are formed, the MAP1A light chain interacts with the MAP1B heavy chain, to create a complex that regulates microtubule stability. However, a separate gene encodes another light chain, called LC3, which is very often part of this MAP1A-MAP1B complex (Fink et al. 1996; Kutschera et al. 1998). The role of this trimeric complex is to bind along the sides of microtubules and stabilize the filament structure. However, it was suggested that MAP1B could also regulate microtubule stability directly affecting the depolymerisation rate. Phosphorylated MAP1B sensitizes microtubules to the binding of depolymerisation factors. This mechanism seems to be important in the regulation of microtubule growth rate (Vandecandelaere et al. 1996). The Map2/Tau family includes three members, MAP2 and Tau, which are normally enriched in neurons, and a non-neuronal protein called MAP4 (Dehmelt and Halpain 2005).

All MAP2/Tau proteins have a characteristic microtubule-binding protein domain at the carboxyl-terminus, containing a KXGS motif, which can be phosphorylated (Drewes et al. 1995).

As previously explained, microtubules have an intrinsic ability, that allows the filament to alternate switching between a growing and a shortening phase. In this context, the role of the MAP2/Tau proteins is to stabilize the microtubules and reduce the rate of the shortening phase (Al-Bassam et al. 2002). It has also been demonstrated that MAP2 can create clusters around the microtubules, and therefore induce the suppression of the shortening phase (Itoh and Hotani 1994). Moreover, a specific four-microtubule repeat isoform of Tau exhibits robust depolymerisation suppression as it binds to the microtubule filament (Panda et al. 2003).
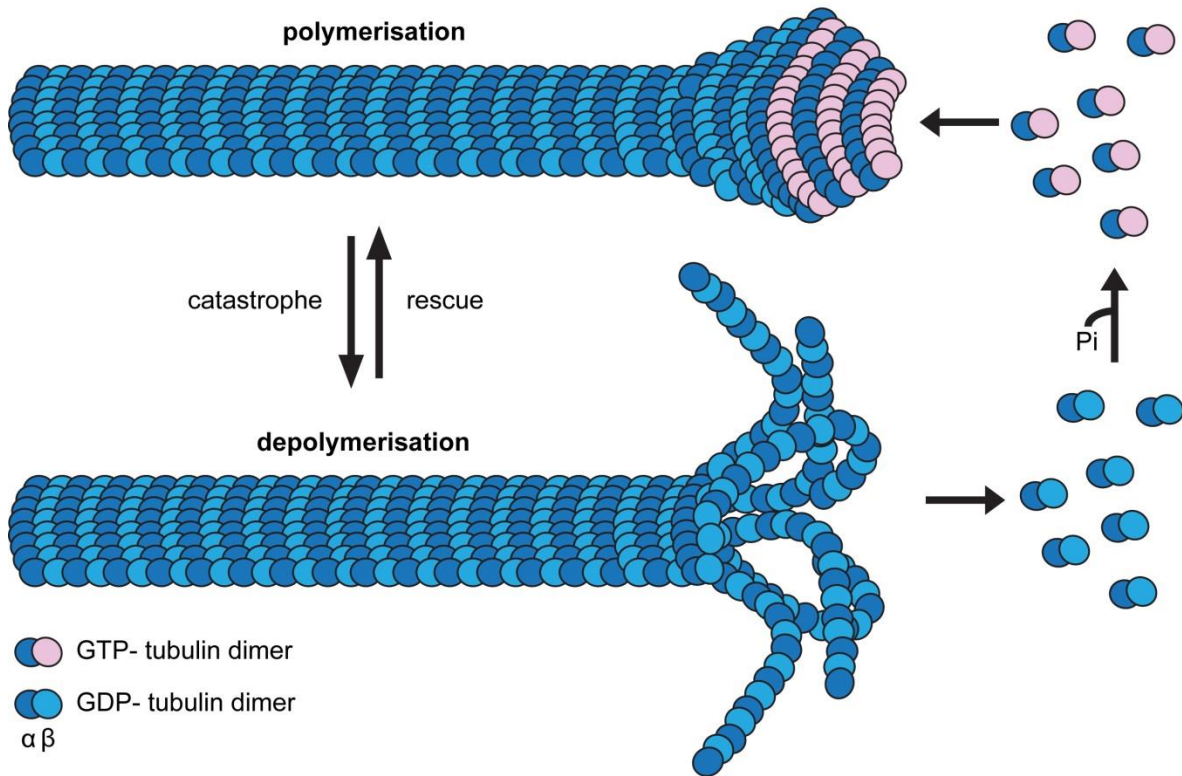
Figure 2. Microtubules polymerisation. Polymerisation and depolymerisation of microtubules is driven by the binding, hydrolysis and exchange of a guanine nucleotide on the β-tubulin monomer. This mechanism does not involve the α-tubulin monomer, where the GTP is not exchangeable and cannot be hydrolyzed. GTP hydrolysis is necessary for switching between catastrophe (rapid depolymerisation) and rescue (rapid polymerisation).

2.1.3 Intermediate filaments

In most of eukaryotic cells intermediate filaments (IF) are assembled in a basket like structure around the nucleus that project throughout the cytoplasm. Intermediate filaments are protein fibers with a diameter of 8 to 10 nm (Lazarides 1982; Steinert et al. 1984). They are usually found in epithelial, neuronal and muscle cells, where they appear to be crucial by providing mechanical strength to cells and tissues (Fuchs and Cleveland 1998). We recognize four main types of IF, that can be distinguished by their aa sequence.

Type I consist of two subfamilies of keratins: acidic keratins and neutral keratins. Keratins are heteropolymeric proteins formed by an equal amount of subunit of each of the two protein subfamilies, and are particularly enriched in epithelial cells (Moll et al. 1982).

Type II includes three proteins: vimetin, expressed usually in mesenchymal cells, glial fibrillary acidic protein, expressed in glial cells, Schwann cells and astrocytes of the

nervous system, and desmin, found abundantly in muscle cells (Lazarides 1982). These proteins are normally assembled in homopolymers but will also interact with other Type II proteins to form heteropolymers.

Type III is made by neurofilaments and is a major component of axons and dendrites (Geisler et al. 1982).

Type IV proteins are the nuclear lamina, that have a crucial role during mitosis (Aebi et al. 1986).

All these proteins are encoded by a multigene family, and therefore share part of their aa sequence. In particular these proteins show similarity in a region of 310 aa, that forms a coiled coil structure that allows the proteins to create homodimers. These dimers can line up together and form a protofilaments of 48 nm. The protofilaments can associate in a staggered way to form larger structures. Finally, each IF is formed by eight protofilaments, for a total of 32 coiled coil-dimers (Geisler et al. 1985) (Figure 3).
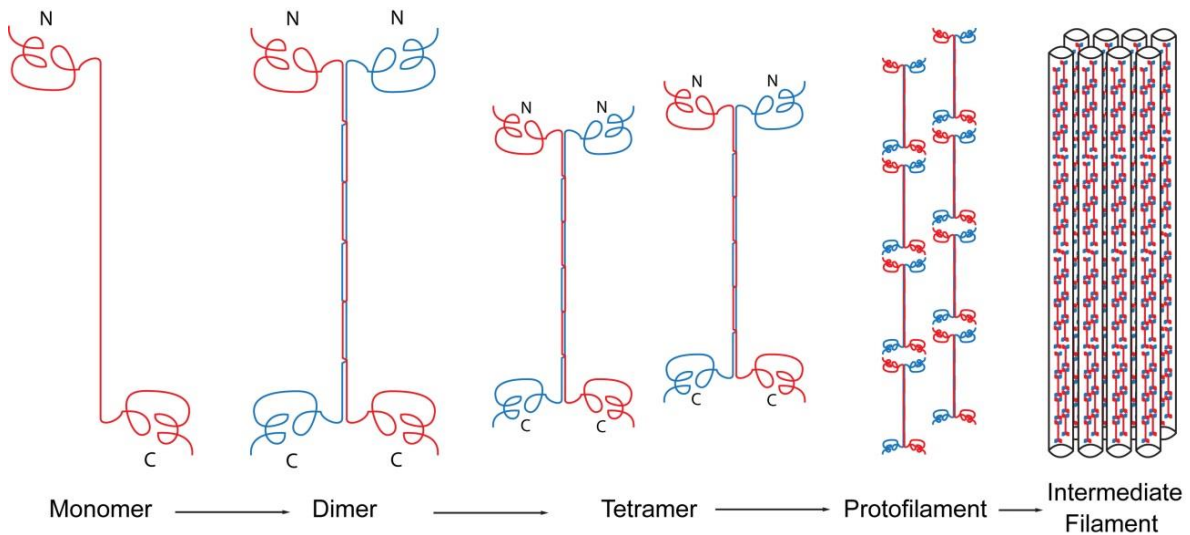
Figure 3. Intermediate filaments polymerisation. The intermediate filaments are extended proteins composed largely of an alpha helix. Two monomers form a coiled coil structure around each other to form a dimer, and two dimers align together to form a tetrameric protofilament. These protofilaments can associate in a staggered way to form a larger structure. Finally, eight protofilaments are arranged in parallel to form the intermediate filament, which contains 32 coiled coil dimers.

## 2.1.4   The cytoskeleton and cell migration

Cell migration is a multistep process that involves changes in the cytoskeleton, ECM and the cell-substrate adhesion (Sheetz et al. 1998; Ridley et al. 2003). Many cell types

migrate as single cells, including leukocytes, fibroblasts and neuronal cells, while epithelial and endothelial cells migrate in groups during development, wound healing and angiogenesis (Krawczyk 1971; Sanchez-Madrid and del Pozo 1999; Marin and Rubenstein 2003; Lamalice et al. 2007).

Cell migration usually starts in response to extracellular cues such as signals from the ECM, diffusible factors or neighbor cells. These cues are translated by transmembrane receptors into intracellular signals. Many different molecules are involved in intracellular signaling during cell migration including: Rho GTPases, mitogen-activated protein kinases (MAPKs), protein kinase C (PKC) and tyrosine kinases (TKs) (Van Aelst and D'Souza-Schorey 1997; Ridley 2001; Huang et al. 2004). Cell migration can be divided in 4 separate steps: lamellipodium protrusion, adhesion formation, cell body contraction and rear retraction (Lauffenburger and Horwitz 1996). The initial response of a cell to a migrating stimulus is to polarize and to extend protrusions, such as lamellipodia and filopodia, in the direction of the stimulus.

The lamellipodia are large protrusions that consist of branched actin networks and are formed by the actin-nucleating activity of the Arp2/3 complex (Pollard et al. 2000). Once the lamellipodium starts to protrude, it establishes novel cell-substrate adhesions, called focal complexes, which allow the cell to attach and extend to the ECM (Lauffenburger and Horwitz 1996). In fast migrating cells focal complexes allow lamellipodia to move over them, while in slow migrating cells they can mature in focal adhesion creating a tither linked with the ECM (Lauffenburger and Horwitz 1996). Nevertheless, in both cases focal adhesions and complexes turnover is crucial to guarantee the progression of cell migration (Cox and Huttenlocher 1998). Focal adhesions are often connected to actin stress fibers, which are actomyosin bundles that play an important role in their maturation and dynamics (Tojkander et al. 2012). Filopodia are long and unbranched actin filaments that protrude out of the lamellipodium. It has been suggested that filopodia formation could be driven by actin treadmilling, where single actin filaments within a bundle elongate at their barbed ends. Filopodia act as sensing machinery that detects changes in extracellular signals and transmits them back into the cell (Welch and Mullins 2002). On the other hand cell body contraction is dependent on actomyosin contractility and is crucial to propel cell body and nucleus translocation during migration (Mitchison and Cramer 1996). Rear retraction is strongly dependent on the cell type and the strength of the adhesions to the ECM. The detachment of the rear requires the degradation of focal adhesions, which can be driven by proteases such as calpain, and the simultaneous contraction of the actin cytoskeleton

16

(Palecek et al. 1998) (Figure 4). Although the majority of the studies have concentrated on the role of the actin cytoskeleton during cell migration, there are evidences that also microtubules can contribute to this process. Microtubules appear to be involved in tail retraction, which is due to their ability to target focal adhesions and promote their turn over (Kaverina et al. 1999; Ballestrem et al. 2000).
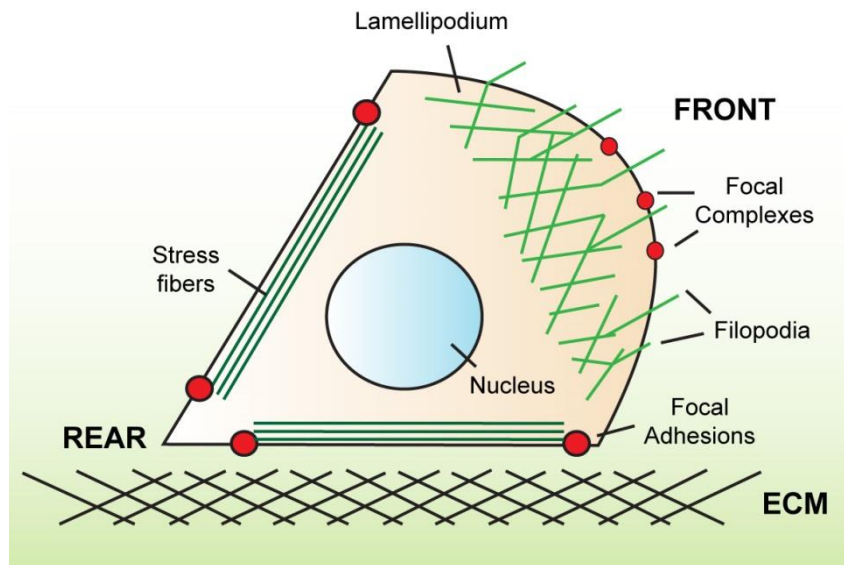
Figure 4. Schematic of cell migration. The initial response of a cell to an extracellular stimulus is to polarize and extend protrusions in the direction of migration. These protrusions can be large and broad lamellipodia or spike-like filopodia, which are stabilized by adhering to the ECM. These adhesions must be disassembled at the cell rear, allowing the cell to detach and migrate.
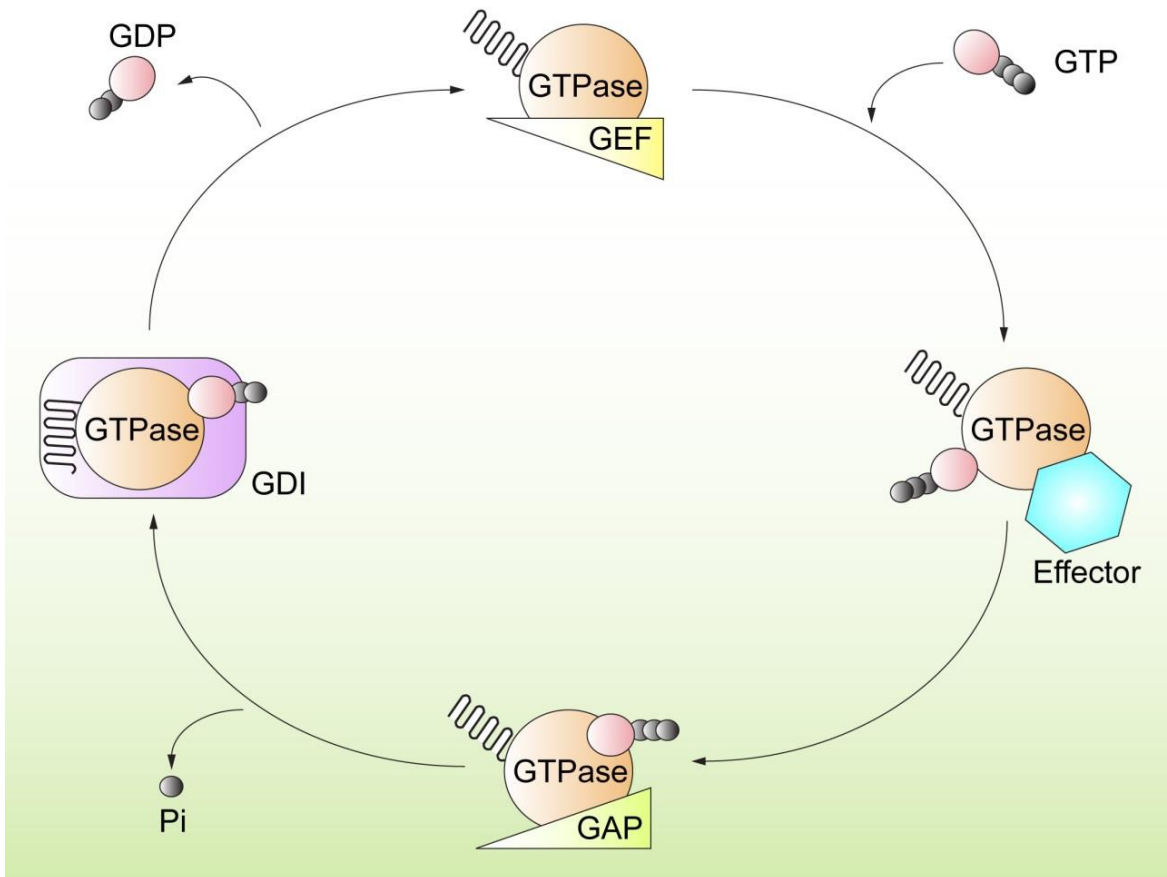
2.2 Rho GTPases

Rho GTPases are members of the larger Ras superfamily of proteins. This family includes Rho (RhoA, RhoB, RhoC, RhoD, RhoT), Rac (Rac1, Rac2, Rac3), Cdc42, TC10, TCl, Wrch1, Chp/wrch2, RhoG, RhoH/TTF, and Rnd (Rnd1, Rnd2, Rnd3/RhoE).

The members of the Rho GTPase family which have been characterized most extensively are RhoA, Rac1 and Cdc42. They are known in particular for their role in the regulation of the actin cytoskeleton. In classic fibroblast studies RhoA, Rac1 and Cdc42 activation triggers the reorganization of the actin cytoskeleton into different structures, leading to focal adhesions and stress fibers (Chrzanowska-Wodnicka and Burridge 1996), lamellipodia (Ridley et al. 1992) and filopodia (Kozma et al. 1995) respectively. Rho GTPases have also been shown to have an effect on microtubules dynamics, membrane trafficking and transcriptional activation. Therefore, through the regulation of these processes they have been linked to various cellular functions such as cytokinesis, cell growth, cell motility, cell invasion and neuronal development (Luo 2000; Ridley 2001; da Silva and Dotti 2002).

Normally most of the Rho GTPase proteins (90-95%) are inactive and located in the cytosol. The cytosolic pool acts as a reservoir allowing a rapid translocation to the membrane and activation of specific signals. This "instantaneous translocation/activation" is important for the cells in order to respond quickly to a certain stimulus. Rho GTPases are guanine nucleotide binding proteins that oscillate in between an inactive and active state, depending on the binding to guanosine diphosphate (GDP) or triphosphate (GTP) (Boguski and McCormick 1993). The switch between these two states is controlled by two other protein families called guanine nucleotide exchange factors (GEFs) and GTPase activating proteins (GAPs) (Cherfils and Zeghouf 2013).

GEF proteins are recruited to the plasma membrane in response to upstream signals. This allows the activation of the GTPases by the exchange of bound GDP for GTP. The GTP bound forms can associate with downstream effectors to initiate a downstream response (Schmidt and Hall 2002). This activation is maintained by the intrinsic GTPase activity of these proteins, which can be induced by the GAP proteins, resulting in the stoppage of the signal (Scheffzek and Ahmadian 2005). Another group of Rho GTPase regulators, called

the GTP dissociation inhibitor (GDIs) family, act as negative regulators, preventing the dissociation of GDP and the nucleotide exchange (Garcia-Mata et al. 2011) (Figure 5).

Figure 5. The Rho GTPases cycle. Rho GTPases cycle between an active (GTP-bound) and an inactive (GDP-bound) state. In the active state, they can interact with over 60 target proteins (effectors), leading to the activation of a vast variety of signaling pathways. The Rho GTPase cycle is highly regulated by three classes of proteins: the guanine nucleotide exchange factors (GEFs) catalyse nucleotide exchange and mediate activation; the GTPase-activating proteins (GAPs) stimulate GTP hydrolysis, leading to inactivation; the guanine nucleotide exchange inhibitors (GDIs), which act extracting the inactive GTPase from membranes and keeping it in its inactive state in the cytosol.

2.2.1 Upstream signals

The Rho family of GTPases is the link between the plasma membrane receptors and the assembly and organization of the actin cytoskeleton. In Swiss 3T3 fibroblasts, different external cues have been shown to activate the Rho GTPase cascade. Addition of lysophosphatidic acid (LPA) to fibroblasts induces the formation of stress fibers and their

response is completely blocked by the C3 transferase, a bacterial coenzyme that inactivates Rho proteins (Ridley and Hall 1992).

On the other hand, growth factors such as platelet-derived growth factor (PDGF), insulin and bombesin stimulate the formation of lamellipodia and membrane ruffles (Ridley et al. 1992). This response is inhibited by a dominant negative (DN) form of Rac, RacN17, inferring that Rac is the link between these factors and actin polymerisation at the plasma membrane. Bradykinin, an angiotensin-converting-enzyme inhibitor (ACE) inhibitor, is able to activate Cdc42 and stimulate filopodia formation; this phenotype can be rescued by the DN form of Cdc42, Cdc42N17 (Kozma et al. 1995).

The actin cytoskeleton rearrangements driven by PDGF and insulin have been linked to the activation of phosphatidylinositol-3-kinase (PI3K). PI3K seems to work upstream of Rac inducing membrane ruffling, a motile cell surface that contains a meshwork of actin filaments, in response to extracellular growth factors. Wortmannin, a PI3K inhibitor, is able to block membrane ruffles induced by PDGF, epidermal growth factor (EGF) and insulin (Nobes et al. 1995). Moreover, PDGF is able to stimulate and increase the levels of active Rac via PI3K (Hawkins et al. 1995). A constitutively activated (CA) form of PI3K is able to increase formation of membrane ruffles and stress fibers in a Rac1- and RhoA-dependent manner (Reif et al. 1996). This result suggests that different upstream signals are linked to the activation of completely different effector pathways that lead to diverse biological activities.

In fibroblasts, adhesion to the ECM induces the aggregation of clusters of integrin receptors that control rearrangements of the cytoskeleton. These rearrangements involve the activation of different Rho GTPase pathways. RhoA stimulates formation of focal contacts and stress fibers via focal adhesion kinase (FAK) and phosphorylation of paxillin, a focal adhesion-associated adaptor protein (Barry et al. 1997). On the other hand, Cdc42 controls the integrin dependent activation of Rac1 via PI3K, which stimulates the formation of membrane ruffles (Clark et al. 1998). Moreover, Cdc42 and RhoA regulate cell proliferation via phosphorylation of Erk2, a member of the Ras/Raf pathway (Clark et al. 1998).

2.2.2 GEF proteins

The guanine nucleotide exchange factors are a protein family that stimulates the exchange of bound GDP with GTP to generate the activated form of a GTPase. Normally, GEFs bind to the GDP-bound form of the GTPase and destabilize the GDP-GTPase complex while stabilizing a nucleotide-free reaction intermediate. However, because of the high intracellular ratio of GTP:GDP, the release of GDP is rapidly replaced by GTP, leading to activation of the GTPase (Figure 6) (Cherfils and Chardin 1999).

GEFs for Rho GTPases can be divided in two main subfamilies. The first subfamily is the Dbl homology-plekstrin homology domain (DH-PH)-containing family, which is represented by 69 mammalian members (Zheng 2001). The second subfamily consists of the Dock180-related proteins, which contain 11 mammalian members, and are characterized by a Dock homology region (DHR)-2 domain (Laurin and Cote 2014).

The first mammalian GEF, Dbl, was found to contain an approximately 180 aa sequence, which was able to catalyze nucleotide exchange on human Cdc42 (Hart et al. 1991). This conserved DH domain was then found to be crucial for GEF activity (Hart et al. 1994). However, besides three conserved regions, consisting of 10-30 aa (CR1, CR2 and CR3), DH domains share little homology with each other. GEFs that share the same substrate, sometimes have <20% homology in their sequence (Aghazadeh et al. 1998). Several GEFs seem to be highly specific for one Rho GTPase, like Fgd1/Cdc42 or Lsc/RhoA (Hart et al. 1996; Zheng et al. 1996), while others activate several, like Vav2/Cdc42, Rac1 and RhoA or Dbl/RhoA and Cdc42 (Hart et al. 1994; Olson et al. 1996).

Almost all the GEFs contain a PH domain at the C-terminal of a DH domain. PH domains are known to bind to phosphorylated phosphoinositides (PIPs) and proteins, and functionally they seem to have two main roles (Rebecchi and Scarlata 1998). Firstly, they can directly affect the catalytic activity of the DH domain, and secondly, they can help GEFs reach the appropriate intracellular location (Rossman et al. 2002). Interestingly, only two GEFs, called ArhGEf10 and ArhGEf10L, do not have a PH domain. However, these proteins contain a transmembrane domain that determines membrane targeting of the protein (Garcia-Mata and Burridge 2007).

Besides the DH-PH module, which represents the minimal structure to promote nucleotide exchange, GEFs also contain other domains such as, SH2, SH3, Ser/Thr or Tyr kinase, Rho-Gap, Ras-GEF, Ran-GEF, PDZ and additional PH domains, which seem to be

involved in coupling GEF to upstream receptors or to transmit signals through multiple signaling pathways (Rossman et al. 2002).

The other GEF subfamily is characterized by a different catalytic domain called DHR-2 domain. This domain was found for the first time in Dock180, a protein able to induce morphological changes in 3T3 fibroblasts (Hasegawa et al. 1996). Although this protein was lacking of the DH domain, it was able to bind and activate Rac1. At the same time, another protein called zizimin-1 was also found to lack the DH domain but selectively associated with activated Cdc42 (Lin et al. 2006). Dock180 and zizimin-1 share two specific regions called DHR-1 and DHR-2. The DHR-2 domain (also called CZH-2 or DOCKER) was found to be a novel GEF domain (Meller et al. 2005).

The DHR-2 domain is very large, consisting of 450-550 aa. However, as for the DH domain, very little sequence similarity (around 16-17%) is shared between the different members of this GEF family (Meller et al. 2005).

Studies in *C.Elegans* have demonstrated that CED12/ELMO is involved in the activation of Rac1 via Dock180. ELMO is an approximately 700 aa protein characterized by Armadillo repeats, a PH domain at the C-terminal, and a proline rich motif at the N-terminal. ELMO is not directly able to bind Rac1, however is crucial for enhancing Rac1 activation by DOCK180. It has been proposed that ELMO and DOCK180 act as a binary GEF, where the DHR-2 domain of DOCK180 engages Rac1, and the PH-domain of ELMO stabilizes the complex (Brugnera et al. 2002).

In mammalian cells, ELMO regulates DOCK180 function in different ways. By binding to active RhoG, ELMO can target DOCK180 to the cell membrane in order to activate Rac1, and alternatively the PH-domain of ELMO can bind and stabilize the DHR-2-Rac1 complex (Katoh and Negishi 2003).
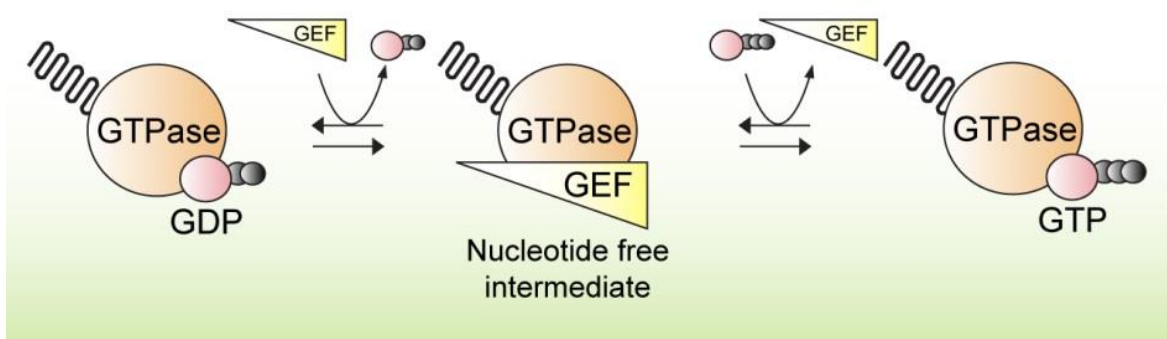
2.2.3 GAP proteins

GTP hydrolysis returns Rho GTPases to their inactive state, thus terminating downstream signaling. This reaction, which is intrinsically very slow, can be accelerated by up to five orders of magnitude through interaction with GAP proteins (Scheffzek and Ahmadian 2005).

GAP activity is contained in a stretch of 100-350 aa called G-domain. This primary sequence folds into an α/β structure with residues from conserved G-motifs forming a shallow surface pocked that accommodates the guanine nucleotides GTP or GDP. The G-domain is generally accompanied by other domains frequently involved in signaling or localization, such as SH2, SH3, PH, PDZ, proline rich and paxillin binding subdomains (Scheffzek and Ahmadian 2005).

Regarding the ability to accelerate GTP hydrolysis, two explanatory models have been proposed. In the first model the GTPase provides the catalytic machinery, while the GAP stabilizes the conformation of the catalytic components (Neal et al. 1988). Alternatively the second model proposes that GAPs supply a catalytic residue, which could possibly be arginine, to the active site of the GTPase (Figure 7) (Rensland et al. 1991).

The first RhoGAP activity was found in a protein then called p50RhoGAP (Hall 1990). Up to now, 68 different RhoGAPs have been identified from the human genome analysis (Peck et al. 2002).

Many RhoGAPs are specific for more than one Rho GTPase, however there are few exceptions. For instance, p190RhoGAP shows specificity to RhoA, such as RhoGAPX-1, while ArhGAP15 exhibits Rac1 specificity (Prakash et al. 2000; Arthur and Burridge 2001; Seoh et al. 2003). The multi-domain BCR, stimulates both Rac1 or Cdc42, while p50RhoGAP acts *in vitro* toward Cdc42, Rac1 and RhoA (Barfod et al. 1993; Lancaster et al. 1994; Chuang et al. 1995).

Several RhoGAPs possess dual or multiple catalytic domains such as GEF and GAP domains, indicative of tight coordination of signaling pathways. For example, both Abr and BCR contain tandem DH-PH domains and a C-terminal GAP domain (Chuang et al. 1995). The GAP domain of these proteins is catalically active towards both Rac1 and Cdc42,

while the DH-PH domain is moderately active as a GEF for Rac1, RhoA and Cdc42. It has been recently shown that Abr acts as a Rho GTPase regulator of single cell wound healing. In this model of interaction Abr is able to amplify the local increase of RhoA activity via its GEF domain for RhoA, while is able, at the same time, to inactive Cdc42 via its GAP domain. The result is a sharp segregation two separate zones of activity for RhoA and Cdc42 that control wound healing (Benink and Bement 2005).
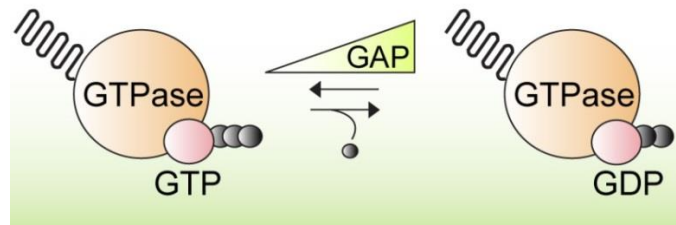
Figure 7. GAP proteins cycle. GTPase activating proteins (GAPs) stimulate and accelerate the GTPase-GTP hydrolysis. This mechanism allows Rho GTPases to return to their inactive state and to terminate downstream signaling. The mechanism that accelerates GTP hydrolysis seems to involve either the stabilization of the GTPase catalytic conformation or the supply of a catalytic residue, such as arginine, into the active site of the GTPase.

2.2.4   GDI proteins

The inactive pool of Rho GTPases is stably maintained in the cytosol by associating with Rho-specific guanine nucleotide dissociating inhibitors (Rho GDIs).

There are three genes encoding Rho GDIs in mammals. Rho GDI1 (also called Rho GDIα), is ubiquitously expressed and able to interact with a wide range of GTPases, including RhoA, Rac1, Cdc42, RhoC and Rac2. Rho GDI2 (also known as Rho GDIβ) is highly expressed in hematopoietic cells and some tumors. This protein is able to associate with several GTPases but with a lower affinity than Rho GDI1. Finally there is Rho GDI3 (or RhoGDIγ), which is highly expressed in the nervous system and interacts predominantly with RhoB and RhoG (Garcia-Mata et al. 2011). Rho GDIs were characterized as proteins able to inhibit some features of Rho proteins (except Ras, Ran and Rab), such as releasing of GDP and loading of GTP. However, RhoGDIs do not inhibit the binding of the Rho GTPase to the nucleotide but only the release of nucleotide (Ueda et al. 1990). Moreover, Rho GDIs are able to extract Rho GTPases from the cell membrane to prevent their inappropriate activation and to protect them from misfolding

and degradation. This occurs by the binding of Rho GDIs to the hydrophobic isoprenoid sequence at the C-terminal of the Rho GTPase. Isoprenylation is crucial for the correct subcellular localization of Rho GTPases. However due to its nature, in the absence of a membrane, this sequence impairs the ability of the Rho GTPase to fold properly. Therefore, acting as a chaperone proteins, Rho GDIs shield the isoprenyl moiety from water in the cytosol by inserting it into a hydrophobic pocket. This allows the cytosolic stabilization of the Rho GTPase pool which is then ready to quickly be recruited to the membrane (Cox and Der 1992) (Figure 8).
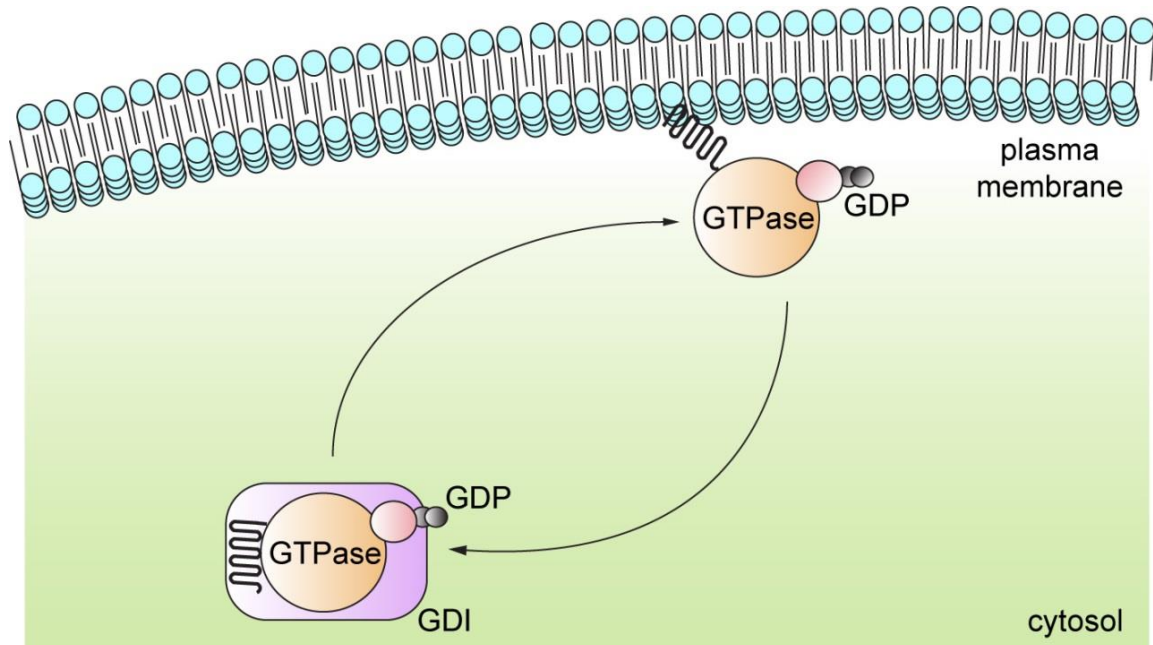
Figure 8. Rho GDI cycle. Rho GDIs are able to extract Rho GTPases from the cell membrane to prevent their inappropriate activation and to protect them from misfolding and degradation, therefore acting as an inhibitor but also as a reservoir for rapid Rho GTPase activation. The mechanism of action involves the Rho GDI binding of the hydrophobic isoprenoid sequence at the C-terminal of the Rho GTPase.

2.2.5 RhoA, Rac1, Cdc42 and their effectors

Rac and Cdc42 share some of their effectors (Figure 9). One of them is the p21-activated kinase (PAK) family of serine/threonine kinases. This family is made by six members (Pak1-6), of which Pak1 and 3 have been mostly studied and are involved in the regulation of the actin cytoskeleton dynamics as well as in gene expression (Jaffer and Chernoff 2002). These kinases normally exist in a latent state, due to their autoinhibitory N-terminal

region, which assumes a conformation that prevents the activation of the C-terminal kinase domain. Upon binding with activated Rac or Cdc42, the autoinhibitory region is no longer able to inhibit the kinase and PAK is activated via autophosphorylation (Buchwald et al. 2001). There are several mechanisms that PAK uses to regulate the cytoskeleton. One of them involves the phosphorylation and activation of Lin-11, Isl-1, and Mec-3 (LIM) domain-containing kinases (Edwards et al. 1999). The kinases once activated phosphorylate and inhibit cofilin, which act as depolymerizing/severing factors for actin filaments (Yang et al. 1998). The result of this inhibition is the stabilization of the actin filament and the promotion of actin polymerisation (Stanyon and Bernard 1999). Another mechanism that PAK uses to regulate the actin cytoskeleton, is to interfere with the myosin light chain (MLC) function, via the direct phosphorylation and inhibition of the myosin light chain kinase (MLCK). This function seems to have an impact on the disassembly of actin stress fibers (Sanders et al. 1999). It appears from recent studies that PAK proteins are also regulators of the microtubule cytoskeleton, in particular through the phosphorylation of stathmin/Op18 at Ser16. Op18 has a microtubule destabilization function, therefore the phosphorylation of this protein by PAK, inhibits its ability to bind the microtubules, leading to their stabilization (Daub et al. 2001). PAK activation can be regulated by another effector of Rac1 called Cdk5/p35. Cyclin-dependent kinase 5 (Cdk5) and its neuron-specific regulator p35, which is able to associate with activated Rac1, can cause hyperphosphorylation of PAK1, resulting in the down-regulation of Pak1 activity. Therefore, Rac1 can control PAK1 activity duration, via the activation of the Cdk5/p35 complex (Nikolic et al. 1998).

Another mechanism that Rac1 and Cdc42 use to regulate the actin cytoskeleton involves the Wiskott-Aldrich-syndrome family of scaffolding proteins. Rac1 regulates the activity of three members of this family, called WASP family verprolin homology domain-containing proteins (WAVE 1-3), while Cdc42 regulates the Wiskott-Aldrich-syndrome protein (WASP) and its neuronal form (N-WASP). As previously described, both WASP and WAVE proteins regulate the actin cytoskeleton via the activation of the Arp2/3 complex (Machesky et al. 1999; Millard et al. 2004; Smith and Li 2004).

WASP and N-WASP are known to bind the activated form of Cdc42 (Rohatgi et al. 1999). The interaction between these proteins induces a conformational change that releases the WASP VCA domain from autoinhibition, allowing the activation of the Arp2/3 complex and the nucleation of actin filaments (Kim et al. 2000). Recently, it has been shown that another protein, called transducer of Cdc42-dependent actin assembly (Toca-1), is crucial

for Cdc42-dependent actin polymerisation. Toca-1 is able to bind both Cdc42 and N-WASP, and promote actin nucleation directly activating N-WASP or inhibiting WIP1, which is a negative regulator of N-WASP (Ho et al. 2004).

The WAVE proteins are able to mediate actin nucleation, without binding directly to Rac1. In its inactive state, WAVE proteins exist in a complex responsive to Rac1 signaling (Eden et al. 2002). The WAVE complex includes Nck-associated protein (Nap125), Abl interactor 2 (abi2), fragile X mental retardation protein (FMRP)-interactin proteins 1 and 2 (CYFIP1, CYFIP2) and the heat-shock protein, HSPC300. Remarkably, Nap125 is able to interact with activated Rac1, via CYFIP1, inducing the dissociation of the complex, and activation via WAVE of the Arp2/3 complex (Kobayashi et al. 1998). This mechanism is used by Rac1 to induce actin nucleation of lamellipodial actin filaments (Steffen et al. 2004). The insulin receptor substrate of 53KDa (IRSp53) is an effector of both Rac1 and Cdc42, which links these two GTPases to the activation of WAVE2 and mammalian Ena (Mena) (Miki et al. 2000). IRSp53 has an autoinhibitory function that involves the partial binding of its N-terminal domain with the Cdc42/Rac1 interactive binding (CRIB) domain. The binding of the Rho GTPases to the CRIB, or to the SH3 domain of IRSp53, is able to relieve the inhibition and to initiate actin filament assembly (Krugmann et al. 2001). IRSp53 can activate Mena to induce filopodia formation and Wave 2 to promote both lamellipodia and filopodia formation (Krugmann et al. 2001).

RhoA controls the activation of two major downstream effectors, which are members of the rho associated protein kinase (ROCK) family and the Diaphanous formin (Dia) subfamily (Figure 9). ROCK proteins are serine/threonine kinases that control the actin cytoskeleton in several ways (Leung et al. 1995; Riento and Ridley 2003). They can regulate actin filament bundling, via MLC phosphorylation, or phosphorylation of MLC phosphatase (PPtase), which indirectly increases phosphorylation of MLC (Amano et al. 1996). Moreover, ROCK proteins promote f-actin nucleation via phosphorylation of LIMK, which phosphorylates and inactivates the actin severing protein cofilin (Maekawa et al. 1999).

There are several members of the Diaphanous-related formin subfamily that interact with activated Rho GTPases, including: mDIA1 (which binds RhoA and RhoC), mDIA2 (which binds RhoA and Cdc42) and mDIA3 (which binds RhoA, Cdc42, Rac1 and RhoD) (Wallar and Alberts 2003). The binding of an activated Rho GTPase seems to disrupt the autoinhibitory interaction between the N- and C-terminal domains of the mDIA proteins (Alberts 2001). It has been shown that mDIA1 is able to bind to prolin via its formin homology domain (FH1); this allows mDIA1 to use prolin-bound actin monomers for

filament nucleation (Li and Higgs 2003). Recent data show evidence that mDIA can also be used downstream of RhoA to regulate the stabilization and orientation of microtubules (Ishizaki et al. 2001). mDIA could have an effect on actin fiber formation in cooperation with ROCK proteins (Maekawa et al. 1999).
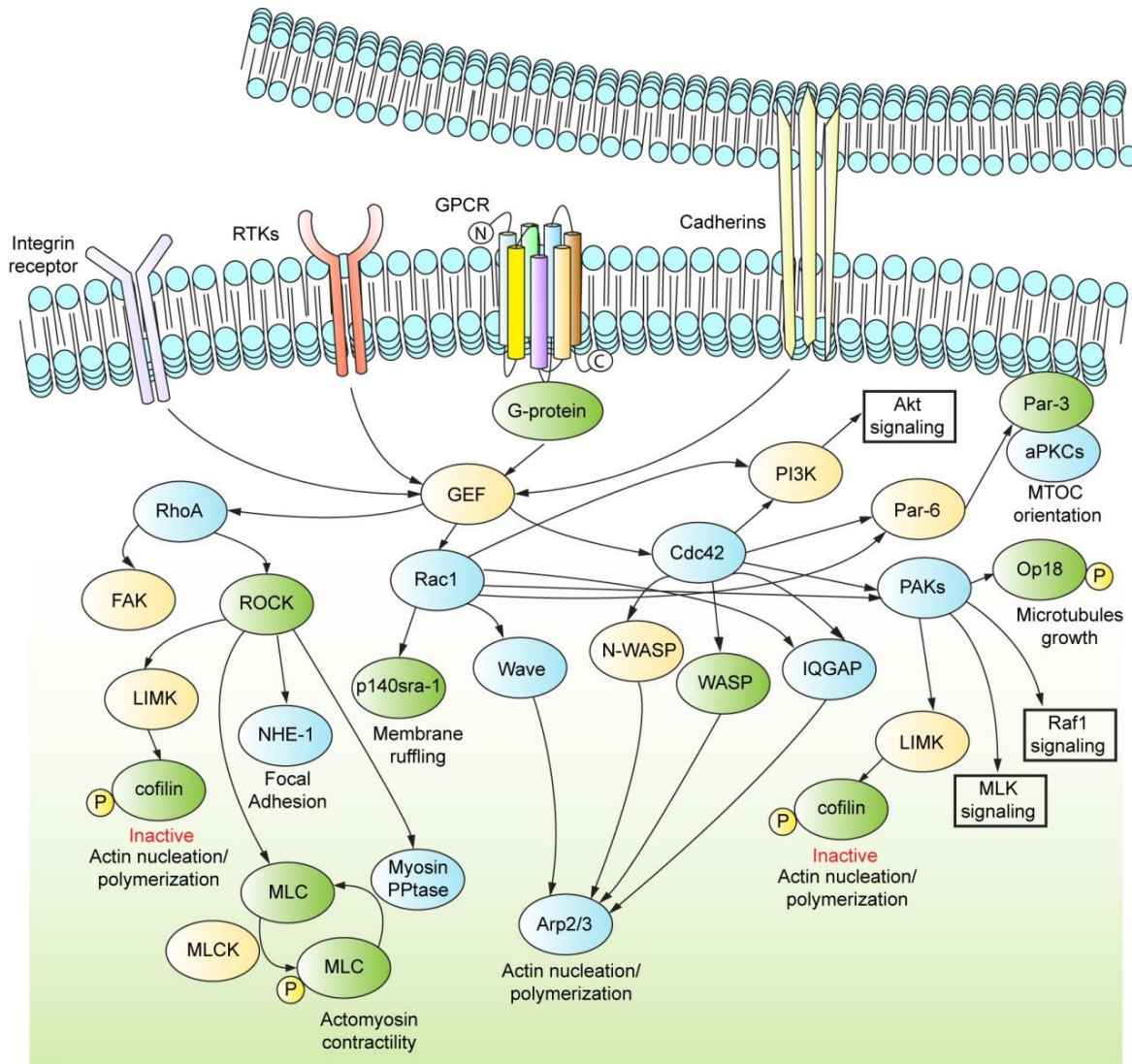
Figure 9. The Rho GTPases central pathways. The Rho family of small GTP-binding proteins comprises a group of signaling molecules that are activated by a variety of growth factors, cytokines, adhesion molecules, integrins, G-proteins and regulate a wide range of biological processes, including cytoskeletal reorganization, cytokinesis, cell motility, cell invasion and neuronal development. The best-characterized family members of the Rho family GTPases are RhoA, Rac1 and Cdc42. Each controls the formation of distinct cytoskeletal components in mammalian cells. Activation of Rac1 induces the formation of lamellipodia, while activation of Cdc42 stimulates the polymerisation of actin to filopodia. Contrarily RhoA regulates focal adhesion and stress fibers formation. A number of proteins have been identified as targets of Rho. These targets include ROCK, Myosin PPtase and FAK. ROCK is the major target of Rho. ROCK phosphorylates both MLC and

Myosin PPtase, thus playing an important role in actomyosin contractility. ROCK also activates LIMK. LIMK phosphorylates and inactivates cofilin, leading to actin-depolymerisation. RhoA plays an important role in regulating the organization of the cytoskeleton by promoting the assembly of focal adhesions and actin stress fibers and by activating FAK.

Rac and Cdc42 also have numerous effectors that mediate effects on the cytoskeleton. Rac binds to WAVE to promote actin polymerisation in lamellipodia through activation of the ARP2/3 complex. Both Rac1 and Cdc42 bind and activate the PAK kinases. PAKs have multiple substrates, including LIMK, which leads to actin polymerisation, stathmin, which stabilizes microtubule plus ends. Rac and Cdc42 also bind to the actin-binding protein IQGAP, which is implicated in the regulation of cell-cell adhesion and microtubule orientation. Both Rac and Cdc42 also bind and stimulate PI3K, which activates Akt. WASP and N-WASP are critical downstream effectors of CDC42 that mediate formation of filopodia. Recent findings show that Cdc42 and Rac, involved in the dynamics of actin cytoskeleton and cell polarity, bind to a protein complex containing PAR-6, PAR-3 and aPKC (atypical Protein Kinase-C).

2.3 Neurite outgrowth

Neurite outgrowth is an early stage of neuronal differentiation. Neuritogenesis starts via the activation of membrane receptors upon extracellular cues. The activation of intracellular cascades triggers changes in the actin and tubulin cytoskeleton and gene transcription that results in the initiation and consequently in the stabilization of the neurite shaft. The Rho family of GTPases is mainly involved in the regulation of these events and represents one of the key players in the coordination of the different phases of neurite outgrowth (da Silva and Dotti 2002).
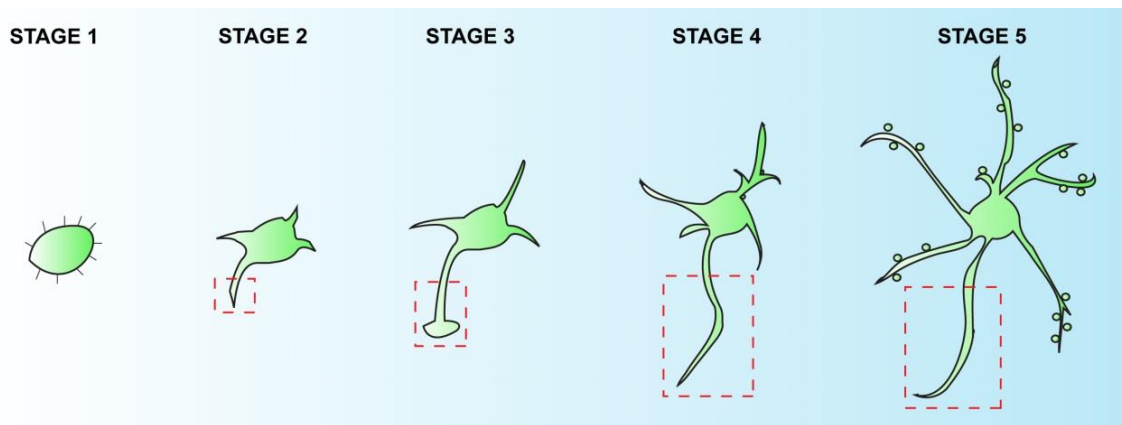
Figure 10. Neuronal stages of differentiation. Neuronal polarization is characterized by different stages. At stage 1, immature neurons exhibit lamellipodia and filopodia protrusion, and this activity leads to the extension of multiple immature neurites in stage 2. Stage 3 represents a crucial step to break neuronal symmetry. In this stage a single neurite grows rapidly to become an axon, while other neurites acquire dendritic identity. Stage 4 is characterized by axonal and dendritic outgrowth. Finally, stage 5 differentiated neurons exhibit dendritic spines. Dashed box represents the axonal differentiation.

2.3.1 Extracellular cues and cytoskeleton

Neuritogenesis plays a crucial role in brain development. During this process the original round shape of the neuroblast is broken by extracellular cues to create a solitary neurite characterized by a specific actin-rich tip called the growth cone (da Silva and Dotti 2002). The disruption of the cellular symmetry allows cells to polarize and subsequently to differentiate the neurite into an axon or a dendrite (Dotti et al. 1988) (Figure 10). Cells and environment play a crucial role in determining the number, the morphology, the orientation

and the speed of growth of the neurites (Sanes 1983). Neuritogenesis depends on a basic engine, which is the actin cytoskeleton that generates forces within the cell that allow migration and neurite protrusion (Mitchison and Cramer 1996). Moreover, microtubules play an important role providing the force to maintain elongated neurites and to regulate the speed of growth (Drubin et al. 1985).

Initially *in vivo* neurons seem to differentiate one neurite, which will become an axon that allows the round cells to switch into a migratory shape. Finally, once the neuron has reached its final position in the brain, the cell undergoes a supplementary stage of differentiation that allows the formation of dendrites (Hinds and Hinds 1978). On the other hand, hippocampus or hypothalamus neurons cultured *in vitro*, follow a different mechanism of differentiation. Initially, the neuroblast protrudes many short neurites and later only one of them differentiates into an axon (Dotti et al. 1988; Craig and Banker 1994).

The different mechanisms of differentiation can be explained by the distribution of extracellular signals. In fact, *in vivo*, where these signals are graded, the cells are induced to sprout only one axon, at the side of the membrane-ligand contact. These gradients will allow the cell to crawl to their final destination. Once the site is reached, a new set of extracellular cues will trigger the differentiation of the dendrites (He et al. 2002). On the other hand in vitro, the cells are stimulated to extend several neurites by the homogenous cues that surround their environment (Esch et al. 1999). However, later specific pathways allow these cells to finally differentiate only one axon.

The cellular machinery that is involved in the interaction with the surrounding environment is the neuronal growth cone. The growth cone is formed by a central region, called the c-domain, which contains membrane organelles and microtubules that are essential in the maintenance of growth, and by a peripheral region, called the p-domain, formed by filopodia and veil-lamellipodia (Goldberg and Burmeister 1989). Filopodia are made of actin bundles that allow rapid extensions and sense the surrounding environment. Lamellipodia are filled with a tight network of actin filaments, which promote growth cone movement and neurite extension (Letourneau 1983) (Figure 11).

The morphology and the orientation of early neurites reflect the nature of the molecules in the surrounding environment. ECM proteins such as collagen, laminin and Slit proteins and soluble molecules, such as fibroblast growth factor (FGF), transforming growth factor beta (TGF-β), vascular endothelial growth factor (VEGF) and neurotrophins are able to

31

influence early neuronal differentiation (Brose and Tessier-Lavigne 2000; Tucker et al. 2001; da Silva and Dotti 2002).

For instance, the integrin-laminin complex seems to play a crucial role in the initiation of neuronal differentiation. Integrins are membrane glycoprotein receptors, which function as non-covalent αβ heterodimers to mediate cell-cell and cell-matrix interactions (Giancotti and Ruoslahti 1999). Laminin binds to the integrin receptor inducing a local change in the neuronal membrane that allows the formation of filopodia and lamellipodia. This first interaction between the cell membrane and the ECM enhances the number of integrin-laminin contacts, leading to an increase in intracellular signaling events that result in the protrusion of a nascent neurite (Ivins et al. 2000). Moreover, the exploring filopodia at the tip of the growth cone can generate a peak of intracellular calcium through the activation of a cluster of integrin receptors. This burst of calcium promotes filopodia formation and neurite extension stimulating actin polymerisation (Gomez et al. 2001).
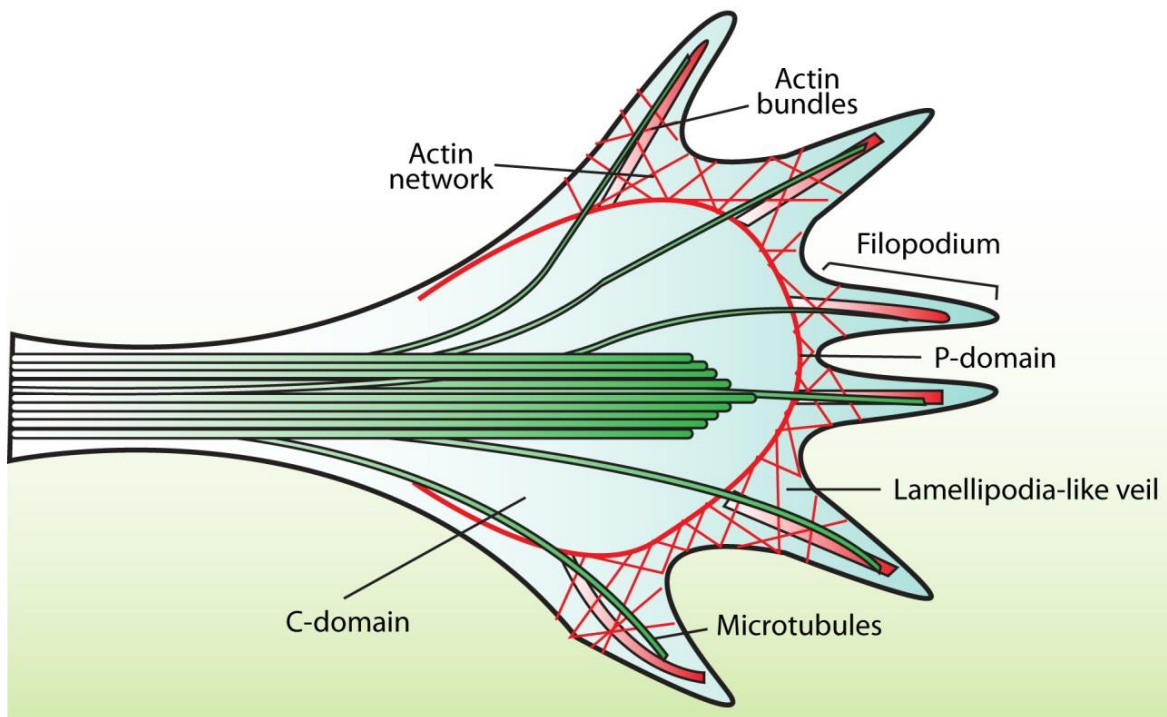
**Figure 11. The structure of neuronal growth cones.** The leading edge of the growth cone is made up of filopodia, which act as a sensing machinery to explore the environment, and the lamellipodia, which drive growth cone movements. Together these two components create the P-domain. Additionally some microtubules can explore this region. The C-domain contains microtubule bundles and organelles, and is crucial for neurite extension.

2.3.2 Rho GTPases role in neurite outgrowth

The involvement of Rho GTPases in the regulation of neurite outgrowth is very well known, and it is believed that different GTPases can act antagonistically toward each other to regulate this process (da Silva and Dotti 2002). Studies using DN forms of Rac1 and Cdc42 supported the hypothesis that these GTPases regulate neurite initiation and outgrowth. DN mutant forms of Rac1 and Cdc42 inhibit neurite outgrowth in PC12 and N1E-115 cells upon NGF stimulation (Sarner et al. 2000; Aoki et al. 2004). Moreover, using FRET technology, it has been demonstrated that Rac1 and Cdc42 are broadly activated at the cell periphery immediately after the addition of NGF in PC12 cells. Subsequently, repetitive cycles of activation and inactivation are observed at the motile tips of protrusion. In particular Rac1 activity seems to be localized in the distal half of the neurite tip, while Cdc42 is concentrated in the filopodia projecting from the tip (Aoki et al. 2004). NGF-induced activation of Rac1, which in turn induces protrusions, is concomitant with decreased RhoA activity (Yamaguchi et al. 2001). Instead, RhoA activation is generally associated with inhibition of neurite protrusion or extension, both in PC-12 and N1E-115 cells (Yamaguchi et al. 2001). CA RhoA is able to prevent neurite initiation (Katoh et al. 1998a; Kranenburg et al. 1999), and DN RhoA, induces neurite protrusion, lamellipodia and filopodia formation, mimicking the effect of Rac1 and Cdc42 (Kozma et al. 1997; Kranenburg et al. 1999).

In this context, it becomes clear that Rac1 and Cdc42 stimulate neurite protrusion and formation of lamellipodia and filopodia, while RhoA is negatively controlling neurite initiation and extension (da Silva and Dotti 2002) (Figure 12).

However, in contrast to these findings, several examples have shown that CA or DN forms of Rac1 and Cdc42 induce opposite phenotype to what is expected. For instance, CA Rac1 decreases neurite length in rat cortical neurons and DN Rac1 promotes neurite outgrowth in chick DRG (Jin and Strittmatter 1997; Sarner et al. 2000). These results may reflect the different roles of Rho GTPases in various species and cell lines, however, at the same time the data highlight the need for GTPases to cycle between the GDP and the GTP states in order to tightly regulate neurite formation and extension.
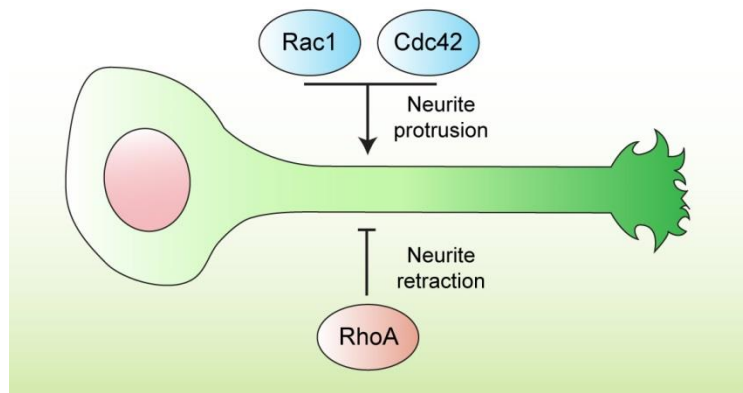
Figure 12. Rho GTPases regulation of neurite outgrowth. In the classical model, Rho GTPases control protrusion and retraction of the neurite. In particular, Rac and Cdc42 promote the formation of protrusions that trigger the actin mediated movement towards the stimulus that induces neurite outgrowth. On the other hand, RhoA promotes neurite retraction by the increase in actomyosin contractility via its effector ROCK.

2.3.2.1 Rac1 and Cdc42 signaling

NGF is well known for its capacity to stimulate neurite formation in neuronal cells, and the pathway that involves NGF in the regulation of this process has also been largely elucidated (Negishi and Katoh 2002).

The neurotropic tyrosine kinase receptor A (TrkA) mediates NGF-driven activation of Rac1 and Cdc42, while PI3K is required for NGF-induced activation of Rac1 and Cdc42, as wells as NGF-mediated inactivation of RhoA (Nusser et al. 2002; Aoki et al. 2004). PI3K and Ras regulate neurite outgrowth via the activation of Rac1 and Cdc42, while these two GTPases can autonomously regulate this process (Sarner et al. 2000) (Figure13). Therefore a pathway has been proposed that involves NGF-TrkA-Ras-PI3K-Rac1 and Cdc42, which promotes neurite protrusion (Sarner et al. 2000). Besides working downstream of Ras, it has been found that Rac1 and Cdc42 mediated neurite outgrowth can be promoted by another GTPase called Rin. Rin is mostly expressed in adult neurons and binds calmodulin (CaM), a calcium-binding messenger protein (Lee et al. 1996). Curiously, Rin expression in PC12 cells promotes neurite outgrowth through the activation of Rac1 and Cdc42. This phenotype can be rescued by DN forms of Rac1 and Cdc42. Moreover, Rin also regulates RhoA activation, and RhoA knock down (KD) increases the formation of neurite branches in Rin expressing cells (Hoshino and Nakamura 2003).

The GEF proteins are positive regulators of Rho GTPase activation, and several of them play a role in Rac1 and Cdc42-driven neurite formation.

Tiam1 is a Rac1 GEF, which is highly expressed in the neuronal system (Habets et al. 1994). In N1E-115 cells, Tiam1 overexpression induces cell spreading and neurite outgrowth, through the interaction between laminin and the integrin receptor α6β1 and the activation of Rac1. This effect can be compensated by overexpression of CA RhoA (Leeuwen et al. 1997). STEF, another GEF for Rac1, is also able to promote neurite outgrowth and this phenotype can be rescued by DN forms of Rac1 (Matsuo et al. 2002). Trio is a multidomain protein containing two GEF domains (GEFDs). GEFD1 controls Rac1 and RhoG activation, while GEFD2 controls RhoA activation (Bellanger et al. 2000). It has been shown that Trio binds the netrin receptor DCC in embryonic brain lysates, through the interaction with Pak1. This interaction induces the activation of Rac1, which leads to neurite extensions in cortical neurons (Bellanger et al. 2000). Another GEF that has an impact on neurite outgrowth and branching formation is Dock4. This is part of the DOCK family of GEFs, characterized by 11 members (Dock1-11) (Laurin and Cote 2014). Multiple studies have demonstrated that Dock4 is capable of controlling cell migration by transducing several upstream signals, such as Wnt, PDGF and RhoG, via activation of Rac1 (Hiramoto et al. 2006). Moreover, it has been recently shown in Neuro2A cells that Dock4 activates Rac1 and promotes neurite outgrowth and branching formation, through its interaction with ELMO2 (Xiao et al. 2013).

VAV2 is the second member of the VAV GEF family of oncogenes, and is known to activate all three main GTPases (Liu and Burridge 2000). In *Xenopus* spinal neurons, both gain and loss of Vav2 function inhibit neurite protrusion, while only Vav2 overexpression enhances neurite formation and branching. Furthermore, Vav2 overexpression protects neurons from RhoA-mediated neurite collapse, suggesting that Vav2 activates Rac1 in spinal neurons (Moon and Gomez 2010).

Another protein that acts through Rac1 and Cdc42 to promote neurite outgrowth is cluster of differentiation 47 (CD47). CD47 is a transmembrane protein that belongs to the immunoglobulin (Ig) superfamily. It has been shown in N1E-115 cells that CD47 is able to activate Rac1 and Cdc42 and promoting neurite outgrowth and filopodia formation (Miyashita et al. 2004).

Once activated, Rac1 and Cdc42 promote neurite outgrowth by binding and activating downstream effectors. PAK kinases promote neurite protrusion interacting with both Rac1

and Cdc42. Pak1 directly induces neurite outgrowth in PC12 cells, and indirectly in cortical neurons via its association with Rac1 and p35 (Daniels et al. 1998; Nikolic et al. 1998). Pak5 is highly enriched in mammalian brain and induces neurite and filopodia formation in N1E-115 cells. At the same time, Pak5 antagonizes the effect of RhoA on neurite outgrowth, suggesting that it could act downstream of Rac and Cdc42 to regulate this process (Dan et al. 2002).

Cdc42 has some unique effectors that regulate neurite outgrowth, such as myotonic dystrophy kinase-related Cdc42-binding kinase (MRCK), N-WASP, and Cdc42Hs-associated kinase-1 (Ack1). In PC12 cells, NGF-induced neurite outgrowth can be blocked by an N-WASP mutant, which is unable to bind Cdc42 and therefore to activate the Arp2/3 complex (Banzai et al. 2000).

2.3.2.2 RhoA signaling

RhoA plays an important role in remodeling neuronal protrusions and promoting neurite retraction antagonizing the effect of Rac1 and Cdc42 (da Silva and Dotti 2002) (Figure13). RhoA activation and neurite collapse activity have been linked to different stimuli, such as LPA-induced activation of G-protein coupled receptor, thrombin receptor peptide (TRP) induced activation of thrombin receptor, prostaglandin E receptor EP3 subunit activation, sphungisune-1-poshpate receptor activation and addition of serum to cells (Katoh et al. 1996; Postma et al. 1996; Katoh et al. 1998b). Addition of LPA and TRP induce rapid neurite collapse and cell rounding. These effects can be compensated by the addition of C3 exoenzyme, which specifically inhibits RhoA activation (Jalink et al. 1994). LPA activates RhoA through heterodymeric G proteins such as Gα12, Gα13 and Gαq (Tigyi et al. 1996).

RhoA activation can be also regulated by specific GEF proteins. GEF-H1 is a microtubule-associated GEF protein that is member of the Dbl family of GEFs (Zheng 2001). In HeLa cells GEF-H1 controls RhoA activation inducing the formation of stress fibers and contractile cell morphology. The KD of GEF-H1 is able to prevent nocodazole-induced cell contraction. These results support the evidence that GEF-H1 activates a pathway including RhoA/ROCK/MLC, which plays a role in cell contractility (Chang et al. 2008). This GEF could also be used during neurite outgrowth, controlling RhoA mediated neurite collapse.

PDZ-RhoGEF is a member of the DH family of GEFs characterized by a peculiar regulator of G protein signaling domain (RGS), which allows this protein to interact with Gα12 and Gα13 and induce RhoA activation via G protein couple receptor (GPCRs) (Fukuhara et al. 1999). PDZ-RhoGEF has been shown to form a complex with Plexin-b1 receptor in primary hippocampal neurons. Plexin b1, which is activated by semaphorin 4D, a secreted protein that regulates axonal guidance, induces the recruitment of Rac1 to the membrane preventing its activation. Simultaneously, Plexin b1 increases RhoA activity via PDZ-RhoGEF. This mechanism has an impact in controlling axonal growth cone collapse (Swiercz et al. 2002).

Furthermore, different RhoGAPs are involved in neurite retraction, such as p190RhoGAP and Grit. p190RhoGAP is the main substrate of Src (Src/Fyn) in the nervous system (Brouns et al. 2001). Overexpression of p190RhoGAP induces neurite outgrowth on laminin in N1E-115 cells, and outgrowth and branching in Neuro2A cells (Billuart et al. 2001). Grit is highly expressed in neurons, where it interacts directly with the NGF receptor and functions as a GAP for RhoA and Cdc42. Grit overexpression promotes neurite formation upon NGF stimulation in PC12 cells, suggesting that in these cells RhoA activity is involved in promoting neurite retraction (Nakamura et al. 2002).

The main effector of RhoA, which mediates neurite retraction, is ROCK. Both wild type and the CA mutant form of ROCK, induce neurite retraction and cell rounding, even under stimuli such as NGF, BDNF, NT-3, and on a laminin-coated surface in rat hippocampal neurons (Amano et al. 1996; Katoh et al. 1998b). On the other hand, the ROCK-inhibitor Y27632 and DN ROCK, promote neurite formation and inhibit LPA-induced neurite collapse (Hirose et al. 1998). The promoting effect of RhoA and ROCK on neurite retraction is driven by an increase in actomyosin contractility. ROCK is able to directly phosphorylate MLC, inducing LPA-driven MLC phosphorylation in N1E-115 cells (Amano et al. 1996; Hirose et al. 1998; Kranenburg et al. 1999). NGF and C3 exoenzyme treatment of PC12 cells show a decrease in MLC phosphorylation. These results suggest that NGF induced neurite outgrowth is in part promoted by the inhibition of the RhoA/ROCK signaling pathway, which results in myosin light-chain phosphatase (MLCP) activation and a transient decrease in phosphorylated MLC (Fujita et al. 2001).

An additional substrate for ROCK to regulate actin cytoskeleton is LIM kinase. As previously described LIM kinase are serine/threonine kinases that phosphorylate and inactivate the actin severing factor cofilin. Treatment with LPA in N1E-115 cells, results in

37

increased cofilin phosphorylation, which is driven by ROCK-dependent phosphorylation of LIM kinases (Maekawa et al. 1999).

The actin monomer binding protein profilin is known to act downstream of RhoA/ROCK signaling to regulate actin stability during neuritogenesis in mammalians hippocampal neurons. Profilin exists in different isoforms, such as profilin I (PI), profilin II (PIIa) and profilin IIb (PIIb) (Witke et al. 1998; Da Silva et al. 2003). ROCK has been shown to associate with PIIa. PIIA overexpression is capable of antagonizing NT-3, NGF and BDNF-driven neurite formation, as previously described for RhoA, suggesting that this protein could act downstream RhoA/ROCK to regulate neurite outgrowth (Da Silva et al. 2003).
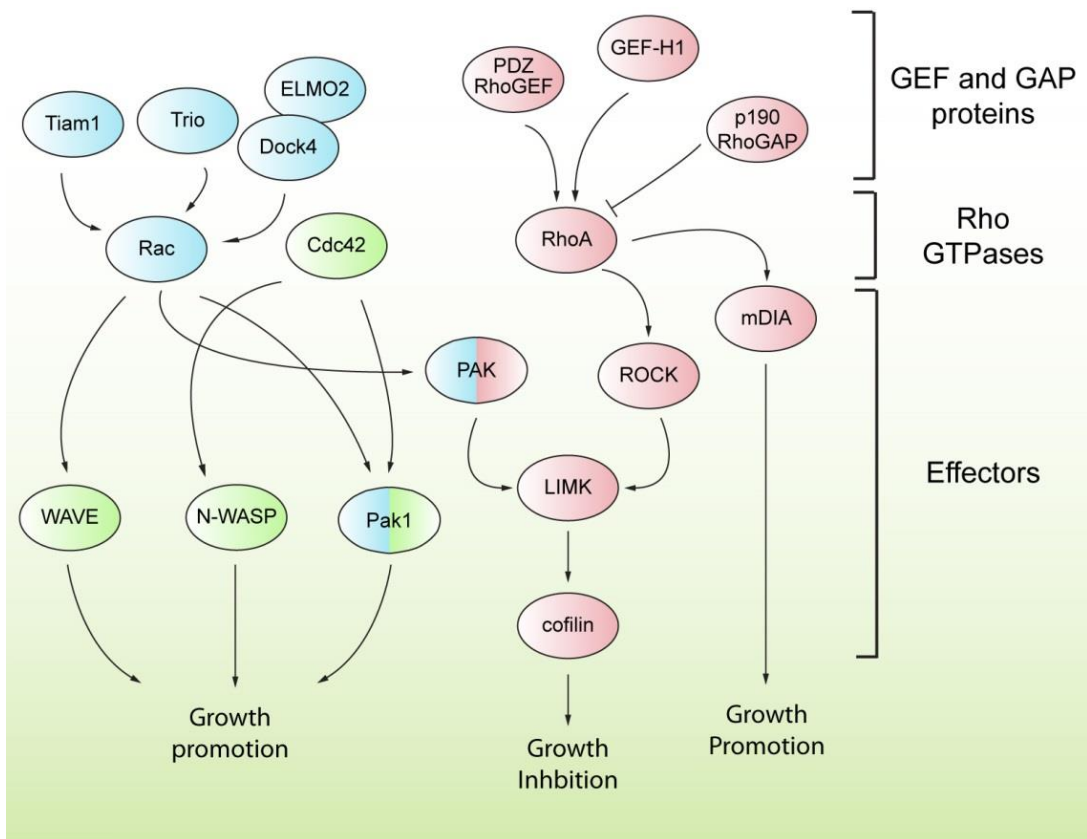
Figure 13. Rho GTPase signaling pathways in neurite outgrowth. When neurite formation is required, a positive signal is triggered into the cell, and activates GEF proteins. The GEFs enhance the exchange of GDP with GTP, leading to the activation of Rho GTPases. GTP-loaded Rho GTPases interact with several effectors to initiate a downstream response. Rac1 and Cdc42 induce the protrusion of the neurite, via their effectors WAVE and N-WASP, by the activation of the Arp2/3 complex, which enhances actin polymerisation. On the other hand, RhoA can induce collapse of the neurite, via its effector

ROCK, which phosphorylates MLC. However, RhoA can also trigger actin polymerisation, via its formin effector mDIA and this mechanism seems to be involved in the polymerisation of filopodia unbranched actin filaments.

2.3.2.3 Other Rho GTPases

The Rho family of GTPases includes more than 20 members. Besides RhoA, Rac1 and Cdc42, additional Rho GTPases, such as RhoG, Rin1/2 and TC10 have been implicated in several signaling pathways that regulate neurite outgrowth.

RhoG, which is downstream of Ras, is able to promote neurite outgrowth through activation of Rac1 and Cdc42 (Katoh et al. 2000). In PC12 cells, upon NGF stimulation, RhoG is able to enhance neurite protrusion in a Rac1 and Cdc42-dependent manner. DN forms of RhoG can suppress neurite outgrowth even in the presence of activated Rac1, while CA RhoG is able to promote neurite protrusion and increase the levels of endogenous Rac1 and Cdc42 (Katoh et al. 2000). RhoG activity is regulated by GEF and GAP proteins. Trio is a multidomain GEF, which is able to activate RhoG and promote neurite outgrowth. Since the GEFD1 domain of Trio is able to activate both Rac1 and RhoG, it has been proposed that the Trio/RhoG/Rac1 pathway and Cdc42 could induce neurite outgrowth in PC12 cells (Estrach et al. 2002).

Recently it has been shown that RhoG is also able to interact in a complex with ELMO and Dock180 to activate Rac1. Coexpression of CA RhoG, Dock180 and ELMO, induces relocation of DOCK180 and ELMO from the cytosol to the plasma membrane, and increases the activation of Rac1. Diversely, Dock180 and ELMO mutants are able to prevent NGF-induced PC12 cells neurite protrusion (Katoh and Negishi 2003).

Kinectin is a MAP protein, which is involved in intracellular organelle motility (Ong et al. 2000). It has been shown that kinectin is able to bind activated RhoG, causing a change in the microtubule transport of lysosomes in non-neuronal cells. This could be the link between RhoG and microtubule transport, which may be important for neuronal differentiation (Vignal et al. 2001).

Rnd proteins, which include Rnd1, Rnd2 and Rnd3 (RhoE), are members of the Rho family of GTPases and appear to promote neurite and branching formation, antagonizing RhoA signaling and regulating changes in the actin and microtubule cytoskeleton (Guasch et al. 1998; Nobes et al. 1998).

Rnd1 and Rnd3 prevent stress fiber and focal adhesion formation, and Rnd1 promotes neurite formation in a Rac-dependent manner by disrupting RhoA-driven cortical actin filaments (Guasch et al. 1998; Nobes et al. 1998).

In non-neuronal cells, Rnd proteins have been shown to be involved in the reorganization of the actin cytoskeleton by reducing active RhoA levels, sequestering ROCK and preventing MLCP phosphorylation (Aoki et al. 2000).

Rnd2 has been linked to neurite and branching formation via its interaction with rapostlin. Rapostlin is an F-bar domain protein involved in the binding of microtubules and in the actin and microtubule-filaments reorganization. In PC12 cells and hippocampal neurons, rapostlin induces formation of neurite and branching in response to Rnd2 activation (Fujita et al. 2002).

TC10 is another member of the Rho family of GTPases that is important in controlling neurite outgrowth. TC10 is highly expressed in muscular tissues and brain and promotes neurite differentiation in PC12 and N1E-115 cells (Abe et al. 2003). This GTPase can associate with certain Rac1 and Cdc42 effectors, such as Pak, N-WASP and MRCK. TC10-driven neurite formation is mediated by the activation of the Arp2/3 complex via N-WASP (Abe et al. 2003). In support of these results DN forms of N-WASP have shown to inhibit TC10 induces neurite outgrowth (Abe et al. 2003).

2.4 Spatio-temporal Rho GTPase signaling

Rho GTPases are molecular switches that sense changes in the extracellular and intracellular environment, and translate these stimuli into downstream signals that control a wide variety of processes such as: cytoskeletal reorganization, cell division and gene expression. A network of GEF, GAP and GDI proteins regulate the rapid activation and inactivation of Rho GTPases, which in turn stimulate downstream signaling cascades. It is thought that the specific effector pathways that are triggered depend on the spatio-temporal activation of Rho GTPases, in response to precise upstream cues. Therefore, it is important to move toward a new paradigm that explores the regulation of Rho GTPases in space and time in order to better understand signaling specificity (Pertz 2010).

2.4.1   Rho GTPases spatio-temporal signaling modules

A series of classic experiments using dominant positive (DP) and DN mutant forms of Rho GTPases, and biochemical pull down assays have been need to study Rho GTPase signaling. These approaches have proven that Rho GTPases are key regulators of the cytoskeleton in a wide variety of cellular processes. In the context of the cytoskeletal regulation during cell migration, the use of these classic tools established that Rac1 controls lamellipodia formation leading to membrane protrusion (Ridley et al. 1992), Cdc42 controls filopodia formation (Kozma et al. 1995), and RhoA controls stress fiber formation and contractility of the rear (Chrzanowska-Wodnicka and Burridge 1996). However, when Rac1 and Cdc42 activity was analyzed using genetic ablation, the cells were still able to form lamellipodia and filopodia, and migrate (Czuchra et al. 2005; Wheeler et al. 2006). This observation suggests that the role of Rac1 and Cdc42 in the regulation of cell migration is not as crucial as previously thought. On the other hand, RhoA has been always associated with cell contractility via its effector ROCK. However, it has been demonstrated that RhoA can also regulate microtubule stability during cell migration via its effector mDIA, therefore suggesting that RhoA could act both in the regulation of membrane protrusions (at the cell front) and contractility (at the cell rear) using different effectors (Amano et al. 1996; Li and Higgs 2003). Novel technologies, such as the fluorescence resonance energy transfer (FRET), have been developed to gain insight into the spatio-temporal activation of Rho GTPases. FRET is the radiationless transmission of

energy from a donor to an acceptor molecule. The donor is a chromophore that absorbs energy and the acceptor is the chromophore to which the energy is transferred. The transfer of energy leads to an increase in the acceptor emission intensity, which can be measured by ratiometric analysis of the images (Roy et al. 2008). In the context of Rho GTPases, the donor and the acceptor chromophores are linked to the GTPase and a specific GTPase binding domain sequence, which only binds the GTPase in its active state. Therefore, when the GTPase is activated, the interaction with the binding domain allows the donor and the acceptor to perform FRET (Pertz 2010) (Figure 14). This technology allows the quantifiable visualization of small pools of activated Rho GTPases not accessible by traditional pull down assays.
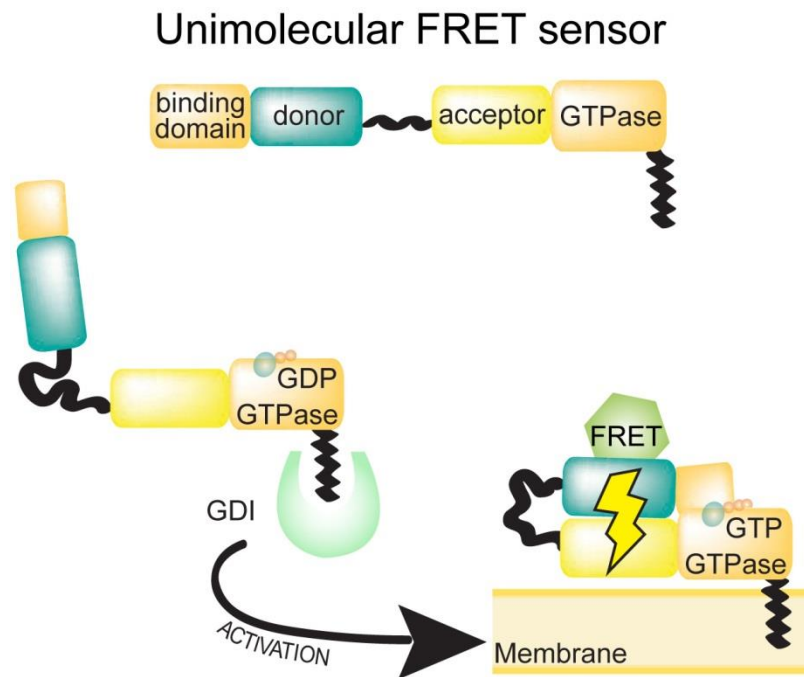
Figure 14. Unimolecular Rho GTPase FRET sensors. Unimolecular FRET probes have been designed to fuse the donor and acceptor fluorophores into a single chain. The Rho GTPase unimolecular probes can be used to monitor the activity of a Rho GTPase over time. When the GTPase is activated, the interaction with the binding domain allows the donor and the acceptor to perform FRET. Moreover, since in the unimolecular probes both fluorophores are identically distributed throughout the cell, the FRET signal can be quantified as a simple ratio between acceptor emission and donor.

For example, the Rac1 FRET-probe, which allows the visualization of GTP-Rac1, was found activated in the lamellipodia of migrating fibroblasts (Kraynov et al. 2000). This result matches with the observation that Rac1 controls lamellipodia formation (Ridley et al. 1992). However the same probe was found activated during uropod retraction in

chemotactic neutrophils, suggesting that this GTPase can be activated both at the front and back during cell migration (Gardiner et al. 2002). Additionally, RhoA FRET-probe was found robustly activated during tail retraction in fibroblasts, accordingly to previous data that described RhoA as the main controller of actomyosin contractility (Chrzanowska-Wodnicka and Burridge 1996). However, surprisingly active RhoA was also found activated at the front of the protrusive lamellipodia, suggesting therefore the existence of two distinct pools of RhoA, which can be activated with a precise timing to specific locations of the cell in order to regulate different processes (Pertz et al. 2006). Moreover, a modified version of the same RhoA probe has been found activated globally during neurite retraction and locally in the growth cone filopodia during neurite protrusion in N1E-115 cells, confirming that spatio-temporal activation of Rho GTPases could be also used to fine tune different events during neurite outgrowth (Fritz et al. 2013). These data have suggested the existence of multiple signaling modules within one cell, which may be made by specific GEFs, GAPs and effector proteins (Figure 15). For instance, during neutrophil chemotaxis, the G_i protein β/γ subunits liberated by the activation of their receptor, can create a complex with the Rac1/Cdc42 GEF β-Pix, the effector PAK and Cdc42, which accumulates at the leading edge and regulates persistent cell migration in these cells. This complex works as an isolated signaling module which locally regulates Cdc42 activation during cell migration (Li et al. 2003). Therefore, since more than 90% of the Rho GTPase pools lies inactivated in the cytosol, the recruitment of specific signaling modules could be the key for a rapid spatio-temporal activation of Rho GTPases.

The picture becomes even more complicated if we consider that spatio-temporal activated Rho GTPases can crosstalk to each other to fine tune specific events (Iden and Collard 2008). For example, it has been demonstrated in single *Xenopus* oocytes that wound closure can be triggered via the formation of exclusive zones of activation of Cdc42 and RhoA. The two Rho GTPases crosstalk to create a region of high contractility (RhoA-ROCK-pMLC) followed by one of low contractility (Cdc42-PAK-LIMK). This mechanism allows the rapid closure of the wound in *Xenopus* oocytes and is finely regulated by the RhoGAP Abr which works as a GEF for RhoA and a GAP for Cdc42, keeping the zones tightly separated (Benink and Bement 2005).

Additionally, using FRET probes and biochemical approaches, it has been proved that the three main GTPases (RhoA, Rac1 and Cdc42) are activated at the leading edge of the protruding membrane during migration in fibroblasts (Machacek et al. 2009). Moreover, using sophisticated methods of computer analysis, which have merged the spatio-

temporal signal of RhoA, Rac1 and Cdc42, it has been proved that these GTPases can cross-talk to each other in space and time (Machacek et al. 2009). In particular, it has been reported that RhoA is activated during membrane protrusion and inactivated during retraction. On the other hand, Rac1 and Cdc42 are activated behind the RhoA zone and later than RhoA during protrusion, but persist in their activation during retraction. These results highlight the existence of a clear crosstalk between Rac1/Cdc42 and RhoA that takes place in a confined subcellular domain, such as the leading edge of a fibroblast, which is on the order of micrometers of length, and occurs in a time shift on the order of tens of seconds.
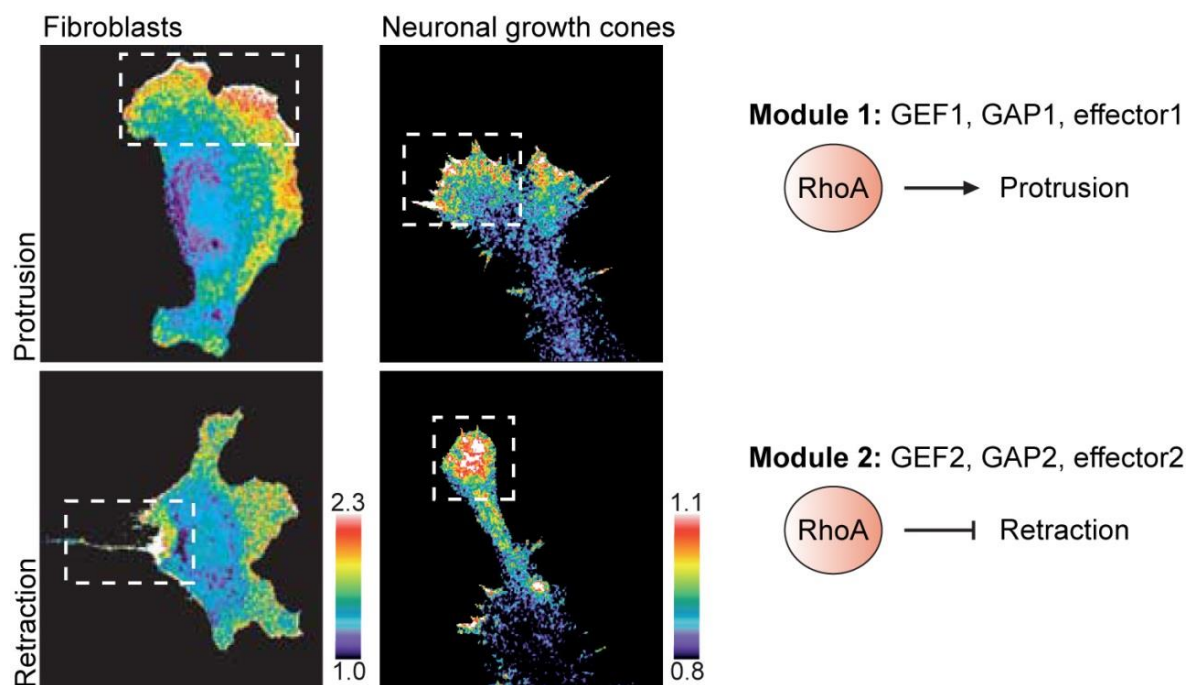
Figure 15. Rho GTPases signaling modules. RhoA FRET-probe analysis allowed the characterization of different signaling modules. In fibroblasts and N1E-115 cells, RhoA probe was found robustly activated during tail and neurite retraction, accordingly to the classic actomyosin contractility pathway that involves this GTPase. However active RhoA also localizes at the front of the protrusive lamellipodia and growth cone filopodia, confirming the hypothesis that Rho GTPases can be activated in space and in time to regulate different processes, and suggesting the involvement of precise signaling module (made by GEF, GAP and effector proteins) that regulate their activity (adapted with permission from Pertz et al., 2006 and Fritz et al., 2013). .

2.4.2 Systematic approach to study Rho GTPases spatio-temporal signaling

The classic tools to study Rho GTPases signaling have given us the opportunity to understand the mechanisms in which these proteins are involved and who their main interactors are. However, when we consider the spatio-temporal resolution in which Rho GTPases are positioned and their tight regulation by GEFs, GAPs, GDIs, crosstalk mechanisms and signaling modules, it becomes clear that global manipulation tools, such as Rho GTPase DN or CA forms, cannot provide appropriate resolution to deconvolute Rho GTPase functionality.

Moreover, due to the global manipulation of the system, classic tools to study Rho GTPase signaling may also introduce artifacts in the results. For example, using a DP Rho GTPase, we would expect an increase in the activity of the entire pattern of effectors that are involved in different signaling modules related to this GTPase. Therefore, hypothetically, using the right tools to extract information from these experiments, we should be able to define every single effect that a DP GTPase has on our system. However, usually the resulting phenotype does not give us information about all the functions in which the GTPase effectors are involved. The explanation comes from the fact that due to the global activation of a certain Rho GTPase, the resulting phenotype can simply be the result of the contribution of one effector, which can be dominant over the others. Moreover, since Rho GTPases act by titrating active GEFs, and since GEF proteins can be specific for more than one GTPase (Rossman et al. 2005), the overexpression of a DN Rho GTPase has the potential to affect several GTPase-driven pathways, creating a phenotype which is far from being specific to just the KD of a single molecule.

Rho GTPase signaling seems to be precisely regulated in space and time; therefore the right approach to understand their subtle regulation would be to analyze the role of every single player participating in a signaling module using systematic approaches.

In this scenario, systems biology methodologies, such as siRNA screenings and high content analysis, could give insight into the spatio-temporal activity of specific signaling modules. A systematic siRNA screening has been performed on GEF and GAP proteins to identify regulators of Rho GTPases that affect migration in tumor cells (Sanz-Moreno et al. 2008). Using this approach, it has been discovered that Dock3, a specific Rac1 effector, is able to promote mesenchymal movement while suppressing amoeboid movements, via the regulation of Rac1 and its effector Wave2. Inversely, RhoA via its effector ROCK,

promotes contractility in order to provide force for amoeboid movements. At the same time, ROCK activates ArhGAP22, which prevents Rac1 from suppressing mesenchymal movements. These data, obtained by a systematic screening and unbiased evaluation of morphological phenotypes show the ability of these two GTPases to control tumor cell movements. Moreover, this work highlights a mechanism of crosstalk between these two proteins that involves the activation of specific effectors such as Wave2 and ROCK.

Systematic approaches can be used to highlight the complexity of the networks in which Rho GTPases are positioned. In the context of neuronal outgrowth, Rho GTPases control neurite protrusion and retraction, which play an important role in the advancement of the growth cone (da Silva and Dotti 2002). However, such a simplistic explanation is in contrast with data coming from proteomic and bioinformatic analysis, which hypothesizes that RhoA, Rac and Cdc42, could be part of a large network, consisting of GEFs, GAPs and effectors involved in the regulation of this process (Pertz et al. 2008) (Figure 16). Such network suggests the existence of multiple Rho GTPase spatio-temporal localized signaling modules that regulate subtle aspects of the neurite outgrowth process, such as neurite initiation, neurite extension, and neurite branch formation. These data again give a hint of how complex Rho GTPase regulation can be and therefore how important it is to find a systematic method to better analyze the role of specific signaling modules.
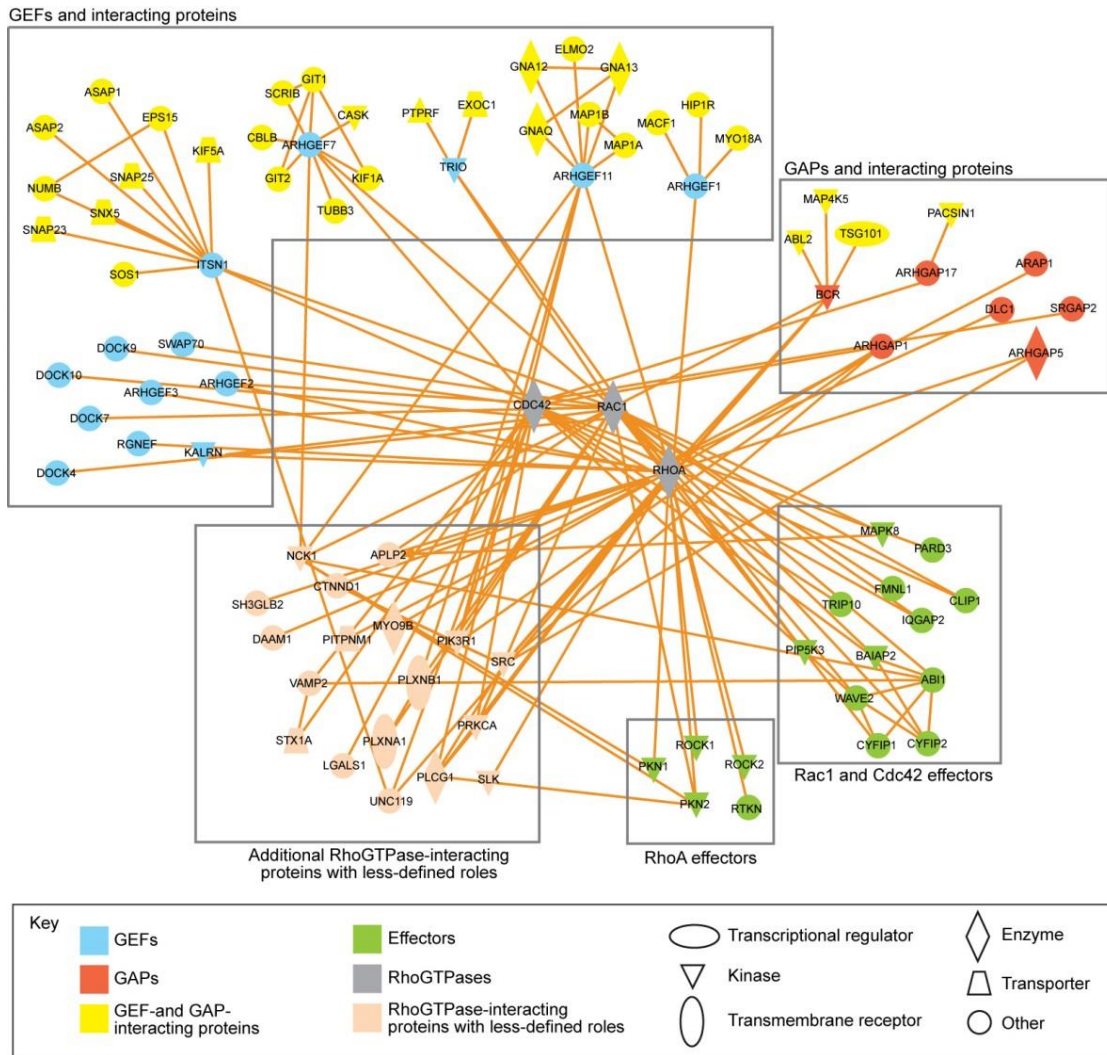
Figure 16. Rac1, Cdc42 and RhoA centered interactome in the neurite. Rac1, Cdc42 and RhoA centered interactome in the neurite. The neurite proteome highlights proteins that are known to interact directly with the three GTPases or with their GEFs and GAPs (adapted with permission from Pertz, 2010).

3. Results

Computer vision profiling of neurite outgrowth morphodynamics reveals spatio-temporal modularity of Rho GTPase signaling

Ludovico Fusco[1,9], Riwal Lefort[2,5,9], Kevin Smith[3,6,9], Fethallah Benmansour[3,7], German Gonzales[3,8], Catherina Barillari[4], Bernd Rinn[4], Francois Fleuret[2], Pascal Fua[3], Olivier Pertz[1]

[1] Institute for Biochemistry and Genetics, Dept. Biomedicine, University of Basel, Mattenstrasse 28, 4058 Basel, Switzerland

[2] Idiap Research Institute, Rue Marconi 19, 1920 Martigny, Switzerland

[3] EPFL CvLab, Route Cantonale, 1015 Lausanne, Switzerland

[4] D-BSSE, Mattenstrasse 26, 4058 Basel, Switzerland

[5] ENSICAEN, Boulevard du Maréchal Juin 6, 14050 Caen, France

[6] Institute for Biochemistry, ETHZ-Honggerberg, Schafmattstrasse 18, 8093 Zurich, Switzerland

[7] F. Hoffmann-La Roche AG, 4070 Basel, Switzerland

[8] Madrid-MIT M+Visión Consortium, Massachusetts Institute of Technology, Cambridge, 02139 Massachusetts, USA

[9] These authors contributed equally.

[*]To whom correspondence should be addressed:

Olivier Pertz, Dept. of Biomedicine, University of Basel, Mattenstrasse 28, 4058 Basel, Switzerland

Phone: +41 61 267 22 03; Fax: +41 61 267 35 66; E-mail : olivier.pertz@unibas.ch

3.1 Abstract

Differentiating neurons both migrate and extend neuronal processes in vitro. The latter process consists of dynamic neurite initiation, elongation, retraction and branching cycles that are likely to be regulated by distinct spatio-temporal signaling networks. Current knowledge of the signaling networks regulating this process stems mostly from experiments in which molecular perturbations are assessed at the steady state, which cannot capture the intrinsically dynamic nature of this process. We present a scalable computer vision pipeline, that coupled with a data analysis platform, allows to automatically annotate neuronal morphodynamic phenotypes in timelapse datasets. In a neuronal-like, cultured cell model system, our approach identifies a stereotypic continuum of morphodynamic events during differentiation. Systematic RNAi perturbations of a candidate Rho GTPase signaling network containing 220 proteins reveal the existence of a limited set of morphodynamic phenotypes, and highlight specific spatio-temporal signaling networks that regulate the different morphogenetic processes involved in neurite outgrowth and/or cell migration.

3.2 Introduction

Neurite outgrowth and neuronal migration are essential to produce and wire the axons and dendrites that connect the adult brain. In cultured cells, neurite outgrowth is highly dynamic, and consists of a series of morphogenetic processes (MPs) such as neurite initiation, elongation, branching, growth cone motility and collapse (da Silva and Dotti 2002). Cultured neuronal cells also actively migrate, which might in part reflect the process of neuronal migration. Precise spatio-temporal signaling networks most likely locally control the cytoskeletal trafficking and adhesion dynamics necessary for each MP to occur. Because neurite outgrowth and cell migration use overlapping cellular machineries, it is conceivable that some molecular components might regulate both processes. These MPs occur on length and time scales of tens of microns and minutes to hours, requiring analysis with adequate spatio-temporal resolution. This has been missed in steady-state measurements, most often at a late differentiation stage. Identification of MP-specific signaling networks thus requires the quantification of the whole morphodynamic continuum of this process.

Rho family GTPases are signaling switches that regulate a wide variety of cellular processes such as actin and adhesion dynamics, gene transcription, and membrane trafficking (Etienne-Manneville and Hall 2002). Rho GTPases are activated by guanine nucleotide exchange factors (GEFs), and switched off by GTPase activating proteins (GAPs). In their activated state, Rho GTPases bind to effectors, which transmit downstream signals. Current models propose that Rac1 and Cdc42 regulate neurite extension, while RhoA controls growth cone collapse and neurite retraction (Sarner et al. 2000; da Silva and Dotti 2002; Aoki et al. 2004). These data are mostly based on the overexpression of Rho GTPase mutants, assayed at steady-state, and therefore do not give insight about the different MPs. Novel fluorescent biosensors that allow to measure Rho GTPase activation dynamics in time and space in single living cells have hinted to more complex models (Pertz 2010). For example, the three canonical Rho GTPases are activated at specific subcellular regions with precise kinetics at the leading edge of motile fibroblasts (Machacek et al. 2009). Recently, RhoA activity was not only observed during growth cone collapse, but also at the tip of filopodia f-actin bundles during growth cone advance (Fritz et al. 2013). This implies the existence of two distinct spatio-temporal RhoA signaling complexes with different functions. Furthermore, the existence of a plethora of

ubiquitously expressed GEFs, GAPs, GTPases and effectors suggests a signaling complexity that is compatible with such exquisite spatio-temporal Rho GTPase regulation. Here, we present an integrated platform that combines high content timelapse imaging and computer vision approaches to perform a multiparametric analysis of neurite outgrowth and cell migration morphodynamics. We combined our platform with an RNAi screen to analyze a potential Rho GTPase interactome, previously identified using a proteomics approach (Pertz et al. 2008). Our data identify spatio-temporal signaling networks that regulate specific MPs during neurite outgrowth and cell migration.

3.3 Results

3.3.1 High content live cell imaging pipeline.

To study neurite outgrowth and cell migration dynamics, we used neuronal-like, mouse N1E-115 cell neuroblastoma cells. To visualize cell morphology, we used a bicistronic vector that expresses Lifeact-GFP, a fusion of green fluorescent protein (GFP) with the f-actin binding peptide Lifeact (Riedl et al. 2008), and a nuclear localization NLS-mCherry fusion, that simultaneously labels the nucleus for unambiguous cell detection (Figure 1a). This construct can be expressed at high level without affecting neurite outgrowth (Supplementary Figure 1a,b), and provides both high contrast on neurites and somata for imaging with air objectives (Figure 1b, Supplementary Movie 1). To perturb different signaling molecules, we co-transfected our reporter plasmid with siRNAs in non-differentiated cells. These cells were subsequently differentiated by overnight serum starvation, replated on laminin-coated coverslips at sparse confluence, and allowed to extend neurites for approximately 20 hours (Supplementary Figure 1c). As proof of concept, we evaluated knock down of previously characterized proteins. *MKK7* siRNA was previously shown to lead to highly unstable, short neurites due to loss of microtubule bundling in the neurite shaft (Feltrin and Pertz 2012); *RhoA* KD leads to increased neurite outgrowth, presumably through loss of ability to collapse (Fritz et al. 2013); and SrGAP2 KD leads to stabilization of filopodia in the growth cone and soma, increasing neurite outgrowth and branching (Pertz et al. 2008). Our protocol enabled efficient knock down of these proteins, which recapitulated the expected phenotypes (Supplementary Figures 1d-f). We also identified a control, non-targeting siRNA that did not alter neurite outgrowth (Supplementary Figure 1g). To perform high content live cell imaging, we optimized our microscope setup for fast, two color imaging of multiple wells. Timelapse analysis started 3 hours post-plating, a time point at which initial neurites already protruded which rendered these cells resistant to phototoxic effects. At this time point, an automated image analysis routine was used to identify 10 fields of view/well with a suitable number of cells with appropriate fluorescence intensities (Supplementary Figures 1h-j). This allowed us to timelapse neurite outgrowth dynamics in 10 fields of view/well across a 24-well plate with 12 minute time resolution for a total of 20 hours.

3.3.2 Computer vision pipeline to quantify neuronal dynamics

To analyze timelapse datasets, we engineered a 3-step, automated computer vision pipeline to segment and track soma and neurite morphodynamics (Figure 1c, Supplementary Movie 2). First, nuclei (mCherry-NLS channel) and their associated somata were identified (Lifeact-GFP channel). Second, somata were tracked throughout a timelapse dataset. Third, neurites for each soma were segmented and tracked over time. This allowed us to annotate each cell soma and neurite with unique identifiers (Figure 1d, Supplementary Movie 2). Importantly, the robustness of the pipeline allowed detection of cellular features across a wide variety of fluorescence intensities that result from our transient transfection protocol. The complete computer vision pipeline is described in Supplementary Note S1 and Supplementary Figure 2. The segmentation and tracking quality were evaluated against human-annotated ground truths datasets.

We then computed relevant features about cell morphodynamics. For that purpose, we modeled the neurite arborescence as a tree, and defined a number of parameters that described both the soma and the neurite (Supplementary Note S2 section 1 and Supplementary Figure 3). These parameters were then used to compute 158 features that comprehensively describe different morphological and morphodynamic aspects during neuronal dynamics. These consist of static cell.time features and dynamic cell.ensemble features (Figure 2a). For cell.time features, all measurements from different cells within one frame at all the different time points of a timelapse movie are considered and therefore provide a population average throughout the whole dynamic neurite outgrowth process. For cell.ensemble features, information about cellular dynamics from all cells in the field of view are analyzed over time. The features were stored as a vector with information on each cell (Supplementary Note S2 section 2), and are comprehensively described in Supplementary Note S2 section 3.

3.3.3 Morphodynamic signature extraction

We then extracted morphodynamic signatures (MDSs) to characterize the effects of RNAi perturbations on neurite outgrowth dynamics (Supplementary Note S3, section 1). For each feature, we performed a statistical z-test that compares its distribution in control and siRNA-treated cells. This enabled us to identify the polarity and penetrance for each feature in response to siRNA perturbations (Figure 2b). To take into account any potential

54

OFF-target effect, we used three distinct siRNAs per gene and computed average z-scores according to the rules that if at least 2 out of 3 siRNAs produce the same phenotype for a given feature (Echeverri et al. 2006), then this phenotype is "ON-target" (Figure 2c). This approach provides a z-score vector, which we refer to as MDS, that indicates penetrance and polarity for each feature in response to a siRNA perturbation throughout the neurite outgrowth process.

To reduce the feature space, we then evaluated the robustness of the MDS of *MKK7* KD across 32 independent experiments (a dataset consisting of 320 movies of non-targeting and *MKK7* siRNA transfected cells each) performed on different days (Supplementary Note S3 section 2). As already shown in Supplementary Figure 1e, *MKK7* KD leads to a highly penetrant phenotype that consists of short unstable neurites (Feltrin and Pertz 2012). For that purpose, we only selected features that exhibited a statistically relevant z-score with identical polarity in at least 70% of the *MKK7* KD experiments (Supplementary Note S3 section 2). This yielded 21 robust features that comprehensively describe neuronal morphodynamics (Supplementary Note S3 section 2.1).

We used our approach to characterize neuronal morphodynamics in *SrGAP2*, *MKK7* and *RhoA* KD cells, already validated to some extent in Supplementary Figure 1e. Representative native and segmented cell images and migration tracks are shown in Fig. 2d and Supplementary movie 3. Extracted MDS signatures (Figure 2e) revealed that our approach successfully captures morphological and morphodynamic phenotypes. *SrGAP2* KD led to increased neurite number, length and branching, as well as increased soma migration. This is consistent with the stabilization of growth cone and soma filopodia, as observed before (Pertz et al. 2008). *MKK7* KD led to short neurites and low soma motility. Consistently with its role in growth cone collapse (Feltrin et al. 2012), *RhoA* KD led to decreased retraction occurrences, producing longer neurites, without however affecting branching. While some of these features can be easily assessed by visual inspection of static images (neurite length/branching) or timelapse datasets (soma speed), others are subtler (soma circularity) and can only be detected by our computer vision approach. Plotting feature distribution in the different perturbed states (Figure 2f) indicates the large level of cellular noise associated with our cell system. These results validate our approach to automatically annotate neuronal morphodynamics.

3.3.4 Characterization of stage specific, neuronal dynamics

Neuronal differentiation involves multiple temporal episodes with distinct morphodynamic behaviors that have until now only been verbally described (da Silva and Dotti 2002). To get quantitative insight into neuronal morphodynamics associated with different temporal episodes, we studied MDSs associated with sequential 1-hour temporal episodes from our 20 hours timelapse movies, using our control siRNA dataset (32 independent experiments/320 movies each). For scale-free representation, we plotted the temporal evolution of the coefficient of variation of a panel of features (Supplementary Note S3 section 3). Because only a fraction of cells extends long neurites in the population, we both considered the whole population, but also specifically gated on the 10 % cells with most robust neurite outgrowth. At the whole cell population level (Figure 3a), robust initiation of multiple short and branched neurites is observed at the onset of differentiation and then steadily decreases during a first phase that lasts 7 hours. This period is also associated with a low soma motility state. After 7 hours, a small cell population extends long unbranched neurites (Figure 3b), and soma motility steadily increases during the remaining period studied. We used a mathematical model (Supplementary Note S3, section 3) to identify cells that represent the average phenotype relevant to select temporal bins of the 10% cells with longest neurites (Figure 3b). These results quantitatively define 2 distinct phases during the neurite outgrowth process. Remarkably, except for phase 2 steady neurite outgrowth, which only occurs in a subset of cells, the dynamic behavior is highly stereotypic for the whole cell population. This suggests the existence of finely tuned genetic programs that regulate each dynamic step of this complex morphogenetic event.

We then applied the same approach to study *MKK7* KD cells (Figure 3c,d), which is characterized by unstable neurite outgrowth (Feltrin and Pertz 2012). Temporal analysis however revealed increased neurite outgrowth in phase 1 compared to control cells, which previously had eluded our visual inspection of timelapse movies. Other parameters such as neurite and branch numbers, as well as cell migration speed were not affected. Short neurites were then observed throughout phase 2. These results suggest that MKK7 regulates two distinct cytoskeletal functions, one in the early, one in the late phase of neurite outgrowth. Such transient phenotypes are typically missed using steady-state assays. Feature distribution plots again represent the noisy, but statistically significant, behavior of cell populations (Figure 3e).

3.3.5 Functional analysis of a Rho GTPase signaling network

We then used our pipeline to analyze timelapse movies of a siRNA screen targeting 220 genes of a potential Rho GTPase signaling network (Supplementary Figure 4). For that purpose, we used a bioinformatics approach to mine our N1E-115 neurite and soma proteome data to identify a mostly neurite-localized Rho GTPase interactome (Pertz et al. 2008). The rationale for the identification of this signaling network is explained in Supplementary Note S4. We used 3 distinct siRNAs/gene, leading to a total of 660 perturbations. These were distributed among 32 experiments, with each 24-well plate containing non-targeting negative and positive *MKK7* siRNA controls, accounting for a total of 7680 timelapse movies and 1.02 TBs of data. A set of quality control metrics showed that similar number of cells/field of view, NLS-mCherry fluorescence intensities were analyzed in different plates of the screen (Supplementary Figure 5a,b). There was no correlation between "OFF-target" effect and specific experimental plates (Supplementary Figure 5c). Overall, 43% of the measurements across different features led to identical z-score polarities for all 3 siRNAs, 52% of the measurements had 2 out of 3 siRNAs yielding identical z-score polarities, while in only 5% of the cases, one siRNA led to a statistically non-significant z-score, and the two other yielded two distinct polarities. Furthermore, we observed that the positive *MKK7* control siRNA associated to each plate yielded a stable MDS across the different experimental plates (Supplementary Figure 5d). These results indicate the stability of our experimental and computer vision analysis pipeline across multiple experiments. KD of each candidate led to a robust phenotype, with an average z-score across all features being statistically significant when compared with the control siRNA.

We then performed hierarchical clustering to identify set of gene perturbations that lead to common MDSs. For that purpose, we computed phenotypic distances between each MDS, and performed bottom-up hierarchical clustering (Supplementary Note S3, section 4 and 4.1). Iterative evaluation of different dendrogram thresholds was performed by visual inspection of the quality of the clusters, as well as inspection of selected phenotypes (Supplementary Figure 6). A good compromise was obtained with a 65 % threshold, meaning that in order to be part of one cluster, 65 % of the features of the MDSs within a cluster had to have a common polarity. Using this approach we identified 24 phenoclusters that comprise 183 out of 220 genes. KD of any of the 36 remaining genes also led to phenotypes, but has to be inspected on a case by case basis.

For intuitive display, we manually sorted these phenoclusters according to the overall polarity of their MDSs (Figure 4). Taking into account the three of the most visually intuitive features accessible at steady state (NumberOfNeurites, NbOfBranchesPerNeuriteMean, MaxExtremeLengthPerNeuriteMean), we grouped these genes in 4 distinct phenotype categories: short neurites, multiple short neurites, long and unbranched neurites, long and branched neurites (Figure 4). To provide a visual representation of these phenotypic categories, we used a mathematical model that selects specific analyzed cells with an extreme phenotype according to these three features. Based on our segmentation, synthetic images of the representative cells are shown (Figure 4, Supplementary Note S3 section 4.2). Indeed, within the cell population context, a large phenotypic continuum around every specific MDS is observed. A second level highly discriminative feature to differentiate phenoclusters was cell migration speed. Taking the latter, as well as the three additional features mentioned above into consideration, we used the same approach to select representative cells for timelapse representation using synthetic images (Supplementary movie 4). Additional discriminative features consist of soma morphology and neurite dynamics, but these are much less visually intuitive.

3.4 Discussion

Our approach allows automated identification of complex morphodynamic phenotypes from timelapse movies, that often escape comprehension by the human eye, and that are more informative than classic steady-state, endpoint assays. The robustness of this platform also provides sufficient throughput for analysis of high volumes of datasets.

We first used this approach to precisely quantify the evolution of different morphodynamic parameter occurring during neurite extension on a time scale of 20 hours (Figure 3a). Our data show that after replating N1E-115 differentiated cells on a laminin substrate, two highly stereotypic phases with specific cell migration and neurite outgrowth behavior are observed. Similar behavior has been described for primary hippocampal neurons, before axonal and dendrite specification occurs (da Silva and Dotti 2002), which is not happening in our neuronal-like cell system. However, such a dynamic behavior has never been formally quantified. For the 10% population of cells with longest neurites, we observe a first phase that lasts about 7 hours, that is characterized by extension of multiple, highly unstable and branched neurites, and a low motile state. In the second stage, for the remaining 13 hours, two neurites get stabilized and extend processively, and a highly motile state is acquired. This might recapitulate neuronal cell migration events observed in vivo (Nadarajah and Parnavelas 2002). Remarkably, the cell population that does not extend robust neurites (Figure 3b) also follows the same stereotypic behavior with regard to the number of neurites, neurite branching and cell motility. This suggests the existence of finely tuned signaling programs as neurite outgrowth proceeds.

We performed an identical analysis for *MKK7* KD cells (Figures 3c-d). MKK7 is part of a Jun kinase (JNK) signaling module that leads to MAP1b phosphorylation and activation, inducing microtubule bundling necessary for robust neurite outgrowth (Feltrin and Pertz 2012). Consistently, loss of robust neurite outgrowth can be well appreciated in phase 2 (Figure 3d). However, our analysis also reveals a burst of outgrowth of branched neurites in phase 1, which had eluded our previous visual inspection of the timelapse movies. This suggests a second role for MKK7 in the regulation of neurite outgrowth during phase 1, and might be consistent with the fact that the MKK7-JNK signaling module regulates additional substrates than MAP1b (Horesh et al. 1999). These results illustrate the benefit

of analyzing such morphodynamic phenotypes. However, we found that this approach requires large timelapse datasets to extract statistically significant information, and therefore is not accessible for our larger siRNA screen.

We then used our pipeline to analyze a candidate Rho GTPase interactome, identified using a combination of proteomic (Pertz et al. 2008) and bioinformatic approaches (Supplementary Figure 4 and Note S4). Most of the different Rho GTPase network components we identified are enriched in the neurite of N1E-115 cells, suggesting that they are involved in the neurite outgrowth process. Consistently, every perturbation in the screen led to a quantifiable phenotype. This illustrates the power of combining a priori knowledge with such phenotypic screens. Our work describes specific proteins that regulate the different MPs relevant to neurite outgrowth in our model system, and unveils an unexpected complexity in the regulation of neurite outgrowth. This opens the possibility to test some of these candidates in more physiologically relevant model systems, that exhibit features such as axonal specification, or complex dendritic arborescences, which are characterized by long unbranched, or highly branched processes respectively. Furthermore, the discovery of a large number of genes of which the perturbation leads to increased neurite outgrowth, provides novel leads for therapeutic intervention in pathologies such as spinal cord regeneration. One important feature that emerges from our global analysis of the comprehensive Rho GTPase network is that this signaling machinery regulates both neurite outgrowth as well as cell migration. Only in very few cases did a perturbation lead to a neurite outgrowth phenotype without affecting cell migration. This does not result from interdependence between the neurite outgrowth and cell migration processes, as perturbation that lead to an identical neurite outgrowth phenotype can lead to distinct cell migration phenotypes, and vice versa. This clearly suggests the existence of defined Rho GTPase signaling network regulating both processes, which is not surprising given the analogy between the cytoskeletal and adhesion dynamics that enable propulsion of a leading edge or a neuronal growth cone (da Silva and Dotti 2002). Another emergent feature is that specification of the neurite number is closely related to cell spreading. In Figure 4, cluster 10 clearly shows an intimate relation between soma spreading, nucleus size (which most likely directly depends on spreading) and number of neurites features correlate together. This will require further work to understand.

Our initial hypothesis was that computation of exhaustive multiparametric MDSs, and the identification of gene perturbations that lead to identical MDSs, would provide hints to

specific spatio-temporal signaling networks that regulate distinct MPs. While our screen allowed us to postulate some possible functional interactions, the relatively restricted phenotypic space we observe (24 phenoclusters for 220 genes) make this a difficult challenge. One can therefore question how much our dataset is explanatory to understand how Rho GTPase signaling networks are wired in time and space? One important hint comes from understanding the spatio-temporal regulation of RhoA activity during N1E-115 neurite outgrowth. Studies with a fluorescent biosensor reporting on RhoA activity (Fritz et al. 2013), clearly describes two distinct Rho GTPase activity pools associated with growth cone advance and collapse. During growth cone advance, RhoA is activated at the tip of f-actin bundles in filopodia, where it might lead to polymerisation of linear actin filaments through its effector mDia (Li and Higgs 2003). During collapse, RhoA is globally activated throughout the growth cone, where it might activate ROCK to induce myosin contractility (Hirose et al. 1998). We observe that both loss of function of RhoA (cluster 12) and ROCK2 (cluster 18) lead to long unbranched neurites with decreased frequency in expansion, indicative of loss of growth cone collapse. Thus both a functional readout about RhoA activity, as well as a perturbation approach, are consistent in predicting a role for RhoA and its effector ROCK2 in growth cone collapse. Importantly, loss of function of PDZ-RhoGEF (Oleksy et al. 2006) (ARHGEF11, cluster 16) phenocopies RhoA and ROCK2 KD phenotypes, suggesting that this could be the GEF that specifically regulates growth cone collapse. Loss of function of p190 RhoGAP (Arthur and Burridge 2001) (ARHGAP5, cluster 8) leads to short, unstable neurites, indicative of increased collapse event. This suggests that p190 RhoGAP negatively regulates the specific RhoA pool that controls growth collapse. These potential interactions now will require validation with various assays including biosensor Rho GTPase activity measurements. However, loss of function of mDia1, the RhoA effector that might be relevant for filopodium regulation during growth cone advance leads to long and branched neurites (DIAPH1, cluster 19). These results suggest that the loss of collapse in RhoA KD cells as well as the RhoA regulation at the filopodium are both important in the regulation of neurite outgrowth. Understanding the potential function of mDia1 loss of function phenotype will require high resolution analysis of the growth cone morphology and morphodynamics, which is not accessible with our technology. This illustrates the limits of our approach, and emphasizes that a correct understanding of Rho GTPase signaling will requires analysis at multiple time and length scales.

Nonetheless, many novel and potentially interesting interactions are suggested by our screen. For instance, the loss of function of the receptor plexin b1 (PLXNB1, cluster 22) shows a long and branched phenotype. In primary hippocampal neurons, the regulation of PDZ-RhoGEF by receptor plexin b1 leads to RhoA activation upon semaphorin 4D stimulation (Swiercz et al. 2002). This activation of RhoA leads to myosin light chain phosphorylation via ROCK, and induces growth cone retraction and collapse. Our results suggest that the plexin b1 receptor also works in a ligand autonomous manner to regulate growth cone collapse via RhoA activation. The finding that loss of function of the plexin b1 receptor leads to a more penetrant phenotype than RhoA loss of function (e.g. long branched versus long unbranched phenotype) might be explained by the ability of the plexin b1 receptor to both negatively regulate RhoA and Rac1 (Swiercz et al. 2002).

Classical steady state studies have proposed that Cdc42 and Rac1 promote neurite protrusion (Sarner et al. 2000; Aoki et al. 2004). However, the results of our screen show that loss of function of Cdc42 (cluster 12), results in long unbranched neurites which surprisingly phenocopies RhoA KD. We therefore speculate that Cdc42 also might regulate growth cone contractility responses. This is suggested by the finding that loss of function of MRCK (Leung et al. 1998) (Cdc42BPB, cluster12), a Cdc42 effector involved in the regulation of actomyosin contractility phenocopies the Cdc42 KD phenotype. Future studies will be necessary to understand the possible requirement of RhoA and Cdc42 in regulation of growth cone collapse.

Consistently with previous results (Sarner et al. 2000; Aoki et al. 2004), Rac1 loss of function leads to short, unstable neurites (cluster 1). Rac1 is thought to control growth cone protrusion by promoting actin polymerisation via the effector Wave2 (Machesky et al. 1999), which controls the Arp2/3 complex. We observed that KD of Wave2 (WASF2, cluster 5) and Wave3 (WASF3, cluster 1), as well as several members of the WAVE complex (Bradley and Koleske 2009), such as CYFIP1 (cluster 3), CYFIP2 (cluster1), Nck1 (cluster 8) and Abi2 (cluster 1) phenocopy the Rac1 KD short neurite phenotype, confirming the crucial role of this protein in the regulation of actin dynamics during neurite outgrowth. Surprisingly, loss of function of several Rac1 GEFs, such as β-Pix (ARHGEF7), Trio and Dock7 (all in cluster 1), recapitulates the Rac1 phenotype. The significance of this redundancy in GEFs that regulate Rac1 will require further experiments which provide a higher spatio-temporal resolution.

Beside the putative spatio-temporal signaling modules that our multi-parametric high content screen uncovered, it is also important to highlight that our work represents a great

resource that can be used by the scientific community, to evaluate the potential function of the Rho GTPase interactome in different processes such as cell migration or neurite outgrowth. To our knowledge, this is the first report that provides insight about the complexity of spatio-temporal Rho GTPase signaling. This provides a starting point to dissect these complex signaling networks, which will require a panel of multi-scale approaches, including the visualization of spatio-temporal Rho GTPase activation profiles using fluorescent biosensors in native and perturbed states.

3.5 Experimental procedures

DNA constructions

For simultaneous expression of Lifeact-GFP and NLS-mCheery, we created a bicistronic expression vector consisting of Lifeact-GFP, an IRES sequence (derived from a pIRES vector [Clontech]), and NLS-mCherry. This construct was built using InFusion technology (Clontech), and was cloned in a pcDNA3.1(+) eukaryotic expression vector (Invitrogen).

Cell Culture and Transfection

N1E-115 neuroblastoma cells (American Tissue Culture Collection) were cultured in Dulbecco's modified Eagle's medium (DMEM) supplemented with 10% FBS, 1% L-glutamine, and 1% penicillin/streptomycin. For differentiation, N1E-115 cells were starved for 24 h in serum-free Neurobasal medium (Invitrogen) supplemented with 1% L-glutamine and 1% penicillin/streptomycin. For the double siRNA-mediated KD and plasmid transfection, cells were transfected as previously described (Chong et al, 2006), using 400 ng of the plasmid pcDNA-Lifeact-GFP-IRES-NLS-mCherry and 20 pmol of Stealth Select siRNAs (Invitrogen). 1 µl of Transfectin (Bio-Rad) was used as transfection reagent. 48 h post-transfection cells were starved in Neurobasal medium. 72 h post-transfection, cells were detached with PUCK's saline and replated on a glass-bottom 24 multi-well plates (MatTek) coated with 10 µg/ml laminin (Millipore-Chemicon). About 3 hours post-seeding, cells were immediately used for timelapse imaging.

Microscopy, Image Acquisition and Analysis

All the experiments were performed on an inverted Eclipse Ti microscope (Nikon) controlled by Metamorph software (Universal Imaging). Laser-based autofocus, a CFI Plan Apo Lambda 10X (NA 0.45) (Nikon) objective and a CoolSnap HQ2 camera (Roper Scientific) were used throughout the experiments. For live cell imaging experiments, rapid switching between the GFP and mCherry channels was performed using two independent LED lamps with excitation at 470 and 585 nm (Cool LED) with a multibandpass EGFP/mCherry filter cube (Chroma technology Corporation).

For measurements of neurite outgrowth at steady state, differentiated, siRNA-transfected cells were replated on 18 mm glass coverslips coated with 10 µg/ml laminin. 24 hours after plating, the cells were fixed and stained with DAPI and an anti-α-tubulin antibody, as

mentioned elsewhere (Feltrin and Pertz 2012). DAPI and tubulin images were acquired in 5x5 matrix of fields of view. The images were then analyzed using the neurite outgrowth Metamorph (Universal Imaging) plugin. For timelapse, live cell imaging of neurite outgrowth dynamics in cells expressing Lifeact-GFP and NLS-mCherry, 25.000 transfected N1E-115 cells were replated on glass-bottom, 24-well plate (MatTek) coated with 10 µg/ml laminin. 4 hours after plating, 10 selected fields of view per well were imaged in Neurobasal medium (Invitrogen) in a heated closed chamber using a CFI Plan Apo Lambda 10X (NA 0.45) objective (Nikon). Selection of adequate fields of view was performed using Metamorph software. For that purpose, the GFP channel was acquired in a 7x7 matrix of fields of view for each of the 24 wells. A macro was then used post-acquisition to select 10 fields of view containing an adequate number of cells exhibiting a specific range in fluorescence intensities and cell areas. This ensured that each field of view displays a similar number of cells and fluorescence intensities, and excludes fields of view with cellular debris. The selected fields of view were automatically translated in a stage position list, which was used for the timelapse experiment. This resulted in acquisition of 240 fields of view in GFP and mCherry channels throughout the 24-well plate every 12 minutes for a total of 19.6 hours.

3.6 Acknowledgements

3.7 Main Figures
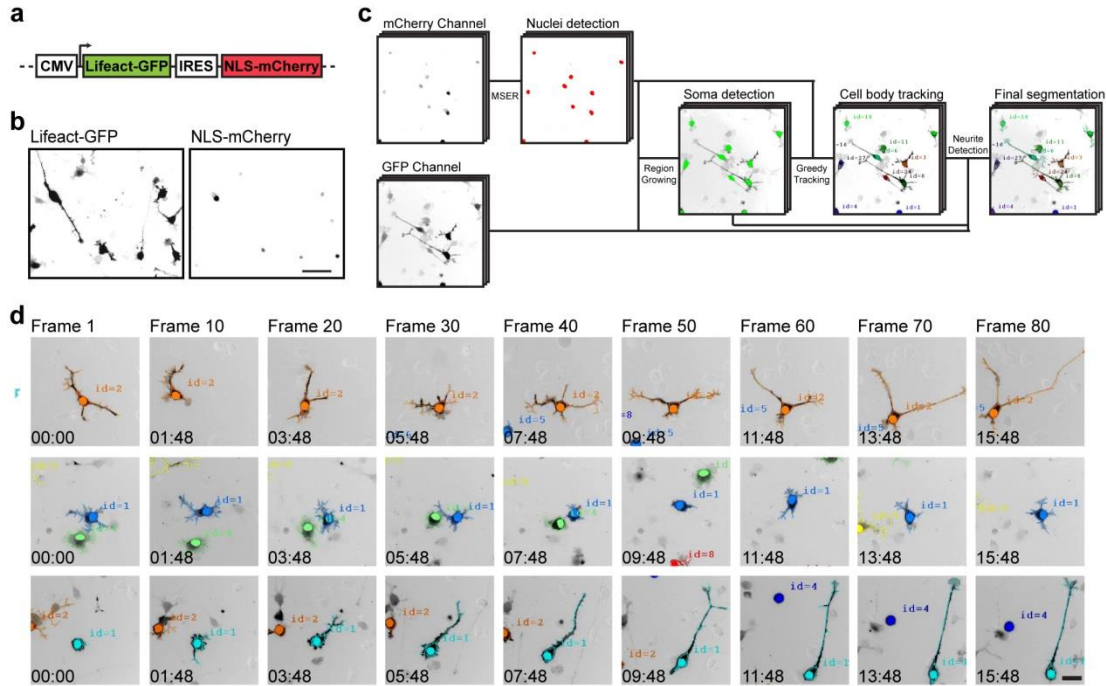
Figure 1. High content imaging of neurite outgrowth dynamics.

(**a**) Structure of fluorescent reporter to monitor neuronal morphology.

(**b**) Representative images of Lifeact-GFP and NLS-mCherry signals. Scale bar: 50 µm.

(**c**) Computer vision pipeline for segmentation of neurite and soma morphodynamics.

(**d**) Representative segmentation of three fields of view in one timelapse movie. Cells with a specific identity label are color-coded. A filled circle identifies cell nucleus, and filament defines soma contour and neurite segmentation. Time scale: hours/minutes. Scale bar: 50 µm.
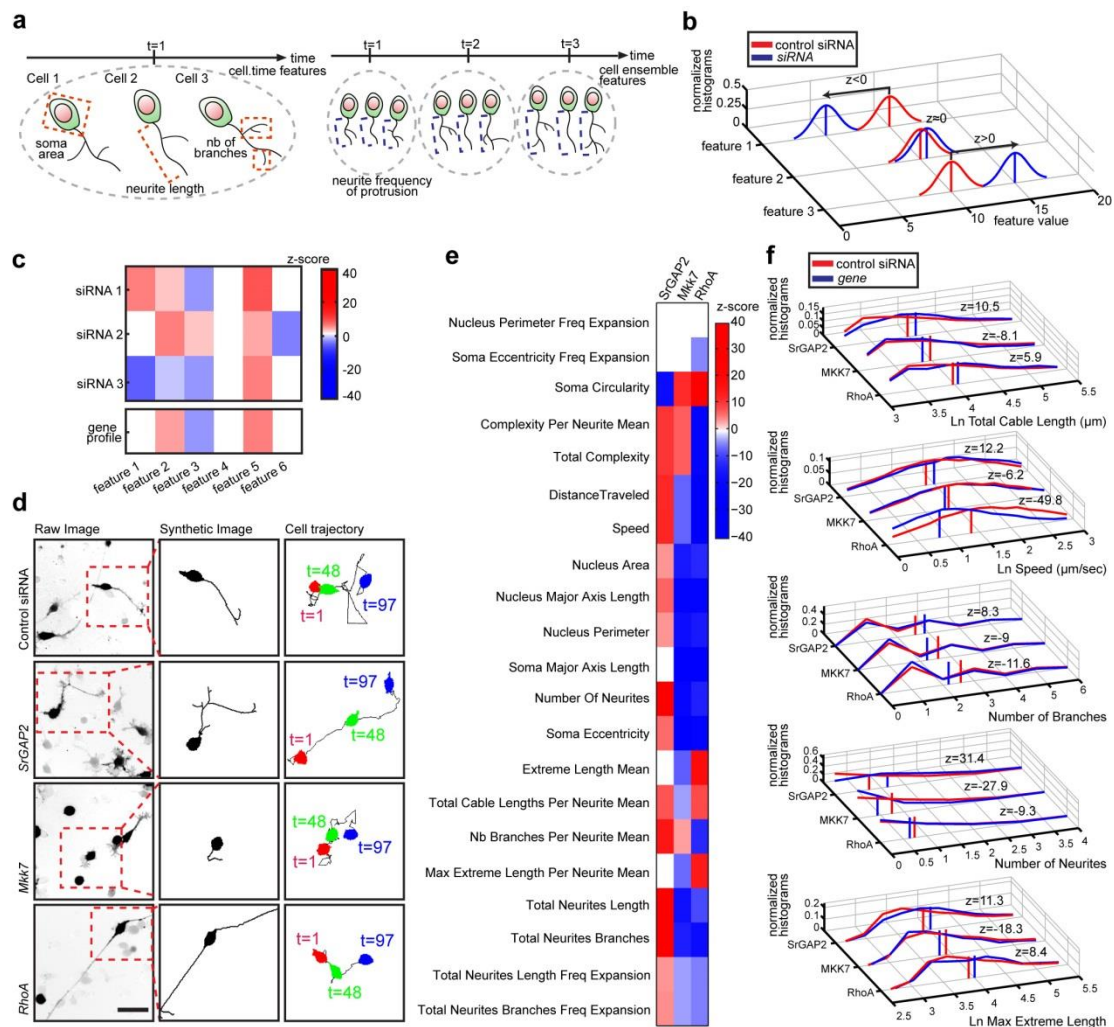
Figure 2. Morphodynamic signature extraction.
(**a**) Schematics of 2 distinct level of feature analysis. Cell.time and cell.ensemble features are considered. (**b**) Feature extraction procedure. Z-score vector defines statistical significance, penetrance and polarity of measured feature distributions of control compared to siRNA-treated cells. (**c**) Deconvolution of RNAi OFF-target effects. For each given feature: i) if the 3 siRNA perturbations lead to a z-score with identical polarity, the average Z-score is computed; ii) if 2 or 3 out of 3 siRNA perturbations lead to a z-score with identical polarity, the average z-score for the 2 features with the same polarity is computed; iii) if the 3 siRNA perturbations yield 3 different z-score polarities, then the z feature score is set to 0. (**d**) Raw image (left panel, inverted black and white contrast), synthetic image (middle panel) and cell migration tracks (right panel) for *SrGAP2*, *MKK7* and *RhoA* siRNA perturbations are shown. (**e**) Gene-associated MDSs represented by a color maps. Z-scores have been arbitrarily scaled. Scale bar: 50 µm. (**f**) Normalized histograms of representative feature distribution profiles. Vertical bars represent the mean. Z-score associated to each feature is also shown.
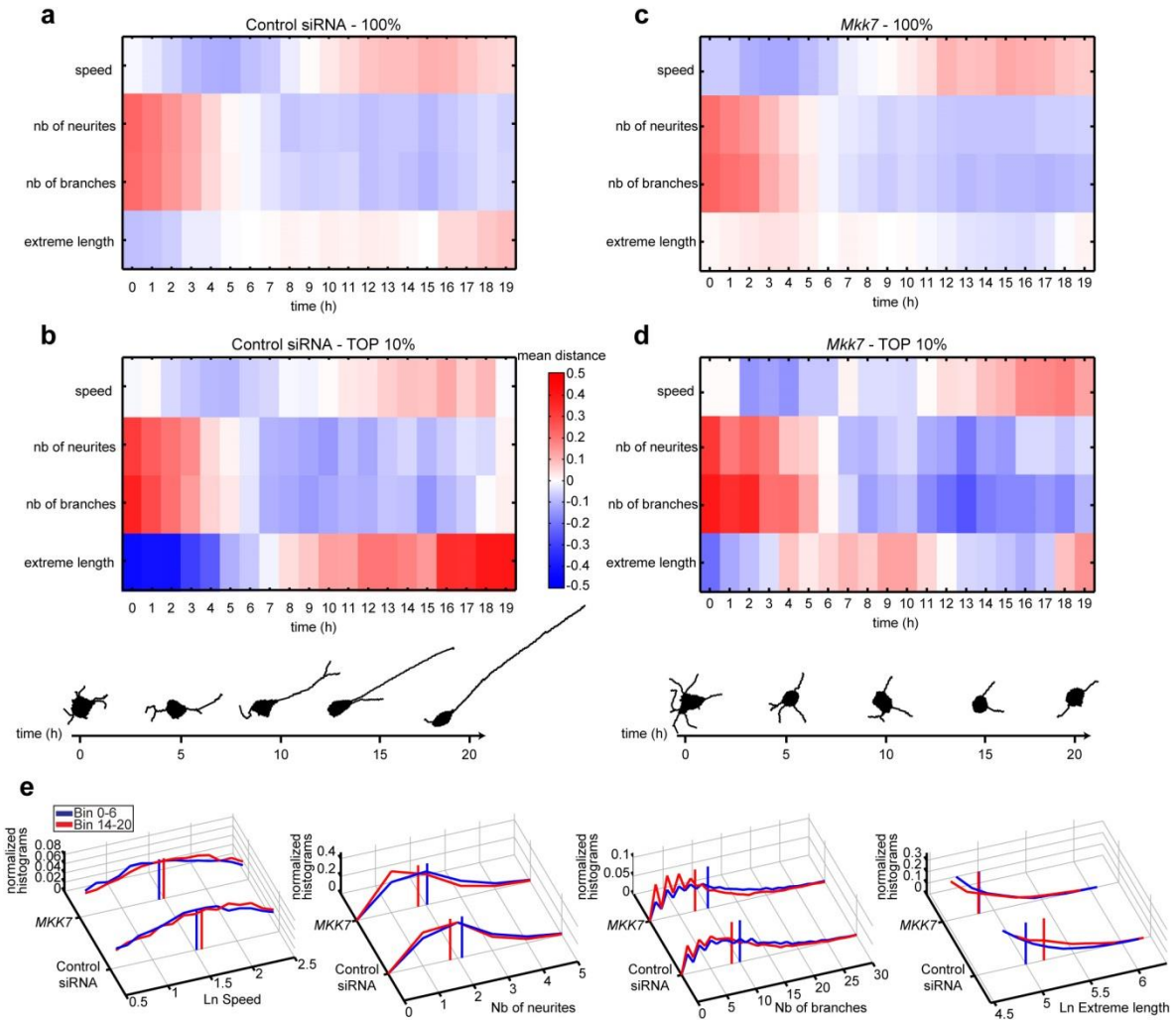
Figure 3. Temporal analysis of neuronal dynamics in control and *MKK7* KD cells.

(**a-d**) Control and *MKK7* KD timelapse sequences from multiple experimental plates were divided in 19 1-hour bins. Coefficient of variation of selected features for each temporal bin for control (**a,b**) and MKK7 KD (**c,d**) cells. Measurements for the whole cell population (**a,c**), and the 10 % cells with highest neurite extreme length (**b,d**). Representative cells from the 10 percentile at the 1, 5, 10, 15, 20 hours timepoints (**b,d**). (**e**) Feature distributions at the 1 and 20 hour timepoints. Vertical bars display distribution averages.

68
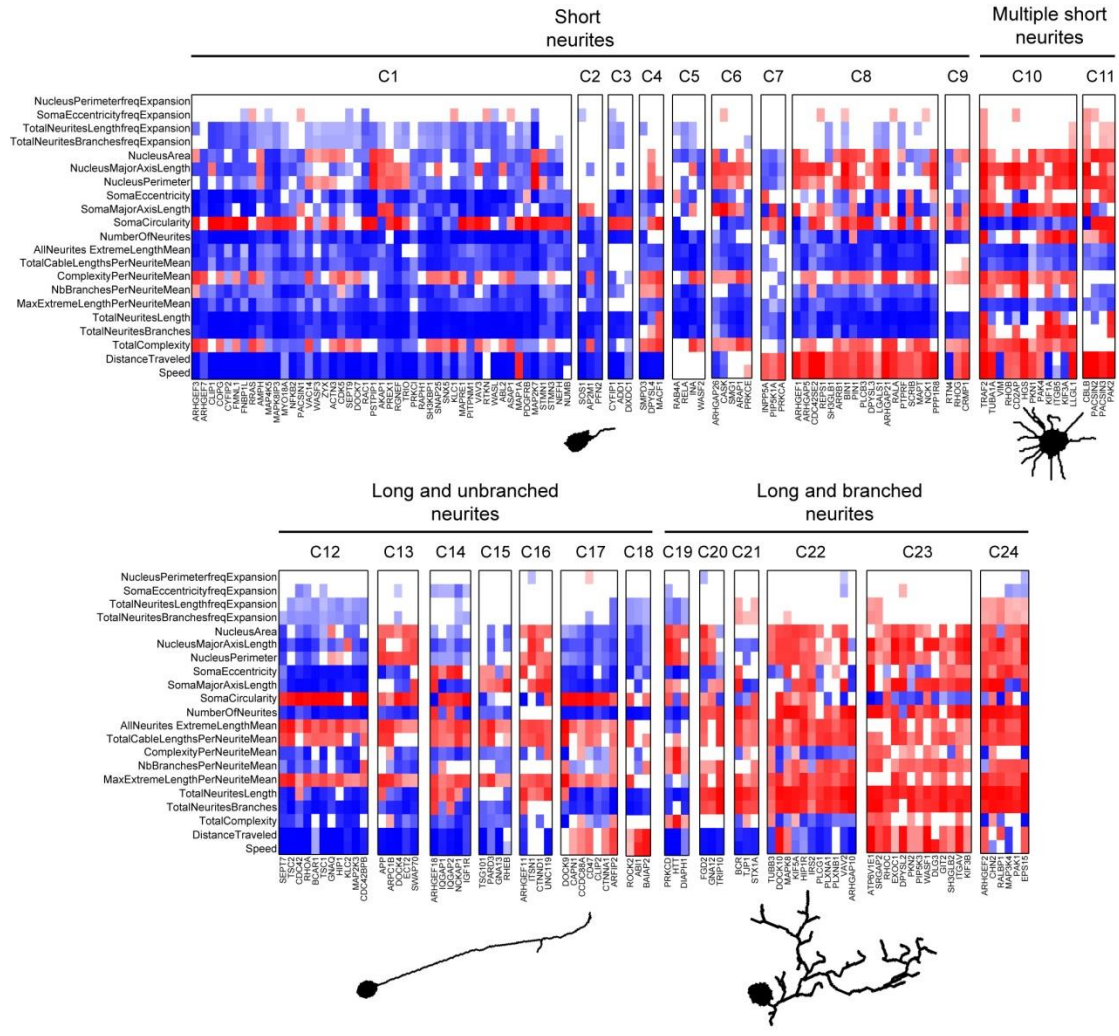
Figure 4. Hierarchical clustering identifies MDS phenoclusters.
Color map of hierarchical clustering of MDSs. A morphodynamic profile index of 65 % was used. Representative images of major different phenotype classes, comprising multiple clusters. Each line represents a specific class for a phenotype that can be understood at steady state.

3.8 References

Aoki K, Nakamura T, Matsuda M. 2004. Spatio-temporal regulation of Rac1 and Cdc42 activity during nerve growth factor-induced neurite outgrowth in PC12 cells. *The Journal of biological chemistry* **279**: 713-719.

Arthur WT, Burridge K. 2001. RhoA inactivation by p190RhoGAP regulates cell spreading and migration by promoting membrane protrusion and polarity. *Molecular biology of the cell* **12**: 2711-2720.

Bradley WD, Koleske AJ. 2009. Regulation of cell migration and morphogenesis by Abl-family kinases: emerging mechanisms and physiological contexts. *Journal of cell science* **122**: 3441-3454.

Chong KW, Lee AY, Koay ES, Seet SJ, Cheung NS. 2006. pH dependent high transfection efficiency of mouse neuroblastomas using TransFectin. *Journal of neuroscience methods* **158**: 56-63.

da Silva JS, Dotti CG. 2002. Breaking the neuronal sphere: regulation of the actin cytoskeleton in neuritogenesis. *Nature reviews Neuroscience* **3**: 694-704.

Echeverri CJ, Beachy PA, Baum B, Boutros M, Buchholz F, Chanda SK, Downward J, Ellenberg J, Fraser AG, Hacohen N et al. 2006. Minimizing the risk of reporting false positives in large-scale RNAi screens. *Nat Methods* **3**: 777-779.

Etienne-Manneville S, Hall A. 2002. Rho GTPases in cell biology. *Nature* **420**: 629-635.

Feltrin D, Fusco L, Witte H, Moretti F, Martin K, Letzelter M, Fluri E, Scheiffele P, Pertz O. 2012. Growth cone MKK7 mRNA targeting regulates MAP1b-dependent microtubule bundling to control neurite elongation. *PLoS biology* **10**: e1001439.

Feltrin D, Pertz O. 2012. Assessment of Rho GTPase signaling during neurite outgrowth. *Methods in molecular biology* **827**: 181-194.

Fritz RD, Letzelter M, Reimann A, Martin K, Fusco L, Ritsma L, Ponsioen B, Fluri E, Schulte-Merker S, van Rheenen J et al. 2013. A versatile toolkit to produce sensitive FRET biosensors to visualize signaling in time and space. *Science signaling* **6**: rs12.

Hirose M, Ishizaki T, Watanabe N, Uehata M, Kranenburg O, Moolenaar WH, Matsumura F, Maekawa M, Bito H, Narumiya S. 1998. Molecular dissection of the Rho-associated protein kinase (p160ROCK)-regulated neurite remodeling in neuroblastoma N1E-115 cells. *The Journal of cell biology* **141**: 1625-1636.

Horesh D, Sapir T, Francis F, Wolf SG, Caspi M, Elbaum M, Chelly J, Reiner O. 1999. Doublecortin, a stabilizer of microtubules. *Human molecular genetics* **8**: 1599-1610.

Leung T, Chen XQ, Tan I, Manser E, Lim L. 1998. Myotonic dystrophy kinase-related Cdc42-binding kinase acts as a Cdc42 effector in promoting cytoskeletal reorganization. *Molecular and cellular biology* **18**: 130-140.

Li F, Higgs HN. 2003. The mouse Formin mDia1 is a potent actin nucleation factor regulated by autoinhibition. *Current biology : CB* **13**: 1335-1340.

Machacek M, Hodgson L, Welch C, Elliott H, Pertz O, Nalbant P, Abell A, Johnson GL, Hahn KM, Danuser G. 2009. Coordination of Rho GTPase activities during cell protrusion. *Nature* **461**: 99-103.

Machesky LM, Mullins RD, Higgs HN, Kaiser DA, Blanchoin L, May RC, Hall ME, Pollard TD. 1999. Scar, a WASp-related protein, activates nucleation of actin filaments by the Arp2/3 complex. *Proceedings of the National Academy of Sciences of the United States of America* **96**: 3739-3744.

Nadarajah B, Parnavelas JG. 2002. Modes of neuronal migration in the developing cerebral cortex. *Nature reviews Neuroscience* **3**: 423-432.

Oleksy A, Opalinski L, Derewenda U, Derewenda ZS, Otlewski J. 2006. The molecular basis of RhoA specificity in the guanine nucleotide exchange factor PDZ-RhoGEF. *The Journal of biological chemistry* **281**: 32891-32897.

Pertz O. 2010. Spatio-temporal Rho GTPase signaling - where are we now? *Journal of cell science* **123**: 1841-1850.

Pertz OC, Wang Y, Yang F, Wang W, Gay LJ, Gristenko MA, Clauss TR, Anderson DJ, Liu T, Auberry KJ et al. 2008. Spatial mapping of the neurite and soma proteomes reveals a functional Cdc42/Rac regulatory network. *Proceedings of the National Academy of Sciences of the United States of America* **105**: 1931-1936.

Riedl J, Crevenna AH, Kessenbrock K, Yu JH, Neukirchen D, Bista M, Bradke F, Jenne D, Holak TA, Werb Z et al. 2008. Lifeact: a versatile marker to visualize F-actin. *Nat Methods* **5**: 605-607.

Sarner S, Kozma R, Ahmed S, Lim L. 2000. Phosphatidylinositol 3-kinase, Cdc42, and Rac1 act downstream of Ras in integrin-dependent neurite outgrowth in N1E-115 neuroblastoma cells. *Molecular and cellular biology* **20**: 158-172.

Swiercz JM, Kuner R, Behrens J, Offermanns S. 2002. Plexin-B1 directly interacts with PDZ-RhoGEF/LARG to regulate RhoA and growth cone morphology. *Neuron* **35**: 51-63.

3.9 Supplementary Information

3.9.1 Supplementary Figures
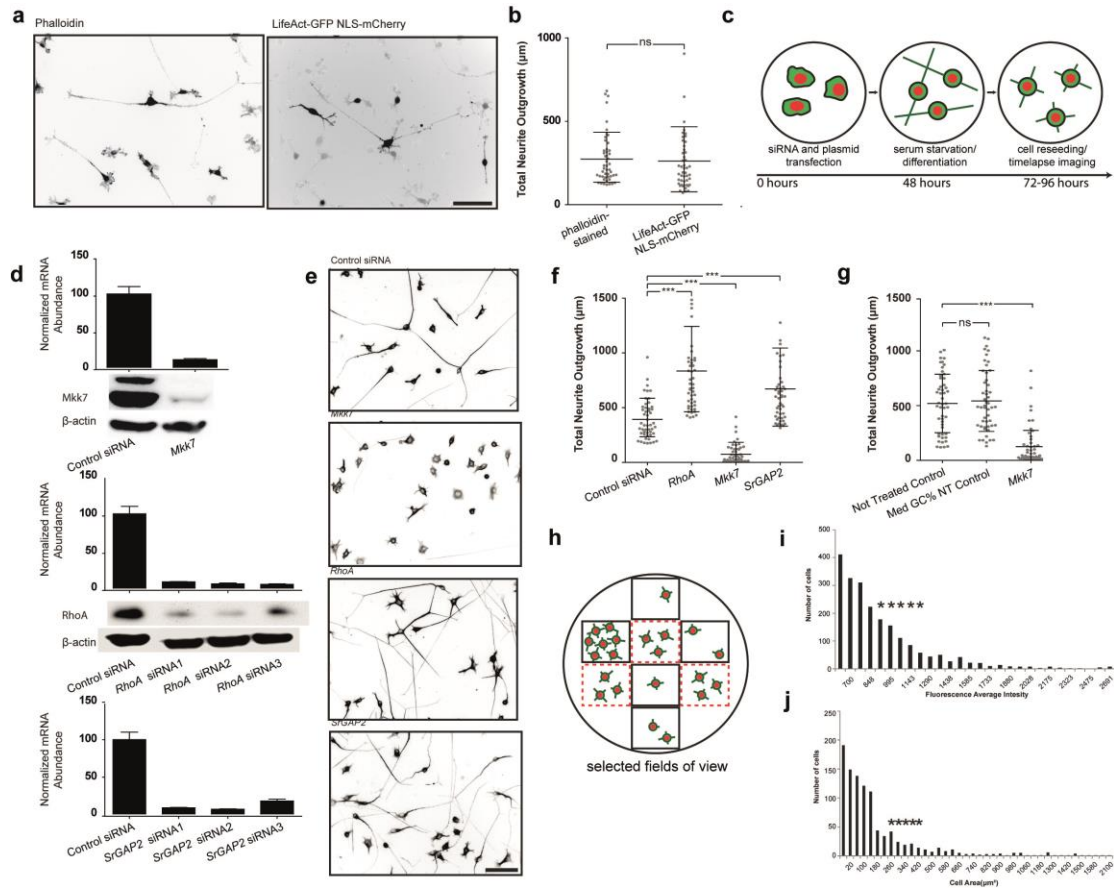
Supplementary Figure 1. High content imaging and RNAi pipeline.

(**a**,**b**) Expression of Lifeact-GFP/NLS-mCherry does not affect neurite outgrowth. Naive or Lifeact-GFP/NLS-mCherry-transfected N1E-115 cells were allowed to differentiate for 24 hours and fixed. Naive cells were stained with phalloidin and DAPI. Metamorph neurite outgrowth plugin was used to quantitate total neurite outgrowth. **(a)** Representative images of phalloidin-stained, and Lifeact-GFP/NLS-mCherry-transfected cell in inverted black and white contrast (ibw contrast). Scale bar: 100 μm. **(b)** Neurite outgrowth analysis of phalloidin-stained, and Lifeact-GFP/NLS-mCherry-transfected cells.

(**c**) Workflow of siRNA and Lifeact-GFP/NLS-mCherry transfection, differentiation, and high content live imaging.

(**d**) KD efficiency in cells transfected with *Mkk7*, *RhoA* and *srGAP2* targeting siRNAs. Quantitative reverse transcriptase - polymerase chain reaction or western blot analysis were used to measure mRNA or protein abundance in control and transfected cells.

(**e**,**f**) Neurite outgrowth phenotypes of control and *Mkk7*, *RhoA* and *srGAP2* KD cells. (**e**) Representative images of tubulin-stained, siRNA-transfected cells (ibw contrast). Scale bar: 100 µm. (**f**) Cells were allowed to differentiate, fixed and stained using anti-α-tubulin antibodies.

(**g**) Total neurite outgrowth of negative siRNA controls and positive *Mkk7* control measurements using Metamorph neurite outgrowth plugin.

(**h-j**) Criteria for selection of fields of view within one well with N1E-115 cells displaying appropriate characteristics for imaging. (**h**) Schematics of well selection with appropriate cell numbers (Lifeact-GFP signal color-coded in green, NLS-mCherry signal color-coded in red). Selected fields of view are indicated by dotted squares. (**i**) Histogram of fluorescence intensities of differentiated N1E-115 cells at the onset of a timelapse microscopy experiment. Asterisks indicate fluorescence ranges used cell selection. (**j**) Histogram of somata surfaces of differentiated N1E-115 cells at the onset of a timelapse microscopy experiment. Asterisks indicate fluorescence ranges used for cell selection. This insures exclusion of fields of view with cellular debris.
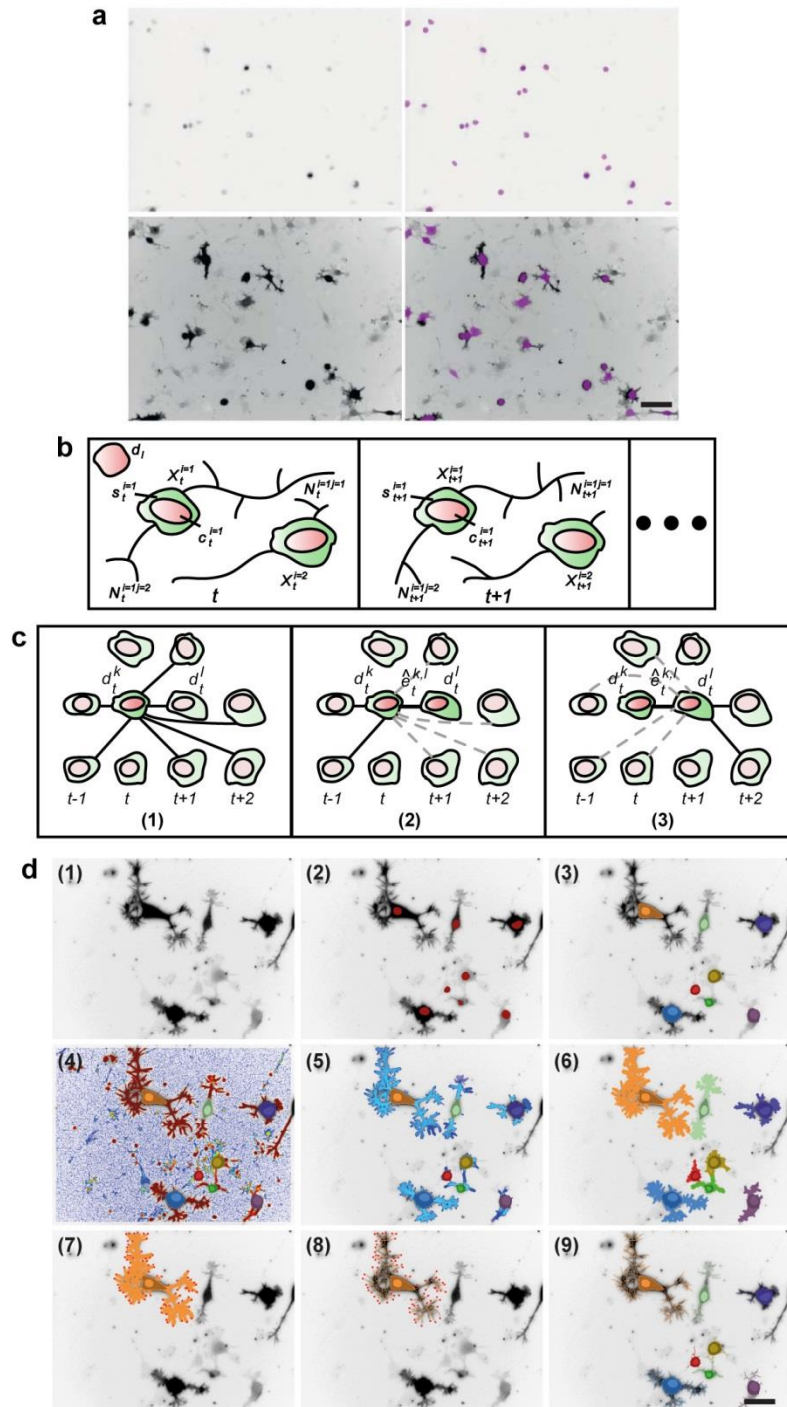
Supplementary Figure 2. Computer vision pipeline for neuronal dynamics.

(**a**) Cell body detection. On the first row, nuclei detections overlaid on top of the NLS-mCherry channel. On the second row, somata detections overlaid on top of the Lifeact-GFP channel. From left to right: the original images, and the automatic detections. Scale bar: 100 μm. (**b**) Neuron tracking notation. At time t a neuron i detection $X^i = \{c_t^i, s_t^i, N_t^i\}$ contains a

nucleus c_t^i, a soma s_t^i, and a set of neurite-filopodia tuples $N_t^i = \{(n_t^{i,1}, F_t^{i,1}), \dots, (n_t^{i,j}, F_t^{i,j}), \dots, (n_t^{i,J}, F_t^{i,J})\}$ which contain J neurites and their associated filopodia shown in red for $j = 1$ and green for $j = 2$. A spurious nucleus detection d_1 is also shown. A neuron i is defined by a time-series of neuron detections $X^i = \{X_a^i, \dots, X_t^i, \dots, X_b^i\}$. The tracking returns a set X^i for each neuron. (**c**) Greedy Tracking. (1) The algorithm begins with each detection fully connected to all future and past detections within a time window W. Above, only d_t^k's edges are shown. (2) Each iteration, the edge $e^{k,l}$ with minimum cost $\hat{w}_e$ is added to $\mathcal{E}'$. Edges connecting d_t^k to future detections are removed from $\mathcal{E}$. (3) Edges connecting d_t^l to the past are removed from $\mathcal{E}$. The process is repeated until $\hat{w}_e > T$. (**d**) Neurite Detection. (1) Illumination correction and normalization are applied to the Lifeact-GFP channel. (2) Nuclei are segmented from the mCherry channel using maximally stable extremal regions. (3) Cell identities are assigned to each nucleus and soma regions are grown using a fast marching algorithm combining euclidean distance from the nucleus and intensity differences. (4) The response of a Hessian-based Frangi tubularity filter is calibrated to reflect the potential that each pixel belongs to a neuron. (5) Cell bodies are extracted by thresholding a geodesic distance based on the potential in (4). (6) Identities are assigned to cell bodies corresponding to the nearest soma according to the geodesic distance. (7) Candidate endpoints for the neurite tree are local maxima of the geodesic distance to the soma. (8) A minimum spanning tree form the soma to each candidate endpoint determines the neurite tree (up to a soft threshold). (9) The process is repeated for each cell, resulting in a set of nuclei, somata, and neurite tree segmentations. Scale bar: 50 μm.
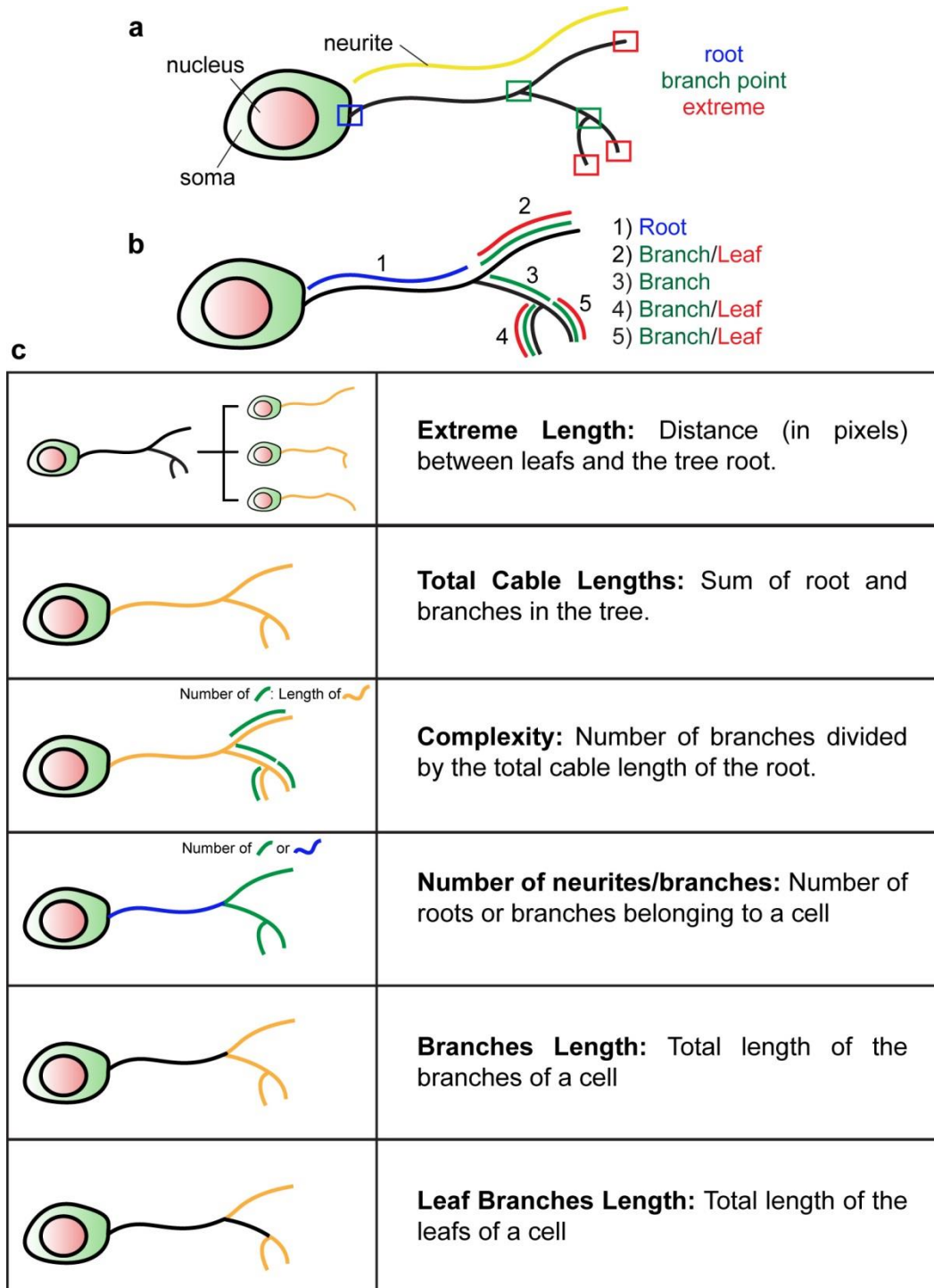
Supplementary Figure 3. Definition of parameters.

(**a**) Schematic of different cell components as described in supplementary note 2.

(**b**) Schematic of a segmented cell. Different colors highlight different segmented components.

(**c**) Representative explanatory pictures of the neurite parameters. Right panels: schematic of features. Left panels: Definition of features.
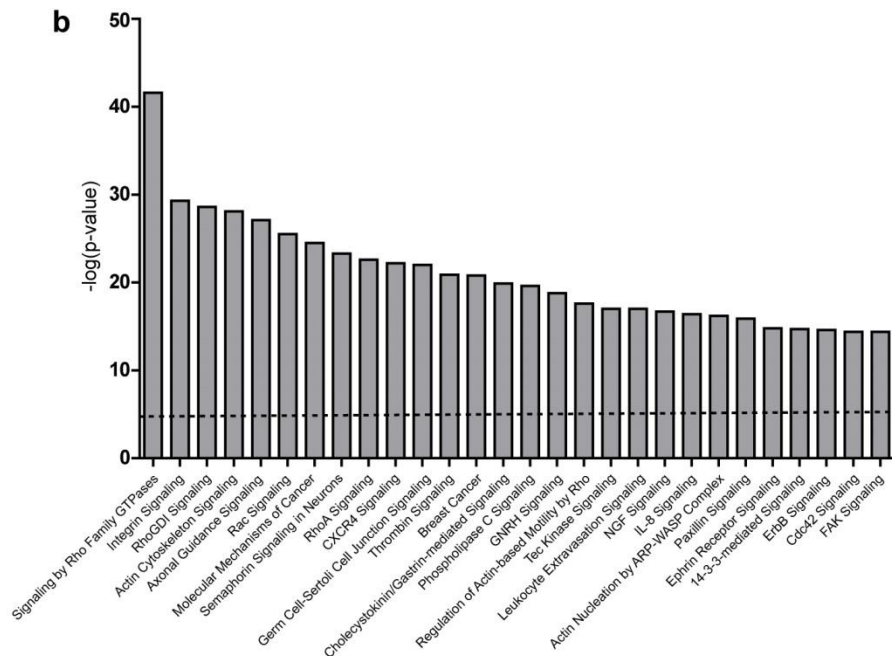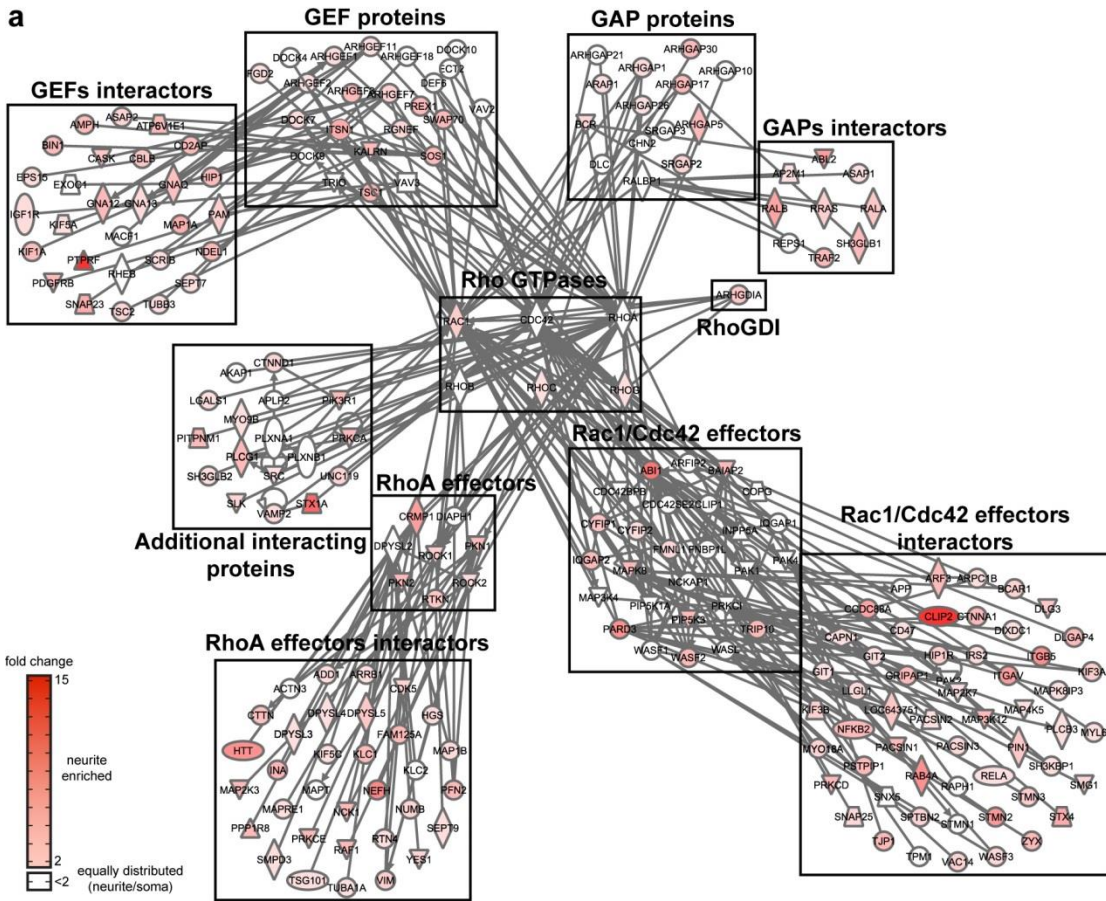
Supplementary Figure. Identification of a potential Rho GTPase signaling network using a proteomics/bioinformatics approach.

(**a**) Potential Rho GTPase signaling network. An extended Rac1, Cdc42, RhoA, RhoB, RhoC, RhoG GTPases interactome is shown. Each line represents a direct protein-protein interaction documented by the Ingenuity Pathway database (http://www.ingenuity.com). Each protein has been detected in N1E-115 cells using a proteomics approach, and is color-coded for neurite/soma fold-enrichment as in the scale provided in the lower left. White color-code indicates proteins that are equally distributed in the neurite and the cell soma. Icon code for different protein functions is shown in the lower right. The specific functions related to Rho GTPase functions are also indicated.

(**b**) Gene ontology analysis of the Rho GTPase signaling network. Green dotted line represents significance threshold as measured by Fishers's test ($P < 0.05$).
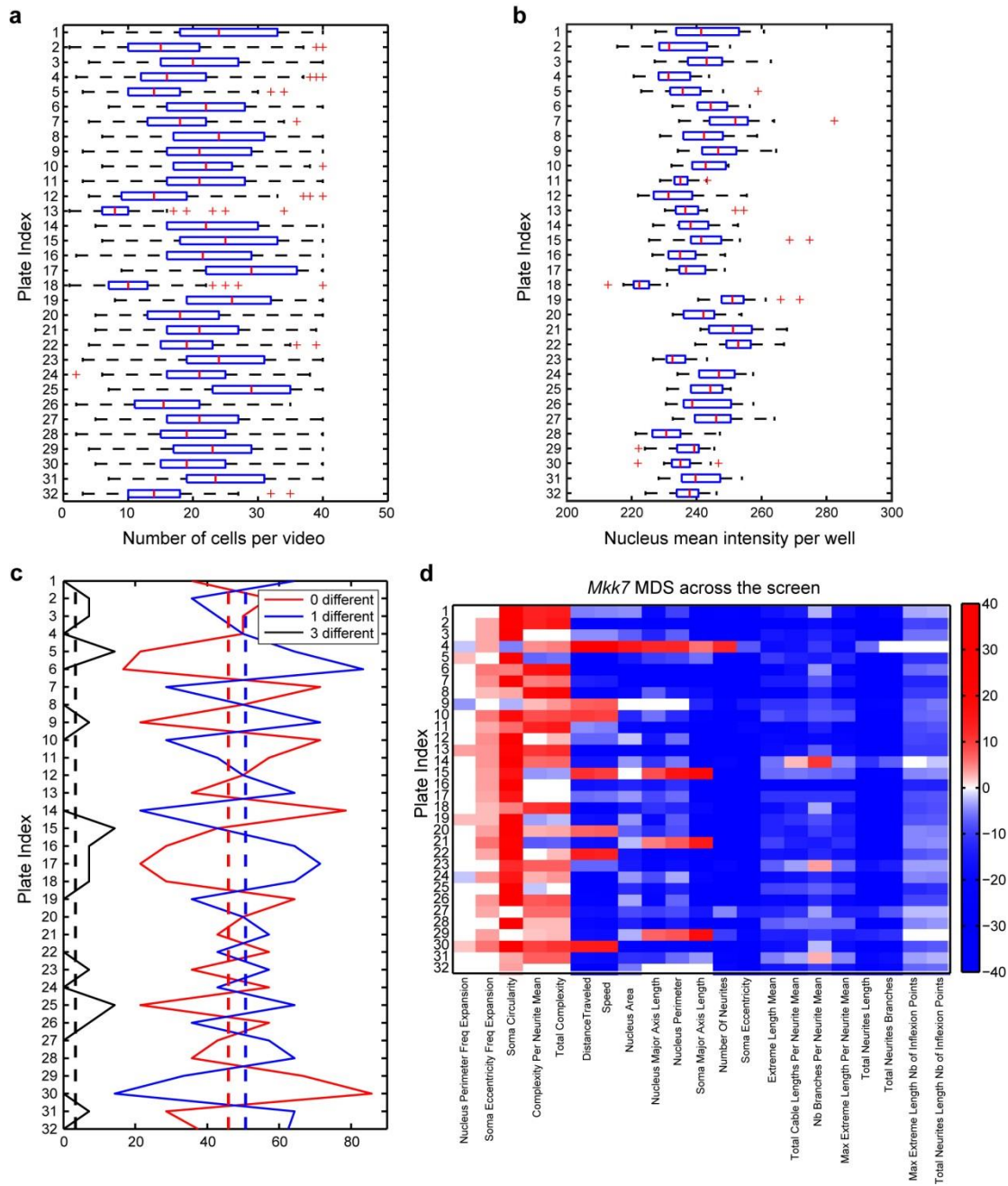
Supplementary Figure 5. Quality control of siRNA screen.

(**a**) Quantification of number of cells per field of view in the different screens. The central red line represents the median, the edges of the box are the 25th and 75th percentiles, the domain is represented in dashed line, and the outliers are plotted individually.

(**b**) Quantification of NLS-mCherry mean fluorescence intensity. The central red line represents the median, the edges of the box are the 25th and 75th percentiles, the domain is represented in dashed line, and the outliers are plotted individually.

(**c**) Per plate off-target effect analysis. For a given feature, there are three possibilities: the three siRNAs generate different phenotypes (black lines), two siRNAs generate the same phenotype but the phenotype of the third siRNA is different (blue lines), or the three siRNAs generate the same phenotype (red lines). For each plate, the proportion of each case is represented by continuous lines. The dashed line represents the average value.

(**d**) MDS of Mkk7 KD cells across 32 independent experiments. Z-score vector maps are shown for each experimental plate. Left bar indicates z-score color code.
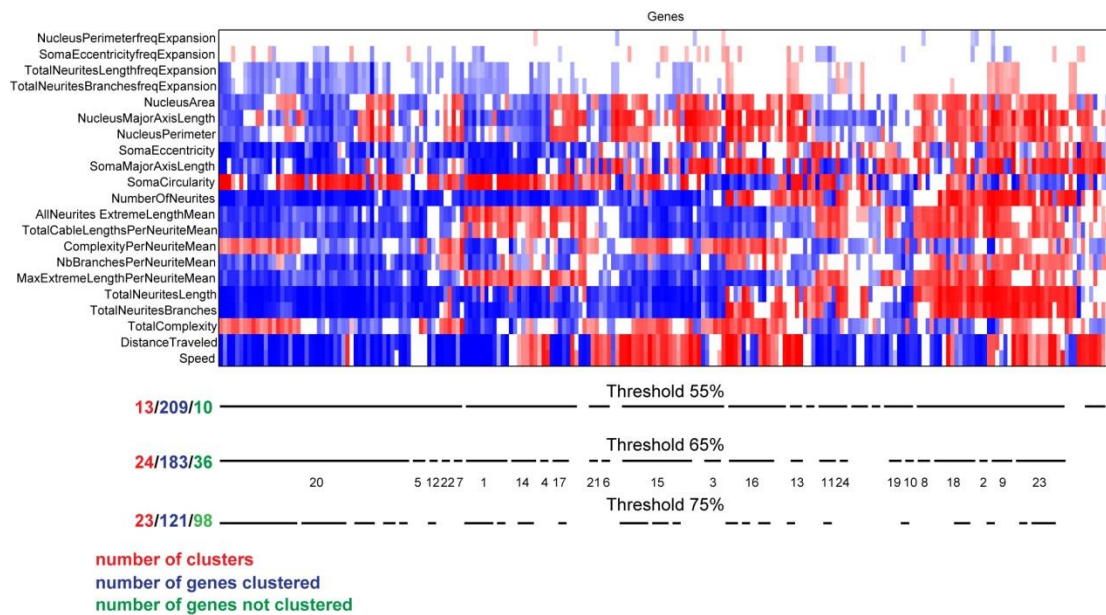
Supplementary Figure. 6. MDS clustering.

Hierarchical clustering of 226 MDSs. MDSs z-scores are color-coded according to scale. Clusters identified with different dendrogram clusters are shown by horizontal black lines. Number of clusters, number of clustered and non-clustered genes are also indicated. For the 65 % threshold, clusters are numbered as in Fig.4a.

3.9.2 Supplementary Note S1. Computer vision analysis of neuronal morphodynamics

We developed an image processing pipeline to segments nuclei, somata and neurites and to track them from Time-Lapse High-Content Screens. In the following, we first describe the data and introduce some notations, then we give a detailed description of our processing pipeline. Finally, we describe our evaluation methodology to assess the quality of the segmentation results.

1. Data description and notations

We worked with sequences of two-channel images, one in which the cytoskeleton is marked with Lifeact-GFP. In the other, the nuclei are marked with NLS- mCherry, (Supplementary Figure 2a). The input to our approach is a series of T images $I = \{I_i, \ldots, I_t, \ldots, I_T\}$ from which we extract K nucleus detections d_T^{k1}. The tracking step described in Sec. 2.2 associates valid detections across time steps while rejecting spurious detections. Since each neuron contains only one nucleus, there is a one-to-one mapping between each valid nucleus detection c_t^i and a neuron X_t^i. Thus, the tracking task is to provide a set of neuron detections $X^i = \{X_a^i, \ldots, X_t^i, \ldots, X_b^i\}$ defining an individual neuron i from time $t = a$ to $t = b$. As depicted in Fig. 1, each neuron detection X_t^i is composed of a nucleus c_t^i, a soma s_t^i, and a set of neurites $N_t^i = \{n_t^{i1}, \ldots, n_t^{ij}, \ldots, n_t^{iJ}\}$. Thus, a complete neuron i at time step t is described by $X^i = \{c_t^i, s_t^i, N_t^i\}$ (Supplementary Figure 2b).

2. Neuron segmentation and tracking

Three stages neuron segmentation and tracking pipeline is proposed. First, as described in section 2.1, we segment nuclei and the associated somata. Since each neuron contains only one nucleus, there is a one-to-one mapping between each valid nucleus and soma, yielding to a neuron cell body. Second, the cell body tracking step described in section 2.2, associates valid cell bodies across time steps while rejecting spurious ones. Finally, using the valid tracked cell bodies, neurites are segmented and tracked over time.

2.1 Nuclei and somata segmentation

The first step in our approach is to extract a set of nucleus detections $\{d^i, \dots, d^k\}$ over the image series. We worked with two-channel images where the cytoskeleton is marked with Lifeact-GFP and nuclei are marked with NLS-mCherry. The nuclei can be reliably detected as a Maximally Stable Extremal Region (MSER) (Matas et al. 2002) of the NLS-mCherry channel, and performing a morphological filling operation. The MSER detector finds regions that are stable over a wide range of thresholds of a gray-scale image. Assuming that the pixels below a given threshold are "black" and all those above or equal are "white"; if we are shown a sequence of thresholded images I_τ with frame τ corresponding to threshold τ, we would see first a white image, then "black" spots corresponding to local intensity minima will appear then grow larger. These "black" spots will eventually merge, until the whole image is black. The set of all connected components in the sequence is the set of all extremal regions. Once the extremal regions are extracted, a maximality criterion is defined and only a few extremal regions are kept, which are the Maximally Stable Extremal Regions.

To extract the Maximally Stable Extremal Regions form the NLS-mCherry channel, we used the VLFeat implementation of MSER. Default parameters of the VLFeat implementation were used to segment the nuclei, except the minimal and maximal size of a nuclei at the given resolution, which were fixed to 70 and 170. The main advantage of MSER compared to the thresholding approach (Gonzalez et al. 2011) is its robustness and insensitivity to contrast change.

Using the nuclei as seed regions, somata are segmented using a region growing and region competition algorithm on the Lifeact-GFP channel, called the green channel. This is done by computing geodesic distances from each nucleus based on the difference of image intensities. For a given image frame I, let $\{d^i, \dots, d^k\}$ be the set of detected nuclei. For each detected nucleus d_k we define a potential as follows:

$$P_k(x) \frac{1}{A\, exp\left(-\frac{(I(x)-\mu_k)^2}{2\beta^2\sigma_k^2}\right)+1} \tag{1}$$

μ^k and σ^k are respectively the mean and standard deviation of the green intensities of the pixels describing d^k. Parameter β, is a multiplicative factor of the intensity standard deviation σ^k, and represents a tolerance of variation between the local foreground (soma) intensities and the local background intensities.

The geodesic distance U_k associated to the nucleus d^k is defined as the solution of the Eikonal equation

$$\left\|\nabla U^k\right\| = P_k \quad \text{such that} \quad U_k\left(d^k\right) = 0 \tag{2}$$

From equation 1, one can see that the more the green intensity of a pixel $I(x)$ is different from the mean intensity μ^k of the detected nuclei, the higher the potential P_k would be, and from equation 2, the higher U_k would be.

The algorithm to compute the geodesic distances U_k, is the Fast Marching algorithm (Cohen et al. 1996; Sethian et al. 1999). Our first approach to segment the somata regions consists on thresholding the geodesic distances $s^k = \{U_k < T_g\}$. However, as this requires computing all the K distances U_k, the complexity depends on the number of detected cells, and may yield to intersecting somata regions (which was happening as well with the region growing approach proposed before [Gonzalez et al. 2011]).

Instead, we used a more efficient approach that computes the geodesic distance from all the detected nuclei simultaneously by launching a region growing and region competition algorithm which complexity does not depend on the number of cells but only on the size of the image, and for which the obtained somata segmentations do not intersect. For that, we define a distance map to all the detected nuclei d^k as:

$$U(x) = \min_{k=1,..,K} U_k(x) \tag{3}$$

The distance map U can be approximated by computing the solution of

$$\|\nabla U\| = P \quad \text{such that} \quad U\left(d^k\right) = 0, \quad \text{for all } k, \tag{4}$$

where

$$P_k(x) \frac{1}{A\,exp\left(-\frac{(I(x)-\mu_k)^2}{2\beta^2\sigma_k^2}\right)+1} \tag{5}$$

and where the index of the closest region k, is decided during the propagation of a variant of the Fast Marching algorithm (Benmansour et al. 2009). The main difference between

84

this variant of the Fast Marching algorithm and the original one (Cohen et al. 1996; Sethian et al. 1999), is that the potential values (more precisely the k index for our case) is not fixed before starting the propagation but is rather decided during the propagation. Computed that way, U defines an approximate geodesic distance to the detections d^k . It combines the local intensity differences and the Euclidean distance. The somata segmentations are finally obtained by thresholding both U and the euclidean distance to the nuclei (those 2 shresholds are denoted T_g and T_e repectivelly). Formally, if $\{R^k\}$ is the Voronoi tessellation associated to U and the set of nuclei $\{d^k\}$ and if the Euclidian distance to the set of nuclei is denoted D then the soma s^k associated to a detection d^k is defined as follows:

$$s^k = R^k \cap \{U < T_g\} \cap \{D < T_e\} \tag{6}$$

Once this intersection is obtained, a morphological filling operation is applied to guarantee that a soma does not contain holes.

An example for nuclei and somata segmentation is depicted on Supplementary Fig. 2b. For all our experiments, we took $A = 1e7$, $\beta = 1.5$, $T_g = 2e - 6$ and $T_e = 7$.

At this point, cell body detections $d_t^i = (c_t^i, s_t^i)$ have been obtained from the whole sequence. A filtering step is applied to these detections to keep only the most reliable ones. First, detections that are too close to the image boundary (with distance from the centroid of the nucleus detection less than 10 pixels) are ignored. Second, the minimal tolerated circularity is 0.2. Finally, the maximal accepted eccentricity is 0.85. Those last 2 criteria are applied to the nuclei detections.

2.2 Cell body tracking

The tracking algorithm searches through the full set of nuclei detections and iteratively associates the most similar pairs of detections, returning lists of valid detections corresponding to each neuron X^i. This is accomplished by constructing a graph $G = (D, E)$ where each node $d_t^k \in D$ corresponds to a detection. For each detection d_t^k in time step t, edges $e \in \mathcal{E}$ are formed between d_t^k and all past and future detections within a time window W . A weight w_e is assigned to each edge according to spatial and temporal distances, and a shape measure $w_e = \alpha \left\| d_{t1}^k - d_{t2}^l \right\| + \beta \left| t1 - t2 \right| + \gamma f \left(v_{t1}^k, v_{t2}^k \right)$, where

$\hat{e}^{k,l}$ connects d_t^k and d_t^l, and v^k is a shape feature vector containing d_t^k's area, perimeter, mean intensity, and major and minor axis lengths of a fitted ellipse. f evaluates differences between a feature a extracted from d_t^k and d_t^l as $f(a^k, a^t) = \left| \frac{a^k - a^l}{a^k + a^l} \right|$. The tracking solution corresponds to a set of edges $\mathcal{E}' \subset \mathcal{E}$ that minimizes the cost $\sum_{e \in \mathcal{E}'} w_e$. To minimize this cost function, we adopt a greedy selection algorithm outlined in Table 1 and summarized in Supplementary Figure 2c that iteratively selects an edge with minimum cost $\hat{w}_e$ and adds it to the set $\mathcal{E}'$, removing future and past connections from the detections $e^{k,l}$ connects. The algorithm iterates until the minimum cost $\hat{w}_e$ is greater than a threshold T. The track for neuron i is extracted from $\mathcal{E}'$ by traversing the graph $(G, \mathcal{E}')$ and appending linked nucleus detections to X^i (Supplementary Figure 2c).

Table 1 **Greedy Tracking association algorithm**

Start with an empty set $\mathcal{E}'$.
 	
repeat
    Find edge $\hat{e}^{k,l}$ with minimum cost $\hat{w}_e$.
    Add $\hat{e}^{k,l}$ to $\mathcal{E}'$, linking detections d_{t1}^k and d_{t2}^l.
    Remove $\hat{e}^{k,l}$ from $\mathcal{E}$.
    if $t1 < t2$ then
        Remove edges between d_{t1}^k and future detections (where $t > t1$) from $\mathcal{E}$
        Remove edges between d_{t2}^l and past detections (where $t < t2$) from $\mathcal{E}$
    else
        Remove edges between d_{t1}^k and past detections (where $t < t1$) from $\mathcal{E}$
        Remove edges between d_{t2}^l and future detections (where $t > t2$) from $\mathcal{E}$
    end if
until $\hat{w}_e > T$

The parameters of this algorithm have been fixed empirically as follows: $W = 4, \alpha = 1, \beta = 50, \gamma = 40$ and $T = 200$. Only tracks containing at least 20 frames are kept. In addition to these parameters, a spatial connection constraint is applied during the

construction of the graph G. In fact, only detections which are at a distance less than 50 pixels are connected to create the set of edges E. Once the tracking is achieved, tracks are sorted according to their total cumulated green intensities, and only the 40 best tracks are kept, as this is a reasonable number of stained enough moving cells which are quite visible for an experienced human eye.

2.3 Neurites segmentation and association

Given an image It and the set of somata present in it $S_t = \{s_t^1 \dots s_t^m\}$, our goal is to associate to each pixel u a label $J_t(u)$ that indicates to which soma it belongs. The probability of $J_t(u)$ can be deduced using Bayes' rule,

$$P(J_t(u) = i | S_t, I_t) = \frac{P(S_t, I_t | J_t(u)=i)}{\sum_{\eta=1}^{m} P(S_t, I_t | J_t(u)=\eta)} \qquad (7)$$

where we have assumed a uniform distribution on $P(J_t(u))$. The numerator is modeled as the probability of the path L that connects maximally the voxel u to the soma $s_t^i, P(S_t, I_t | J_t(u) = i) = \max_{L:u \to s_t^i} \prod_{\{l_r\} \in L} P(I_t(r) | l_r)$, where l_r are indicator variables for the locations forming the path L. We chose this model since an optimal maxima can be found by minimizing its negative likelihood using geodesic shortest path (Cohen et al. 1996) and because it produces connected components.

The extraction of neurites from a time frame I_t proceeds in the following stages:

• Compute tubularity measure T_t [6]. In addition, detected but not tracked somata are ignored, that is the minimal tubularity value is assigned to "detected but not tracked" somata regions, in order to avoid segmenting their boundaries as neurites.

• Estimate the parameters of a sigmoid functions which is applied to the tubularity measure to obtain a potential P_t that drives the Fast Marching algorithm. The parameters of the sigmoid function are estimated using maximum likelihood.

• Launch simultaneously the front propagation Fast Marching algorithm from all the tracked somata. This is done by solving the Eikonal equation $\|\nabla U_t\| = P_t$ and $\|\nabla L_t\| = 1$.

That yields a geodesic distance map U_t, the associated tessellation V_t, and the map of the Euclidian lengths L of the geodesics. The complexity of the algorithm, at this stage, does not depend on the number of tracked somata but depends only on the size of the image.

• Threshold the geodesic distance with a soft threshold T_s and then extract local maxima of L_t in each thresholded region. We took local maxima of L_t as they likely correspond to continuations of elongated shapes (typically neurites). In fact, at a given threshold value of U_t, elongated structures, such as neurites, has higher L_t values than their surrounding points. Here, we prefer to use a soft threshold and to eliminate the spurious branched in the next step using the hard threshold

• Using the Geodesic distance U_t, back-propagate from all the local maxima of L_t, by keeping only points for which the U_t value is above a hard threshold T_h. The idea is that even if the candidate endpoints detected in the previous step are not necessarily all correct, they will quickly converge to interesting elongated structures during the back propagation.

• Finally, we instantiate a Minimum Spanning Tree from each root touching a soma, and create the associated neurite tree.

The different steps of our approach are illustrated in Supplementary Figure 2d.

Parameters of the neurite detection algorithm are as follows:
• Frangi (Frangi et al. 1998) parameters are: FrangiOpt.FrangiScaleRange = 1,2
FrangiOpt.FrangiScaleRatio = 1, FrangiOpt.FrangiBetaOne = .5,
FrangiOpt.FrangiBetaTwo = 15,

• Geodesic distance thresholds: $T_s = -log(10^{-4})$, and $T_h = -log(0.2)$.

• Finally, any neurite containing less than 10 pixels have been ignored.

2.4 Neurite Tracking

Neurites are tracked by applying the algorithm described in Sec 2.2 using the centroids of the neurite trees instead of nucleus centroids, with the additional constraint that edges may only exist between neurites that emanate from the same tracked soma and only from consecutive time detections. The weight w_e of an edge connecting two neurites N_t^i and N_t^j is assigned according to spatial distance and a shape measure

$$w_e = w_{TLC}f\left(\text{TotalCableLenght}(N_t^i), \text{TotalCableLenght}(N_{t'}^i)\right)$$
$$+w_{Centroid}\left\|\text{Centroid}(N_t^i), \text{Centroid}(N_{t'}^i)\right\| +$$
$$w_{\text{SomaContact}}\left\|\text{SomaContact}(N_t^i), \text{Somacontact}(N_{t'}^i)\right\|$$

where $w_{TLC}f = 50, w_{Centroid} = 10, w_{\text{SomaContact}} = 5$, $\text{TotalCableLenght}(N)$,is the total cable length of a neurite N, $\text{Centroid}(N)$ is its centroid, $\text{SomaContact}(N)$ is its contact point with the soma, and $f\left(a^k, a^t\right) = \left|\frac{a^k - a^l}{a^k + a^l}\right|$. As opposed to the weights used for cell body tracking, the weights used here for neurites tracking do not include a temporal distance because the neurites are associated to already tracked cell bodies. During the neurite tracking stage, only neurites that are considered stable have been taken into account. Neurites are considered stable if their total cable length is above 30 pixels. The threshold parameter of the tracking algorithm (Table 1), have been adapted to neurites by taking $T = 800$.

3. Evaluation

The image processing pipeline, described in section 2, segments and tracks cell bodies and neurites. Questions one could raise to evaluate the quality of the segmentation results are:

1.   What is the quality of the cell body components segmentation. More precisely, what is the quality of the nuclei and the somata segmentations. (Static evaluation)

2.   What is the quality of the cell body tracking (cell identity assignment). In other words, does the algorithm track accurately the moving cells? and is it able not to switch identities of two neighboring moving cells? (Dynamic evaluation)

3.   Are the neurites segmented accurately? Neurite trees are complex structures, and are critical to our phenotypic study. How can we assess their quality is a crucial question to answer (Static evaluation)

4.   Are the neurites tracked properly? or a simpler question could be: how accurate is the "neurite to cell body" assignment step? (Dynamic/Static evaluation ?)

In order to evaluate our algorithm in a fair manner, one should bear in mind that, at detection time, we made the choice not to detect and track all visible cells and neurites. For instance, a neuron that enters the field of view for a short period of time (say during 5 frames, for instance) is not kept in the final set of tracks. In addition, as described in section 2.2, tracked cells are sorted according to their cumulated green intensity, and only the 20 best tracks are kept. We made this choice to favors cell body tracks that are bright with a long lifetime. This choice is also justified by the fact that the moving neurons appears with very different contrast: some are very bright and others are quite faint. Assuming that the algorithm will be able to segment and track accurately all the moving neurons is not realistic, and we preferred to focus our efforts in segmenting and tracking accurately the most robust neurons.

In order to evaluate the different critical components of our processing pipeline we need to annotate ground truth data. If one annotates all visible moving neurons, then our segmentation results will be penalized by the objects that have been purposefully ignored by the algorithm. Hence, evaluation scores obtained using such an over complete ground truth would not reflect the quality of the segmentation and tracking results. To sum up, a special care must be made for the ground truth annotation step and for the quantitative evaluation.

4. References

Benmansour, F. & Cohen, L. D. Fast object segmentation by growing minimal paths from a single point on 2d or 3d images. Journal of Mathematical Imaging and Vision 33, 209–221 (2009).

Cohen, L. & Kimmel, R. Global Minimum for Active Contour Models: A Minimal Path Approach. 666–673 (1996).

Frangi, A. F., Niessen, W. J., Vincken, K. L. & Viergever, M. A. Multiscale Vessel Enhancement Filtering. Lecture Notes in Computer Science 1496, 130–137 (1998).

Gonzalez, G., Fusco, L., Pertz, O. & Smith, K. Automated quantification of morphodynamics for high-throughput live cell imaging datasets. EPFL Technical Report (2011).

Matas, J., Chum, O., Urban, M. & Pajdla, T. Robust wide baseline stereo from maximally stable extremal regions. In Proceedings of the British Machine Vision Conference, 36.1–36.10 (BMVA Press, 2002). Doi:10.5244/C.16.36.

Sethian, J. Level Set Methods and Fast Marching Methods Evolving Interfaces in Computational Geometry, Fluid Mechanics, Computer Vision, and Materials Science (Cambridge University Press, 1999).

3.9.3 Supplementary Note S2. Description of morphological and morphodynamic features

After segmentation and tracking of the timelapse datasets, a panel of features that described cell morphology and morphodynamics can be extracted. In this section, we first provide a conceptual framework that defines different cell components of the neuron. We then define a number of features that describe different morphological and morphodynamic processes that depend on these cell components.

1. Definition of cell components

In order to generate a list of features that describe cell morphology and morphodynamics, we defined a series of parameters that describe cell components such as the nucleus, soma and neurite.

Nuclei and soma parameters

Area: Area of a nucleus or a soma.

Perimeter: Perimeter of a nucleus or a soma.

Major Axis Length and Minor Axis Length: An ellipse is fitted through the nucleus and the soma. Major axis A and a minor axis B of the ellipse are measured.

Orientation: Orientation of the major axis length A of the fitted ellipse (radians)

Eccentricity: Eccentricity of the fitted ellipse: $\sqrt{(a^2 - b^2)}$

Circularity: Distance measured between a pure circle and the real shape of the nucleus or the soma.

Neurite parameters

We modeled the neurite arborescence using different elements. A neurite is considered as the trunk of a tree. We define a tree root as the attachment point between the neurite and the soma, a branch point as any intersection point between neurite elements and the extreme point as the extremities of the arborescence. The root is the neurite segment between the tree root and the first branch point, a branch is any elementary part of the

tree, and a leaf is a branch situated at the extremity of the neurite arborescence (Supplementary Figure 3).

Extreme Length: Distances between the tree root and the extreme points.
Total Cable Length: Sum of the lengths of the root and the branches.
Complexity: Number of branches in the tree divided by the total cable length of the tree.
Number of neurites/branches: Number of roots or branches belonging to a cell
Branches Length: Total length of the branches of a cell
Leaf Branches Length: Total length of the leaves of a cell

2. Data structure for feature storage

After cell segmentation and tracking, data in a non-vectorial form is converted in a matrix. We use the following notation. Let $m \in \{1, \dots, M\}$ be the movie index, $c \in \{1, \dots, C_m\}$ the cell index, $t \in \{1, \dots, T\}$ the time index, and $f \in \{1, \dots, F\}$ the feature index.

We split the features into two groups:

1. "cell.time" features characterize the whole cell population within one frame. These features account for a number of static shape properties, as well as some dynamical properties that are obvious at the population level (speed). This data takes the form of a F-dimensional feature vector. The data structure

$$movie(m).cell(c).time(t).feature(f)$$

is organized into a matrix with $T \sum_{m=1}^{M} \sum_{c=1}^{C_m}$ rows and F columns
2. "cell.ensemble" features globally characterize a given cell through time. These features characterize both an average shape and some dynamic features of the neurite out- growth process. The data structure:

$$movie(m).cell(c).time(t).feature(f)$$

is organized into a matrix with $T \sum_{m=1}^{M} \sum_{c=1}^{C_m}$ rows and F columns

3. Feature list

Features are stored in a multilevel data organization. Solid lines separate different organization levels

Movie(m)

...

Movie(m).numberOfTracks: The number of cells in the movie.

Movie(m).InputRootDir:

Movie(m).RedImageFilenames:

Movie(m).GreenImageFilenames:

Movie(m).NumberOfFrames:

Movie(m).Sample

Movie(m).SeqIdx

Movie(m).DateProcessed

Movie(m).TrackedCells

Movie(m). Cell

Movie(m).RedImageFilenames

...

Movie(m).RedImageFilenames.name

Movie(m).RedImageFilenames.date

Movie(m).RedImageFilenames.bytes

Movie(m).RedImageFilenames.isdir

Movie(m).RedImageFilenames.datenum

Movie(m).GreenImageFilenames

...

Movie(m).GreenImageFilenames.name

Movie(m).GreenImageFilenames.date

Movie(m).GreenImageFilenames.bytes

Movie(m).GreenImageFilenames.isdir

Movie(m).GreenImageFilenames.datenum

Movie(m).Cell(c)

...

Movie(m).Cell(c).Distance Traveled: Total distance traveled by the cell (c) (in pixels).

Movie(m).Cell(c).Number Of Neurites: Number of neurites of the cell (c).

Additionally, for each feature in the layer **Movie.Cell(c).Time(t)** the mean was computed. These features are represented by a single value and do not include the variable **Time(t)**, therefore they are reported in the cell layer **Movie(m).Cell(c)**:

Movie(m).Cell(c).Mean: The average value of the feature through the entire movie.

Moreover, for the features of the layer **Movie.Cell(c).Time(t)** specific parameters that allowed the measurement of dynamic information were computed.

Let $F(t)$ be the feature value at time t and let $\Delta F(t) = F(t) - F(t-1)$ be the feature difference between the two consecutive frames $t-1$ and t.

The list of additional features is as follows:

Movie(m).Cell(c).Time Expanding: The number of times where $\Delta F(t)$ is positive which is the number of times where the feature changes positively.

Movie(m).Cell(c).Time Contracting: Number of times where $\Delta F(t)$ is negative which is the number of times where the feature changes negatively.

Movie(m).Cell(c).Number Inflexion Points: Number of times where $\Delta F(t)$ switches from a positive value to a negative value and from a negative value to a positive value.

Movie(m).Cell(c).Freq Expansion: Number of times where $\Delta F(t)$ is positive divided by the number of frames where the cell appears. This is the number of times per second where the feature changes positively.

Movie(m). Cell(c).Time

Movie(m). Cell(c).Time(t)

...

Movie(m).Cell(c).Time(t).Nucleus Area: Nucleus area of the cell (c) at time (t), in pixels.

Movie(m).Cell(c).Time(t).Nucleus Eccentricity: Nucleus eccentricity of the cell (c) at time (t).

Movie(m).Cell(c).Time(t).Nucleus Major Axis Length: Nucleus Major Axis Length of the cell (c) at time (t).

Movie(m).Cell(c).Time(t).Nucleus Minor Axis Length: Nucleus Minor Axis Length of the cell (c) at time (t).

Movie(m).Cell(c).Time(t).Nucleus Orientation: Nucleus Orientation of the cell (c) at time (t).

Movie(m).Cell(c).Time(t).Nucleus Perimeter: Nucleus Perimeter of the cell (c) at time (t).

Movie(m).Cell(c).Time(t).Nucleus Circularity: Nucleus Circularity of the cell (c) at time (t).

Movie(m).Cell(c).Time(t).Soma Area: Soma Area of the cell (c) at time (t).

Movie(m).Cell(c).Time(t).Soma Eccentricity: Soma Eccentricity of the cell (c) at time (t).

Movie(m).Cell(c).Time(t).Soma Major Axis Length: Soma Major Axis Length of the cell (c) at time (t).

Movie(m).Cell(c).Time(t).Soma Minor Axis Length: Soma Minor Axis Length of the cell (c) at time (t).

Movie(m).Cell(c).Time(t).Soma Orientation: Soma Orientation of the cell (c) at time (t).

Movie(m).Cell(c).Time(t).Soma Perimeter: Soma Perimeter of the cell (c) at time (t).

Movie(m).Cell(c).Time(t).Soma Circularity: Soma Circularity of the cell (c) at time (t).

Movie(m).Cell(c).Time(t).Number Of Neurites: Number of roots of the cell (c) at time (t).

Movie(m).Cell(c).Time(t).All Neurites Length Branches Mean: Average branch length of the cell (c) at time (t).

Movie(m).Cell(c).Time(t).All Neurites Leaf Length Branches Mean: Average leaf length of the cell (c) at time (t).

Movie(m).Cell(c).Time(t).All Neurites Extreme Length Mean: Average extreme length of the cell (c) at time (t).

Movie(m).Cell(c).Time(t).Total Cable Lengths Per Neurite Mean: Average neurite total cable length of the cell (c) at time (t).

Movie(m).Cell(c).Time(t).Complexity Per Neurite Mean: Average neurite complexity of the cell (c) at time (t).

Movie(m).Cell(c).Time(t).Number of Branches Per Neurite Mean: Average number of branches per neurite of the cell (c) at time (t).

Movie(m).Cell(c).Time(t).Max Extreme Length Per Neurite Mean: Average max extreme length per neurite of the cell (c) at time (t).

Movie(m).Cell(c).Time(t).Total Neurites Length: Sum of the total cable length of each neurite of the cell (c) at time (t).

Movie(m).Cell(c).Time(t).Total Neurites Branches: Sum of the number of branches of each neurite of the cell (c) at time t.

Movie(m).Cell(c).Time(t).Total Complexity: "Total Neurites Branches" divided by "Total Neurites Length".

Movie(m).Cell(c).Time(t).Distance Traveled: Distance traveled by the soma of the cell (c) between two consecutive frames.

Movie(m).Cell(c).Time(t).Speed: Instantaneous speed of the cell (c) between two consecutive frames

Movie(m).Cell(c).Time(t).Acceleration: Instantaneous acceleration of the cell (c) between two consecutive frames.

Note. The features that do not have a description are included in the original script but are used for analytical purposes and do not have any biological meaning.

3.9.4 Supplementary Note S3. Feature extraction and data analysis

1. Computing single siRNA profiles and gene-specific morphodynamic signatures (MDSs)

1.1 Single siRNA profiles

In order to characterize the phenotype associated to each of the three siRNAs targeting a gene of interest, we associate a feature vector $r = \{r_1, \dots, r_F\}$ with each siRNA perturbation, where $r_f \in \mathbb{R}$ and F denotes the number of features. We considered two sets of samples for the feature f: the samples from the control, and the samples associated with the siRNA perturbation. We applied a z-test with 5% significance (Orvedahl et al. 2011). Let $z_f \in \mathbb{R}$ be the resulting z-score and $h_f \in \{0, 1\}$ be the result of the statistical test, where $h_f = 1$ if the mean of the two distributions are significantly different, $h_f = 0$ otherwise. The siRNA profile is defined as follow:

$$r_f = h_f z_f \tag{1}$$

The component r_f specifies a signed distance measure between the distribution of the feature f of the control, and the distribution of the feature f of the specific siRNA. The sign of r_f gives the feature polarity:

If $r_f > 0$, the polarity is positive and the average feature value is higher for the siRNA than for the control.

If $r_f < 0$, the polarity is negative and the average feature value is lower for the siRNA than for the control.

If $r_f = 0$, the polarity is null and the average feature value is the same for the siRNA and the control.

1.2. Morphodynamic signature

To deconvolute siRNA "off-target effects", we then computed a gene-specific,

morphodynamic signature by "averaging" the 3 single siRNA profiles according to the rules described below. As previously proposed (Echeverri et al. 2006), if at least 2 out of 3 siRNAs produce the same phenotype, this phenotype can be considered as "on target". We therefore assumed that if each independent feature had at least the same polarity in 2 out of 3 siRNAs, then this specific feature was "on-target". More specifically, for a given feature, if the three siRNAs yield the same polarity (positive, negative or null), the feature score is the mean of the z-score. If 2 out of 3 siRNAs yield the same polarity, with the 3rd siRNA having a different polarity, the feature score is the average z-value of the 2 siRNAs with the same polarity. If the 3 siRNAs yield 3 different polarities, we set the z feature score to zero.

Formally, let $ri = \{ri, \ldots, rF\}$ be a siRNA profile given by Equation (1), where F denotes the number of features for each siRNA, i.e. $i \in \{1, 2, 3\}$. Let $\varepsilon \in \{-1, +1\}$ be a binary value and $N(\varepsilon) = |\{i \text{ s.t. } \varepsilon\, r_f^i > 0\}|$ be the number of RNA molecules that are together positively affected ($\varepsilon = 1$) or together negatively affected ($\varepsilon = -1$). The MDS $g = \{g1, \ldots, gF\}$ arises from an average siRNA profile if these one have the same polarity:

$$
g_f = \begin{cases} \frac{1}{N(\varepsilon^*)} \sum_{i \text{ s.t. } \varepsilon\, r_f^i > 0} r_f^i & \text{if } N(\varepsilon^*) > 1 \\ 0 & \end{cases} \tag{2}
$$

otherwise where

$$
\varepsilon^* = \arg\max_\varepsilon N(\varepsilon) \tag{3}
$$

For instance, for a given feature, if two siRNAs yield a significant positive z-scores and if the third siRNA molecule yields a negative z-score, then the feature f value of the gene profile is the mean z-score of the two first RNA molecules. In the following table, we provide some examples:

r_f^1	0	0	0	0	0	-15	10	0	2	12
r_f^2	0	0	0	5	8	8	8	-6	-12	-10
r_f^3	0	10	-5	-8	10	4	6	-4	-15	-8
g_f	0	0	0	0	9	6	8	-5	-3.5	-10

2. Feature reduction

In order to reduce the complexity to obtain well-defined phenoclusters, we reduced the feature space size. For that purpose, we used an automatic feature selection strategy, which is based on feature robustness across different experimental plates. For each one of the 32 experimental plates, a negative control (consisting of a non- targeting siRNA), and a positive control (consisting of a MKK7 siRNA) have been included. In theory, for a given feature, we should have the same z-score in each experimental plate. But, because of the noise arising from experimental conditions variation, some features can change their polarity across the plates. We therefore discarded any feature of which the z-score polarity was dissimilar in at least $S = 70$ of the plates.

Formally, let F be the starting set of features. We want to obtain a subset $\hat{F} = \{\hat{f}_1, \ldots, \hat{f}_F\} \subset F$ such that $f \in \hat{F}$ if, and only if:

$$max \ \{p \text{ s.t.} r_f^p > 0\}, \{p \text{ s.t.} r_f^p < 0\}, \{p \text{ s.t.} r_f^p = 0\} \ > P \, S \qquad (4)$$

where P is the number of plates, r_f^p is the siRNA profile of the MKK7 control in the plate p, and $S \in [0, 1]$ is a threshold value. By setting $S = 0.7$, we reduce the size of the feature space by 87%.

2.1 The features list after feature selection

We operated an automatic feature selection based on feature robustness across different experimental plates, as described in section 2.

The list of features obtained after reduction is the following:

Movie(m).Cell(c).Nucleus Perimeter Freq Expansion

Movie(m).Cell(c).Soma Eccentricity Freq Expansion

Movie(m).Cell(c).Total Neurites Length Freq Expansion

Movie(m).Cell(c).Total Neurites Branches Freq Expansion

Movie.Cell(c).Time(t).Nucleus Area

Movie.Cell(c).Time(t).Nucleus Major Axis Length

Movie.Cell(c).Time(t).Nucleus Perimeter

Movie.Cell(c).Time(t).Soma Eccentricity

Movie.Cell(c).Time(t).Soma Major Axis Length

Movie.Cell(c).Time(t).Soma Circularity

Movie.Cell(c).Time(t).Number Of Neurites

Movie.Cell(c).Time(t).All Neurites Extreme Length Mean

Movie.Cell(c).Time(t).Total Cable Lengths Per Neurite Mean

Movie.Cell(c).Time(t).Complexity Per Neurite Mean

Movie.Cell(c).Time(t).Number of Branches Per Neurite Mean

Movie.Cell(c).Time(t).Max Extreme Length Per Neurite Mean

Movie.Cell(c).Time(t).Total Neurites Length

Movie.Cell(c).Time(t).Total Neurites Branches

Movie.Cell(c).Time(t).Total Complexity

Movie.Cell(c).Time(t).Distance Traveled

Movie.Cell(c).Time(t).Speed

3. Temporal analysis of neurite outgrowth dynamics

With the availability of large timelapse datasets (32 plates with each a non-targeting siRNA as negative and a MKK7 siRNA as positive control), we analyzed the averaged temporal behavior of neurite outgrowth of control and MKK7 KD cells. For this, we divided each timelapse series (of approximately 20 hours) into 20 temporal bins, and computed the mean of the feature value in each bin.

In order to compare the temporal evolution of each feature, we normalized the feature value by its variance. Let $A = \{x_1, \ldots, x_N\}$, where $x_n \in \mathbb{R}$, be the values of a feature for all the cells of a control. We denote by μ_b and σ_b^2 the mean and variance of A

respectively. Let $A^b = \{x_1^b, \ldots, x_N^b\}$, where $x_n^b \in R$, be a subset $A^b \subset A$ such that x_n^b is restricted in the temporal bin b. Similarly, we denote by x_n^b and σ_b^2 the mean and variance of A^b respectively. We normalized the data as follows:

$$x_n^b \leftarrow \frac{x_n^b - \mu}{\sigma}$$

Additionally, we illustrated this temporal analysis by selecting representative cells in figure 3 A-C. Each cell is automatically selected from a model. Let $X = \{X_1, \ldots, X_F\}$ be a model for a targeted cell, where $X_f \in R$ is chosen regarding the variation of μ_b in the analysis of figure 3 A-C. The method consists of selecting the cell $x_{\hat{n}} \in \{x_1, \ldots, x_N\}$, where $x_n \in R^F$, such that:

$$\hat{n} = \arg\min_n \| x_n - X \|^2$$

In order to filter the cells without neurite, we target the 10% cells with longest neurites.

4. Computation of MDSs L_o-distances for hierarchical clustering

Phenotypical clustering requires to compute a distance $D(i,j)$ between two MDSs g^i and g^j. We used a straightforward distance that is only based on the MDS polarity. In other word, the proposed distance depends on the signed distance between the gene profiles:
$D(i,j) = D\left(sign(g^i), sign(g^j)\right)$ where $sign(g^i) = \{sign(g_1^i), \ldots, sign(g_F^i)\}$,
$sign(g_f^i) = 0$ if $g_f^i = 0$, $sign(g_f^i) = 1$ if $g_f^i > 0$, and $sign(g_f^i) = -1$ if $g_f^i < 0$. In other words, two genes have a similar phenotype if their features have the same polarity. This can be computed by using the L_o distance:

$$D(i,j) = \frac{1}{F} \left|\{f \text{ s.t. } sign(g_f^i) = sign(g_f^i)\}\right| = \frac{1}{F} \|sign(g^i) - sign(g^j)\|_0 \qquad (5)$$

The distance gives a percentage of features that are matching between two genes.

4.1. Hierarchical clustering to identify phenoclusters

We used bottom-up hierarchical clustering (Bakal et al. 2006, Yin et al. 2013) to identify set of genes that share common MDSs. Evaluation of the distance between two clusters

was carried out by computing the L_o-distance (5) between the two mean points of the clusters. We set the minimum number of genes per cluster to three, with the consequence that if a cluster is composed of less than three genes, we consider these genes as unclustered.

The number of clusters also depends on the dendrogram threshold which gives the minimum percentage of matching features in each cluster. This percentage is directly connected to the L_o-distance (5). If this threshold is too high there are few clusters, if the threshold is too low the clusters are two noisy. We came to a compromise by manually setting the threshold to 65%. This means that there are 65% of features that match in a given cluster. In this way, we obtain both numerous and feature- homogeneous clusters.

4.2. Identification of cluster representative cells

We then identified representative cells for each phenoclusters to provide synthetic images and timelapse series that are representative of each phenotype. For that purpose, we first identified the single siRNA profile that has the highest similarity with the averaged MDS. For each siRNA, following the method in section 1.2., we computed the occurrence of the on-target features, then, we select the single siRNA profile that has the highest number of on-target features.

Second, we select the cells with an extreme phenotype. More specifically, for a given gene i, we are looking for a cell $x_{\hat{n}}^i \in \{x_1^i, \ldots, x_N^i\}$ where $x_n^i \in \{x_{n,1}^i, \ldots, x_{n,F}^i\}$, such that this cell has features strongly consistent with the centroid $\overline{x}$. The optimization formulation is as follows:

$$\hat{n} = \arg\max_n \sum_{f=1}^{F} \frac{sign\left(g_f^i\right) x_{f,n}^i -}{\sigma_f} \tag{6}$$

where σ_f the standard deviation of the feature f (computed from all the data), $\overline{x_f}$ be the centroid value of the feature f for the control, $sign[g_1^i] = 1$ if the gene profile g_f^i is positive, and sign $sign[g_1^i] = -1$ else.

Importantly, in this analysis, we focused on a subset of features that are easily interpretable, therefore allowing to visually grasp the essence of the specific phenotype. The specific features are enumerated here: number of neurites, number of branches per neurite mean, max extreme length per neurite mean, and speed.

5. References

C. Bakal, et al., "Quantitative Morphological Signatures Define Local Signaling Networks Regulating Cell Morphology", Science, vol. 316, p. 1753-1756, 2007.

C.J. Echeverri, et al., "Minimizing the risk of reporting false positives in large scale RNAi screens", Nature Methods, vol. 3(10), p. 777-779, 2006.

A. Orvedahl, et al., "Image-based genome-wide siRNA screen identifies selective autophagy factors", Nature, vol. 480, p. 113-117, 2011.

Z. Yin, et al., "A screen for morphological complexity identifies regulators of switch-like transitions between discrete cell shape", Nature Cell Biology, vol.15(7), p. 860-871, 2013.

3.9.5 Supplementary Note S4. Identification of a Rho GTPase signaling network.

To identify a Rho GTPase signaling network, we took advantage of our recent proteomic analysis of purified neurite and soma fractions of N1E-115 cells (Pertz et al. 2008). This dataset provides spatial information about the subcellular localization (neurite/soma) for 4855 proteins, through the measurement of relative protein enrichment in purified neurite and soma fractions. Using the Ingenuity Pathways Analysis (IPA) software (http://www.ingenuity.com), we first identified Rho GTPases expressed in our cell system (Rac1, Cdc42, RhoA, RhoB, RhoC, RhoG). We then used these as "bait" to identifying proteins that are documented to interact directly with these Rho GTPases by interrogating the Ingenuity Pathways Knowledge Base, which is a system wide database of biological pathways created from multiple relationships of proteins, genes, and diseases. Only considering proteins identified in our proteomics screen to be neurite-enriched or equally distributed in neurite and soma fractions, we then manually sorted these proteins in GEFs, GAPs, RhoA effectors, Rac1 and Cdc42 effectors, and additional interacting proteins. In a second round, we then used these different protein groups as baits to identify additional interactors that might work upstream of GEFs and GAPs, or downstream of effectors. This yielded a Rho GTPase signaling network of 226 proteins (Supplementary Fig. 4a), in which most proteins are significantly enriched in the neurite. We used Ingenuity analysis pathway software to perform a gene ontology analysis of the protein ensemble in this signaling network (Supplementary Fig.4b). As expected, we observed enrichment of Rho GTPase, adhesion, cytoskeleton and axonal gene ontology terms. Our approach reveals the existence of a neurite-enriched, Rho GTPase signaling network of unanticipated complexity.

References

Pertz, O.C. *et al.* Spatial mapping of the neurite and soma proteomes reveals a functional Cdc42/Rac regulatory network. *Proceedings of the National Academy of Sciences of the United States of America* 105, 1931-1936 (2008).

3.9.6 Supplementary Movies

Movie 1. 20 hour timelapse movie of N1E-115 cells expressing the Lifeact-GFP/NLS-mCherry, extending neurites on a laminin-coated coverslip. GFP and mCherry channels in inverted black and white contrast are shown. Scale bar: 50 µm mm. Timescale: hours/minutes.

Movie 2. Representative timelapse movie of segmented N1E-115 cells extending neurites. Scale bar: 50 µm. Timescale: hours/minutes.

Movie 3. Representative synthetic images of neurite outgrowth dynamics of control, *SrGAP2*, *MKK7* and *RhoA* KD cells. Scale bar: 50 µm. Timescale: hours/minutes.

Movie 4. Representative synthetic images of different phenotypical subgroups. Scale bar: 50 µm. Timescale hours/minutes.

4. Additional results

4.1 Introduction

In our large scale siRNA screen, we concentrated on time and length scales of tenth of minutes and tenth of microns, at which the global neurite outgrowth process occurs. However, when one considers the neurite outgrowth process, a much shorter time and length scale also has to be taken into account.

For instance, the actin cytoskeleton in the growth cone veil and filopodia fluctuates in time scales of single seconds and length scales of single microns (Jang et al. 2010). Any dynamic phenotypes occurring at these time and length scales are not accessible by the computer vision approach we used in our large scale siRNA screen. Furthermore, our studies in which we visualized Rho GTPase activation dynamics using FRET probes, clearly show that their signaling dynamics oscillate on time and length scales of seconds and single microns, respectively (Pertz et al. 2006; Fritz et al. 2013). It is then easily conceivable that dynamic phenotypes when studied at this specific timescale, can impact the global neurite outgrowth process. For example, long neurites may be produced by switching off the spatio-temporal signaling network that regulates growth cone collapse, or by stabilizing the actin cytoskeleton in the growth cone so as to prevent collapse. Thus a phenotype observed at the global neurite outgrowth level might be the consequence of different causes at the local length and time scales. This prompted us to design a computer vision pipeline to study the second/single μm length/time scale. The results of this approach revealed the possible existence of localized spatio-temporal signaling modules, which lead to an analogous global effect on the neurite outgrowth process.

4.2 High resolution morphodynamic signature is crucial to explore Rho GTPase spatio-temporal activity

In order to determine how regional actin cytoskeleton architecture of the growth cone may contribute to larger-scale neurite outgrowth, we decided to further investigate the high resolution (HR) morphodynamic signature (MDS) of two smaller subsets of KD genes previously analyzed in our lower resolution neurite outgrowth screen. These subsets were comprised KDs of the three canonical Rho GTPases, RhoA, Rac1 and Cdc42, and a potential Rac-centered signaling module including the Rac1 GEFs, Beta-Pix, Trio, Dock7, and the Rac1 GAP protein called SrGAP2. (Figure 1a,b)

First, in order to obtain information regarding the actin cytoskeleton in these KD experiments, we acquired single frame, high resolution images of protruding growth cones upon phalloidin staining (Figure 1c). Interestingly, we found that diverse growth cone structural profiles can lead to very similar larger scale neurite outgrowth phenotypes. RhoA, Cdc42 and SrGAP2 KDs show a LR long neurite phenotype, however their growth cone architecture at high resolution appears to be stereotypically and morphologically distinct, even by gross visual analysis. As previously described, SrGAP2 KD is characterized by a high density of growth cone filopodia (Pertz et al. 2008), while RhoA KD shows thin growth cone morphology, with thick filopodia actin bundles protruding outward from the growth cone veil., Similar to RhoA KD, Cdc42 KD shows filopodia protruding outward from the veil; however these filopodia appear thinner with potentially lower levels of filamentous actin bundles. The KDs of Rac1 and the three putative Rac1 GEFs (Trio, Dock7 and β-Pix), each of which share a short neurite LR phenotype, are also characterized by strong visual differences in their HR growth cone morphology. From visual inspection, the growth cone veil appears relatively similar between Rac1 KD and the control, while it appears to be thinner in Trio and β-Pix KD growth cones. Visual analysis reveals that Trio KD shows an additional crisscross filopodia phenotype (Pertz et al. 2008). Dock7 KD shows long filopodia protruding from the veil but, similar to Cdc42, lacks thick filopodia actin bundles. All together these results demonstrate that while the selected KD genes can share similar LR MDS, it is possible to see strong morphological differences when their growth cones are analyzed at HR.

Since Rho GTPases are known to be spatio-temporal regulators of neuronal outgrowth (da Silva and Dotti 2002), we developed an automated segmentation and tracking pipeline to

investigate the HR MDS of the previously described KD genes in a live cell imaging mode. This pipeline (Figure 2) shows how HR growth cone segmentation can be achieved by combining information obtained from separate filopodia and veil/shaft detection steps. We acquired a library of protruding growth cone movies (5 sec intervals for 10 minutes) of N1E115 cells expressing fluorescently labeled Lifeact for each of the KD genes.

As the full growth cone is segmented, both global/functional parameters such as neurite outgrowth, and spatially localized parameters such as veil/shaft protrusion/retraction dynamics, and the individual filopodia lengths can be measured in HR (Figure 3).

We then decided to compare HR and LR neurite outgrowth measurements (Figure 4) for our selection of KD genes, to investigate possible differences in these parameters between the two different scales. Surprisingly, the HR neurite outgrowth results do not always correspond to the LR neurite outgrowth profiles of our KD selection, suggesting a possible separation between the events that control this process at two different scales.

As previously described, the KD of Rac1 and the three GEFs Trio, Dock7 and β-Pix, share a similar LR profile. Moreover it has been shown in various studies that these GEFs are all able to interact with Rac1 and enhance its activity (Bellanger et al. 2000; Pinheiro and Gertler 2006; ten Klooster et al. 2006). Therefore, we compared the HR MDS of Rac1, Trio, Dock7 and β-Pix KD experiments, in order to highlight possible similarities and differences between the HR MDS of these genes.

By analyzing HR neurite outgrowth parameters, we established that the KD of two out of three GEFs (Trio and Dock7) and Rac1 KD are characterized by lower overall neurite outgrowth compared to control siRNA (Figure 5a). Moreover, the spatially localized veil dynamic calculations begin to reveal potential subtleties in the KD phenotype among the putative Rac1 GEFs (Figure 5b). We found that Rac1, Trio and Dock7 KDs are characterized by immobilization of the veil, which may be potentially responsible for their short neurite phenotypes. Interestingly, the dynamic analysis provides evidence that β-Pix KD results in a more motile veil than the KD of Rac1 and the other two GEFs, while still having a negative impact on the promotion of neurite outgrowth (Figure 1a,b).

We then analyzed SrGAP2 KD HR MDS and found that in contrast to the KD of Rac1, Trio, Dock7 and β-Pix, SRGAP2 KD shows an increase in the growth cone protrusion and retraction dynamics (Figure 6a), consistent with SrGAP2's hypothesized role as a Rac1 deactivator (Guerrier et al. 2009). Moreover, SrGAP2 windowing veil dynamic measurement highlights an increase in the veil dynamics compared to control siRNA (Figure 6b), suggesting a possible relationship between veil dynamics and neurite

outgrowth. All together these results highlight the existence of a putative Rac-1 signaling module, involving the GEF proteins Dock7 and Trio, and the GAP protein SrGAP2, which could be involved in the regulation of growth cone veil dynamics.

4.3 Two GAPs for RhoA are involved in the regulation of neurite retraction and filopodia formation

In order to explore the role of GAP proteins in the regulation of RhoA activation, we performed experiments using the RhoA FRET probe (Fritz et al. 2013) to monitor the activity of this GTPase during GAP KD.

We analyzed the MDSs of RhoA and two GAPs that are known to control its activity, Dlc1 and p190RhoGAP (Arthur and Burridge 2001; Ullmannova-Benson et al. 2009). RhoA KD cells show a long neurite phenotype without any increase in the number of branches (Figure 7a), which is consistent with current knowledge that RhoA promotes neurite retraction (da Silva and Dotti 2002). Consistent with the results that p190RhoGAP enhances neurite outgrowth via RhoA inactivation in PC12 cells (Jeon et al. 2012), p190RhoGAP KD shows the opposite phenotype compared to RhoA KD, and is mainly characterized by short neurites with no evident increase in branching (Figure 7a). On the other hand, the KD of Dlc1, which also negatively controls RhoA activation, phenocopies RhoA KD in its neurite phenotype, but in contrast to RhoA KD, shows a higher number of branches (Figure 7a). We then investigated how the knock down of these proteins could affect growth cone morphology. In this case, RhoA, p190RhoGAP and Dlc1 KD growth cones show a similar phenotype characterized by long and dense filopodia actin-bundles protruding outward from the growth cone veil (Figure 7b). In order to better investigate how p190RhoGAP and Dlc1 controls RhoA activation, we performed high resolution RhoA FRET probe imaging by co-transfecting control siRNA, Dlc1 and p190RhoGAP siRNAs, together with pLenti-Lifeact-mCherry (Figure 7c). We then acquired high resolution images in live cells in the FRET, donor and mCherry channel. The ratio images show that, as we previously demonstrated, in cells treated with the control siRNA, RhoA is activated at the tip of the filopodia of the protruding growth cone (Figure 7c, left panels) (Fritz et al. 2013). Moreover it has been shown, that RhoA is also activated globally in the growth cone

during neurite collapse (Fritz et al. 2013). On the other hand, the ratio images of cells treated with p190RhoGAP and Dlc1 siRNAs show a different pattern of RhoA activation. In p190RhoGAP KD cells, the activation of RhoA is extended entirely in the growth cone, suggesting therefore that this GAP could globally control RhoA activation during neurite retraction (Figure 7c, central panels), which is also consistent with the p190RhoGAP MDS results. However, in Dlc1 KD cells, RhoA activity seems to be enhanced particularly in the entire structure of the filopodia (Figure 7c, left panels). This specific accumulation of the RhoA-probe in the filopodia, together with the results of the MDS of Dlc1 KD, suggests the possibility that this GAP could control RhoA activation during growth cone filopodia protrusion.

4.4 Experimental procedures

Cell Culture, Transfection.

N1E-115 neuroblastoma cells (American Tissue Culture Collection) were cultured in Dulbecco's modified Eagle's medium (DMEM) supplemented with 10% FBS, 1% L-glutamine, and 1% penicillin/streptomycin. For differentiation, N1E-115 cells were starved for 24 h in serum-free Neurobasal medium (Invitrogen) supplemented with 1% L-glutamine and 1% penicillin/streptomycin. For the double siRNA-mediated KD and plasmid transfection, cells were transfected as previously described (Chong et al. 2006) using 400 ng of the plasmid pLenti-Lifeact-GFP or pLenti-Lifeact-mCherry and 20 pmol of siRNA, a single gene-specific siRNA (Invitrogen Stealth Select siRNAs (Invitrogen). 1 µl of Transfectin (Bio-Rad) was used as transfection reagent. For the immunofluorescence experiment, only the single gene-specific siRNAs were transfected as previously described. 48 h post-transfection cells were starved in Neurobasal medium. 72 h post-transfection, cells were detached with PUCK's saline and replated on a glass-bottom 24 multi-well plates (MatTek) coated with 10 µg/ml laminin (Millipore-Chemicon). About 24 hours post-seeding, cells were used for timelapse imaging or immunofluorescence experiments.

Immunofluorescence

24 hours after replating, N1E-115 cells were washed with PBS, fixed in PBS containing 4% paraformaldehyde (Sigma Aldrich) for 10 min and permeabilized in PBS containing 1% of Triton-X for 2 min. 18 mm coverslips were then blocked in 2% BSA, 0.1% Triton-X in PBS for 30 min. For the staining, cells were incubated with primary antibodies for 2 hours, and then with secondary antibodies for 1 hour (Alexa-fluor 488 labeled phalloidin, Alexa-fluor 546 secondary antibody, and DAPI [all Invitrogen]), in both cases the same blocking solution was used to dilute the antibodies. Coverslip were then mounted using Dako fluorescent mounting medium (Dako).

**Microscopy, Image Acquisition, and Analysis**

All the experiments were performed on an inverted Eclipse Ti microscope (Nikon), controlled by Metamorph software (Universal Imaging). Laser-based autofocus was used for all experiments. For fluorescent timelapse live cell imaging of neurite dynamics, N1E-115 cells were replated on a laminin-coated glass-bottom multi-well plates (MatTek). 24 hours after plating, cells were imaged in Neurobasal medium (Invitrogen) in a heated closed chamber. The images were acquired every 5 sec using Plan Apo VCoil 60X (NA1.4) (Nikon) objective controlled by MetaMorph (Molecular Devices) and a CoolSnap HQ2 camera (Roper Scientific). SPECTRA X light engine was used as light sources (Lumencor). Filter for 470 nm (excitation of GFP) was used throughout the experiments. The total length of a movie was 10 min. For the acquisition of high resolution images and neurite outgrowth analysis, N1E-115 cells were stained as previously described. The images were acquired using a Plan Apo VCoil 100X (NA1.4) (Nikon) for high resolution images and a CFI Plan Apo Lambda 10X objective (Nikon) for neurite outgrowth and representative images. For the automated neurite segmentation the Metamorph software was used. For FRET live cell imaging acquisition, cells were treated as previously described for fluorescent timelapse live cell imaging. Images were acquired with Plan Apo VCoil 60X (NA1.4) (Nikon) objective controlled by MetaMorph (Molecular Devices). SPECTRA X light engine was used as light sources (Lumencor). Filters for 440 nm (excitation of CFP, mCerulean, and mTeal), 480 nm (excitation of Venus), and 565 nm (excitation of mCherry) were used during acquisition. Acquisitions were done with a CoolSnap HQ2 camera (Roper Scientific). Processing of epifluorescence ratio-imaging data sets was performed with the Biosensor Processing Software 2.1 (Danuser laboratory: http://lccb.hms.harvard.edu/software.html). For the ratio, images were sequentially

thresholded on each channel, background-corrected, and masked before ratios were calculated. Ratio images were then color-coded in MetaMorph (Molecular Devices) so that warm and cold colors represent high and low biosensor activity, respectively.

4.5 Figures
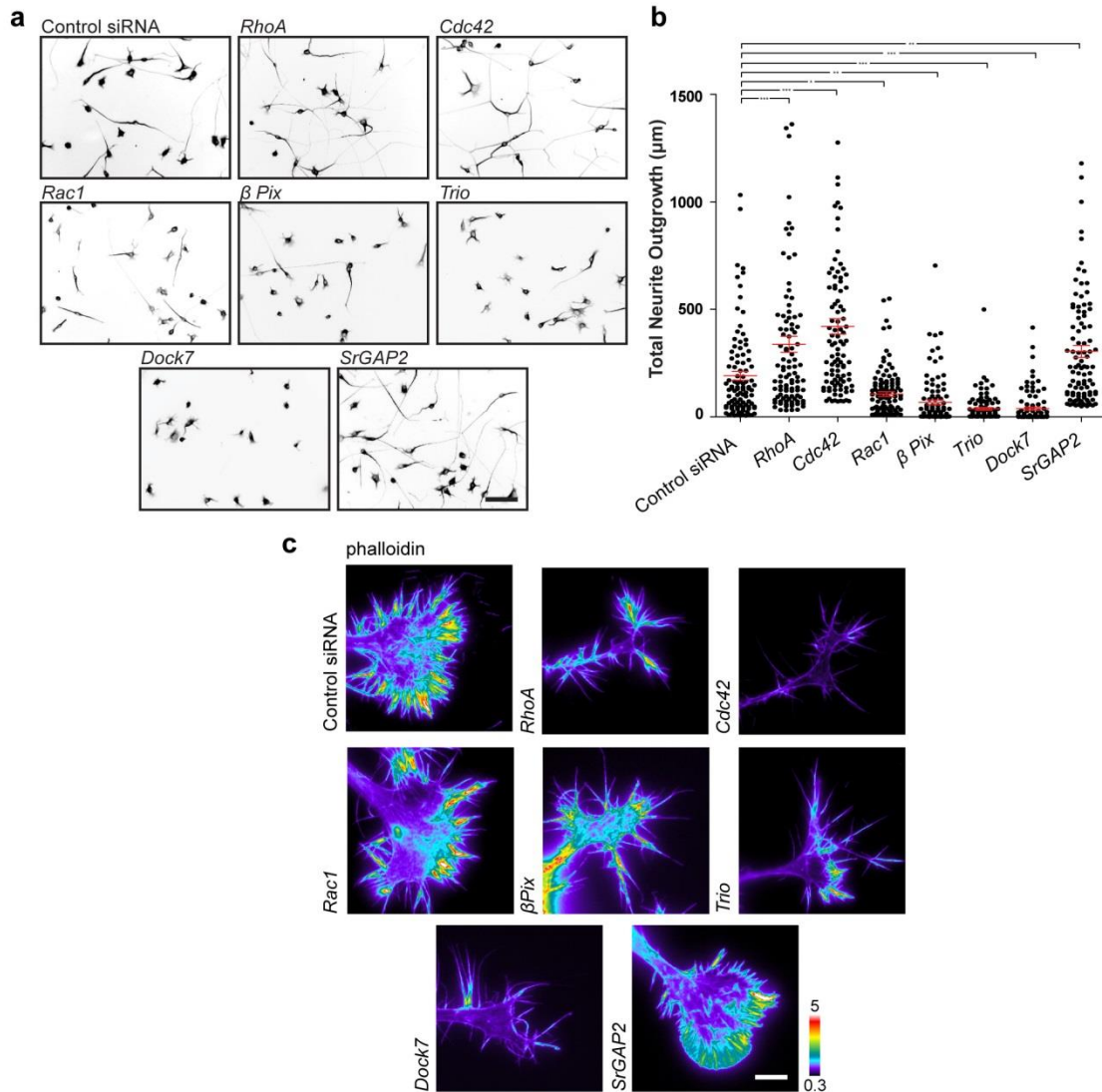
Figure 1. High resolution images, neurite outgrowth and representative images of knock down experiments in N1E-115 cells. (**a**). Representative images of different α-tubulin stained of (b). Scale bar: 50µm. (**b**). Quantified Neurite outgrowth analysis of 24hr differentiated KD experiments using MetaMorph neurite outgrowth plugin. Error bar represent SEM. *** =p<0.001. (**c**). High resolution images of phalloidin stainings of selected KD growth cones. Scale bar = 10 µm
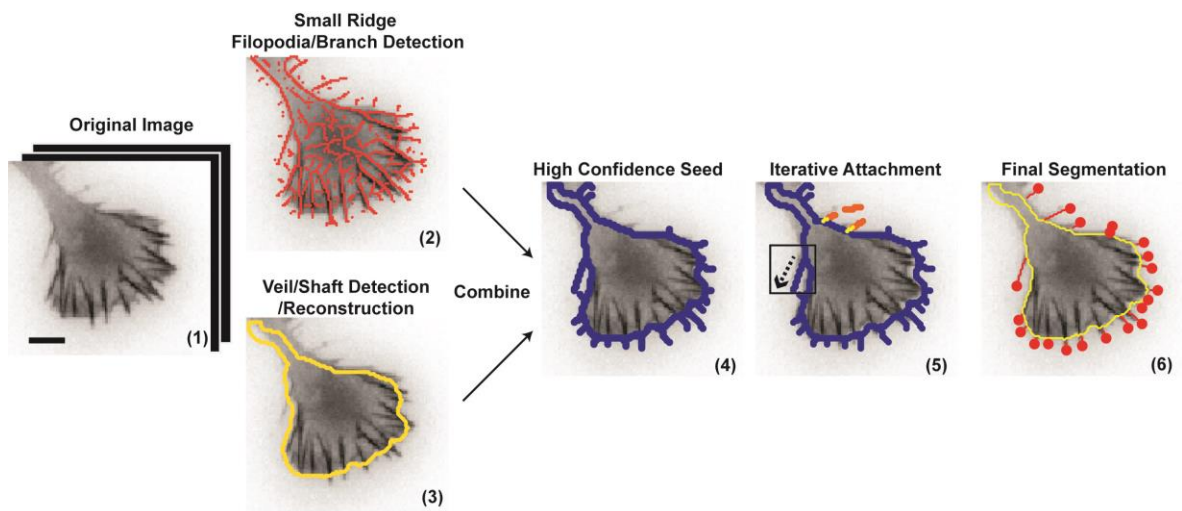
Figure 2. Pipeline of Automated High Resolution Growth Cone Segmentation and Parameter Extraction. Steps of growth cone reconstruction. Preliminary detection/reconstruction of the original image (1) is decomposed into two parallel steps of small-scale ridge detection (2) for detection of diffraction-limited growth cone filopodia/branch structures and larger-scale detection/reconstruction of the more amorphous growth cone veil/shaft (3). The larger scale veil/shaft estimation is then used to filter intersecting high-confidence small-scale ridge detections and obtain a high confidence "seed" (4) for further iterative attachment (5) of lower confidence, candidate ridges corresponding to filopodia and protruding branch structures, which results in a fully reconstructed growth cone segmentation (6). Scale bar: 10 μm
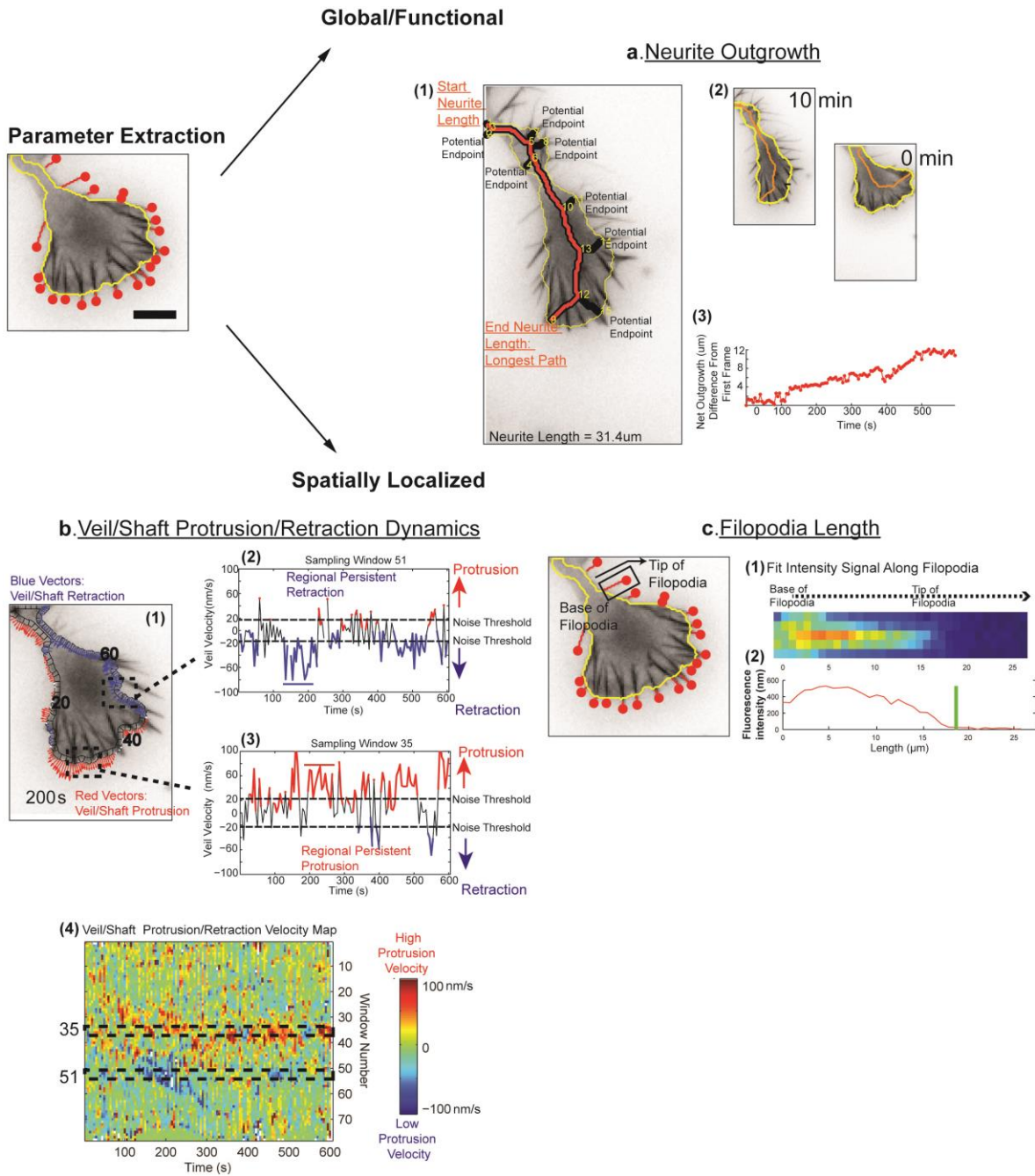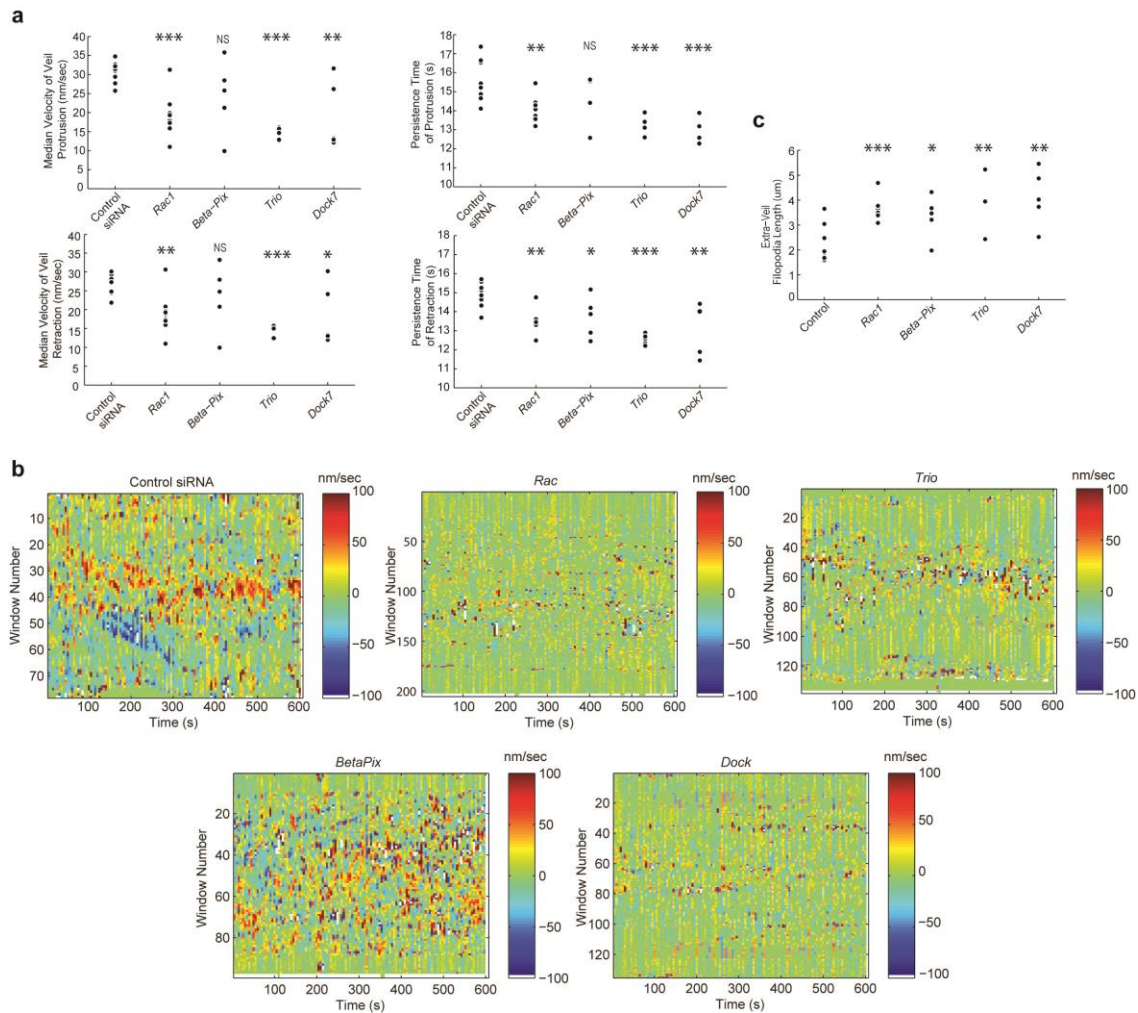
Figure3. Extraction of Growth Cone Structural and Dynamic Parameters. Full growth cone reconstruction allows for parameter extraction of both global/functional parameters such as neurite outgrowth (a) and more spatially localized parameters corresponding to the growth cone veil dynamics and individual filopodia length measurements (b and c). Scale bar: 10 μm (**a**) Definition of high-resolution neurite length. The medial axis transform (orange lines) of the veil/shaft estimation (yellow outline) is treated as a simple graph (yellow numbers, show vertex labels) and the distances of all paths

117

from the neurite shaft entrance to all graph endpoints are measured. (1) The longest of these paths (orange line) is defined as the high-resolution neurite length for the given frame. Differences of high-resolution neurite length measurements between sampled time points provide a good approximation of the change in the neurite length over the given time interval (2) so that neurite outgrowth behavior in time (3) can be monitored. (**b**) Definition of Local Veil Dynamic Parameters. (1) The local displacement of the growth cone veil between two frames can be measured in time and characterized as a veil protrusion (red) or retraction (blue) event, based on if the displacement orientation moves away (protrusion) or towards (retraction) the neurite veil/shaft estimation center. (2-3) A protrusion (red arrow- positive velocity) or retraction (blue arrow– negative velocity) event is defined as those velocities falling above or below the estimated noise threshold. The persistence of a protrusion can be measured as the number of consecutive time points the veil/shaft velocity falls above/below the noise threshold (the red and blue horizontal lines in (2) and (3) mark a single protrusion/retraction event respectively). (4) To obtain a visual representation of the protrusion/retraction patterns over the entire veil/shaft protrusion/retraction maps can be plotted such that each window's corresponding time series is place side-by-side allowing for visualization of coordination among regions. (c) Definition of Filopodia Length Parameter. As a filopodia is typically a diffraction limited object, its length can be most accurately measured by fitting the fluorescence intensity in the direction along the filopodia. Panel (2) shows the fluorescence intensity profile of the filopodia boxed in (1) to a sigmoidal Gaussian error function. The mean of the Gaussian error function defines the tip of the filopodia (green line in 2), where the filopodia intersection with the veil/shaft estimation define the base of the protruding filopodia.
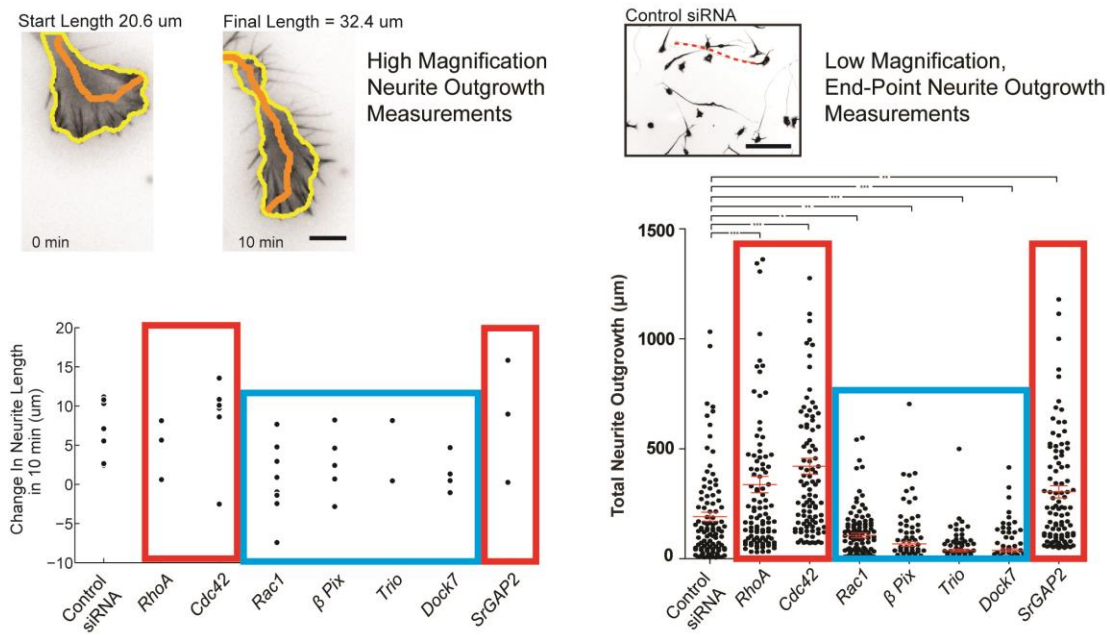
Figure 4. Sampling Neurite Length Metrics at Different Spatial and Temporal Scales. Automated neurite outgrowth measurements performed at higher magnification (left panel), higher time resolution (right panel). Red and blue boxes mark genetic perturbations resulting in enhanced and reduced neurite outgrowth phenotypes, respectively, as determined by low resolution, end-point measurements.

Figure 5. Comparison of Select Structural/Dynamic Features corresponding to Rac1KD, and three putative Rac1 GEFs, Trio, Dock7, and β-Pix via Automated Growth Cone Quantification (**a**) Quantification of local veil protrusion/retraction persistence and velocity as described in Figure 2b. Each point represents the average value per neurite for the entire 10 minute movie. (N = 5-9 growth cones per condition, ~8000-30000 protrusion and retraction measurements per condition). (**b**) Representative Veil Protrusion/Retraction velocity maps as described in Figure 3b comparing Rac1 KD and the KD of the four different Rac1 GEFs to Control. Each map is from a single neurite. (**c**) Automated quantification of growth cone filopodia lengths. Each point represents the average value per neurite for the entire 10 minute movie. (N = 5-9 growth cones per condition, ~16700- 49000 filopodia measurements total per condition. Filopodia were filtered such that only those attached to the neurite veil or shaft were used in the measurement). *** =p<0.001 given a non-parametric, permutation t-test of the means testing KD compared to control.
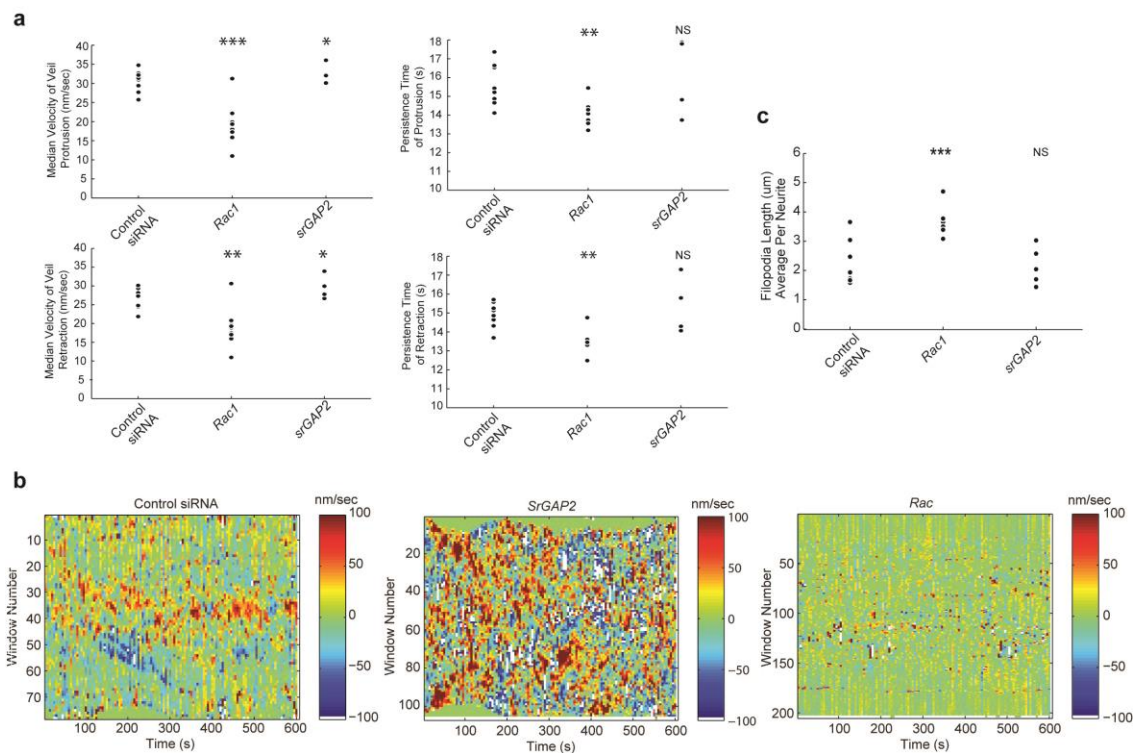
Figure 6. Comparison of select structural/dynamic features corresponding to Rac1KD and srGAP2KD, a putative Rac1 Deactivator via Automated Growth Cone Quantification. (**a**) Quantification of local veil protrusion/retraction persistence and velocity as described in Figure 2b. Each point represents the average value per neurite for the entire 10 minute movie. (N = 5-9 growth cones per condition, ~12500-30000 protrusion and retraction measurements per condition). (**b**) Representative Veil Protrusion/Retraction velocity maps quantified as described in Figure 3b comparing Rac1 KD and srGAP2 KD. Each map is from a single neurite. (**c**) Automated quantification of growth cone filopodia lengths. Each point represents the average value per neurite for the entire 10 minute movie. (N = 5-9 growth cones per condition, 16700- 49000 filopodia measurements total per condition. Filopodia were filtered such that only those attached to the neurite veil or shaft were used in the measurement). *** =p<0.001 given a non-parametric, permutation t-test of the means testing KD compared to control

121
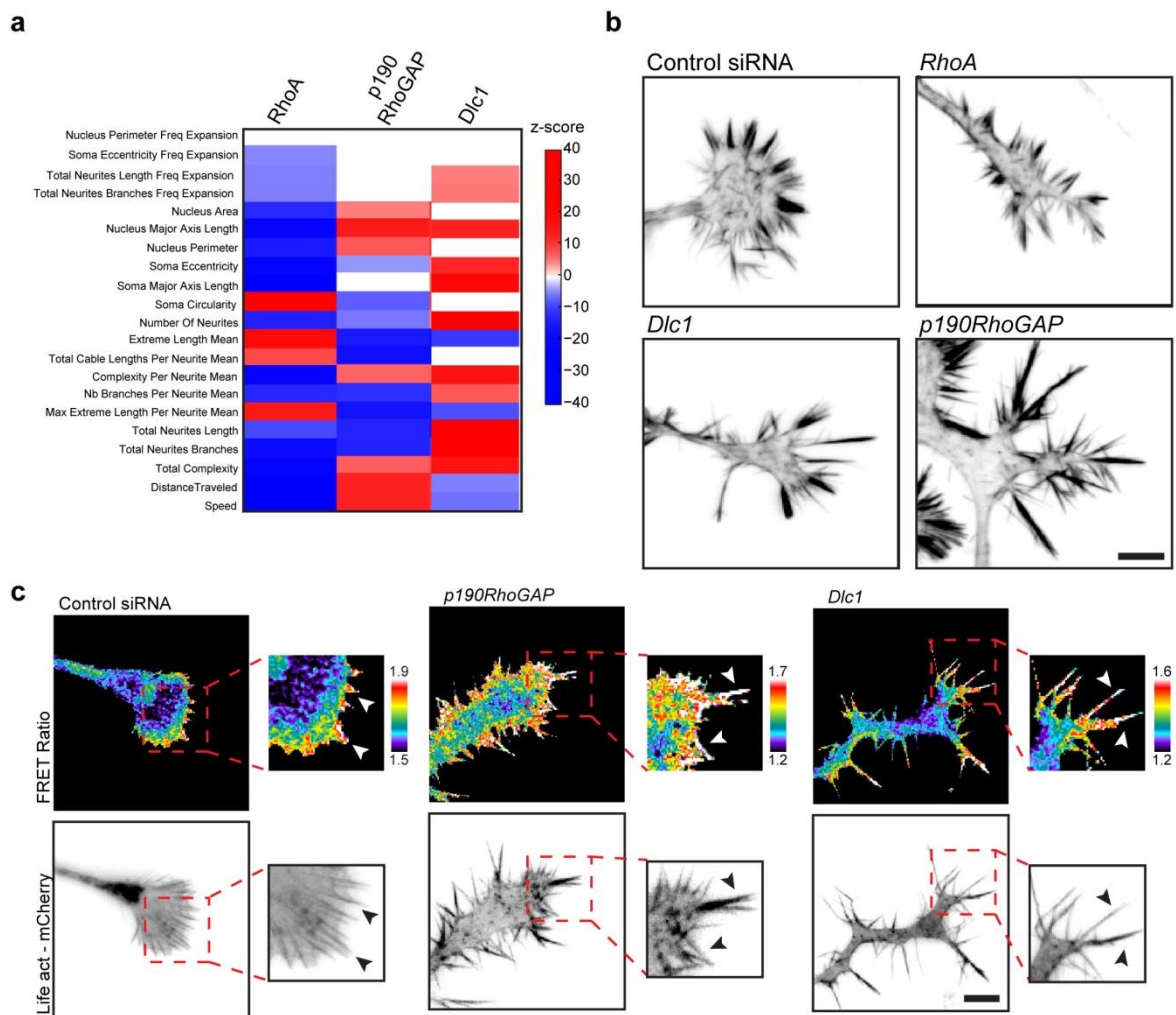
Figure 7: Monitoring of RhoA fret probe activity during p190RhoGAP and Dlc1 KDs. (**a**) MDS analysis of RhoA, p190RhoGAP and Dlc1 KD experiments. (**b**) Representative images of phalloidin stainings of RhoA, p190rhoGAp and Dlc1 KD growth cones. Scale bar = 30μm (**c**) Big squares: RhoA fret Ratio and Lifeact mCherry representative images of control siRNA, p190RhoGAP and Dlc1 KDs. Small square: Detailed images of RhoA fret Ratio and Lifeact mCherry in filopodia. Ratio images are color-coded according to activation intensity. Scale bar = 10μm.

5. Discussion

Neurite outgrowth is an early stage of neuronal development, in which a tubulin-rich protrusion called the neurite, extends outwards from the cell soma. Neurites contain a distinctive actin-rich tip, called the growth cone, which acts as a sensing machinery of the extracellular environment to promote neurite outgrowth and cell migration (da Silva and Dotti 2002). Neurite outgrowth is regulated by several protein families, including small GTPases, PI3K and the PAR complex (Luo 2000; Nishimura et al. 2004; Sanchez et al. 2004; Nishimura et al. 2005; Read and Gorman 2009). In particular, the three main GTPases, RhoA, Rac1 and Cdc42, appear to have a crucial role in the regulation of this process. Classic studies, using DN and CA mutant forms of Rho GTPases, have suggested that Rac1 and Cdc42 promote neurite protrusion, while RhoA controls neurite retraction (da Silva and Dotti 2002). This simplistic seems outdated in light of recent proteomic, bioinformatics and cell biological analysis, which highlight the possible existence of a large network of Rho GTPases, GEFs, GAPs and effector proteins that may be involved in the regulation of neurite outgrowth (Pertz et al. 2008; Pertz 2010)

High content screening platform for the automatic analysis of neurite outgrowth morphodynamics.

We took advantage of our recent proteomic analysis in N1E-115 cells, using purified neurite and soma fractions (Pertz et al. 2008), to identify a Rho GTPase centered interactome, consisting of 220 different proteins, including Rho GTPases, GEFs, GAPs, effectors and interacting proteins. Based upon the knowledge that neurite outgrowth is a dynamic process involving the spatiotemporal activation of Rho GTPases (Pertz et al. 2006; Fritz et al. 2013), we created a high content screening platform characterized by semi-automatic live cell imaging coupled to cutting edge computer vision methods to perform segmentation, tracking and analysis of timelapse movie datasets. This approach allowed us to conduct a multiparametric analysis of neurite outgrowth dynamics, which offers more insight into this process when compared to classical steady state studies which typically use fewer parameters. We used this platform to screen a library of 660 siRNAs, corresponding to the 220 proteins identified in a Rho GTPases centered interactome, in N1E-115 cells. For each of the genes analyzed, we obtained a unique morphodynamic signature (MDS) that highlights the morphological and dynamic differences between a specific gene and an in-plate negative control siRNA (Figure 1).

High content screen platform
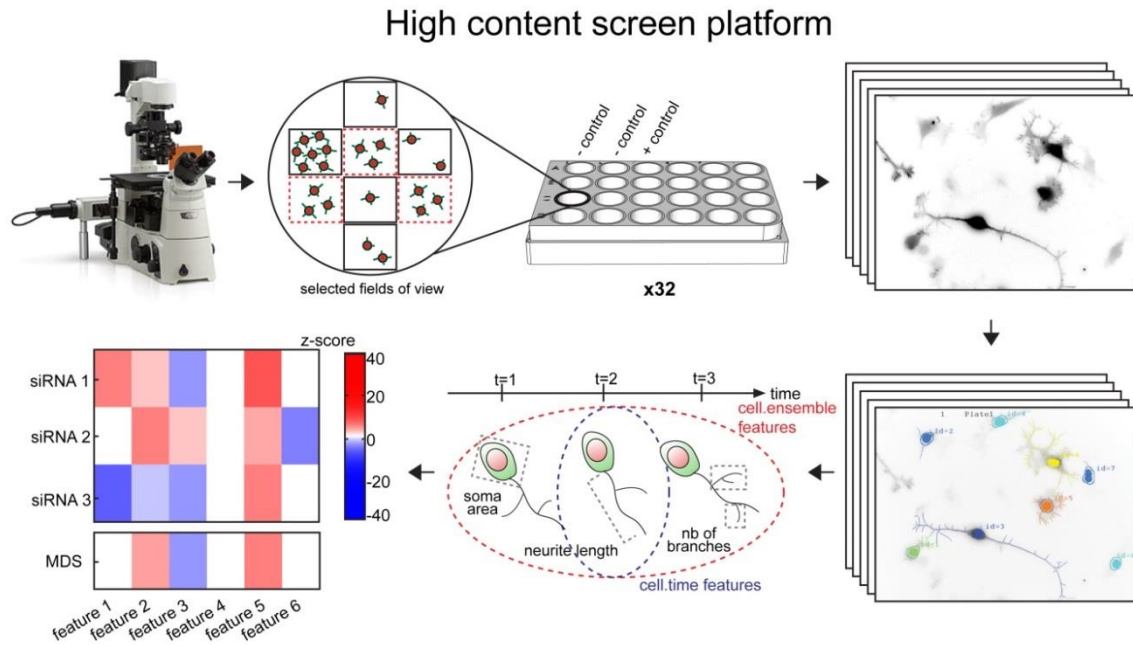
Figure 1. High content screening platform. Schematic of the high content screening platform developed to study live cell imaging neurite outgrowth morphodynamics. 20hr live cell imaging timelapse experiments are acquired upon semi-automatic selection of adequate fields of view. The movies are then segmented and tracked using a newly designed computer vision tracking and segmentation pipeline. The results are analyzed to obtain the MDS for each KD experiment.

Temporal analysis highlights the existence of two distinct phases of differentiation

Neuronal differentiation includes multiple dynamic steps, which have only been verbally described (Higgins et al. 1997; da Silva and Dotti 2002) but not rigorously quantified. In order to gain insight about the different phases that characterize this process, we analyzed the morphodynamic evolution of the differentiation of our negative control siRNA experiments. We pooled together the control siRNA movies from our whole siRNA screen (320 movies) and then we divided the 20 hour movies into bins of 1 hour. Subsequently, we compared specific features, such as neurite length, soma speed, number of branches and neurites between the different bins (Figure 2).

The results of this analysis highlighted the existence of two distinct phases of differentiation. The first phase, which we named the protrusion/retraction phase, is characterized by cells with low motility, and many short and branched neurites (Figure 2, upper right panel, extreme length from time 0 to 10 hours). We believe that in this phase, cells start to sense the environment by protruding and then rapidly retracting many short neurites. The second phase, which we termed the elongation phase, is characterized by cells with high motility, and few long and unbranched neurites, which extend without

retracting (Figure 2, upper right panel, extreme length from time 10 to 20 hours). These data suggest the existence of two distinct genetic programs that control different phases of neuronal differentiation in our *in vitro* model system (Figure 2, left panel).

Furthermore, we applied the same approach to the experiments involving the Mkk7 KD positive control, which was characterized by a short neurite phenotype. We have previously shown that Mkk7 is part of a JNK signaling module that controls MAP1b phosphorylation, which in turn controls microtubule bundling in the neurite to promote its elongation (Feltrin et al. 2012). The results of the temporal analysis show that in the first differentiation phase, Mkk7 KD leads to a burst of neurite outgrowth (Figure 2, lower right panel, extreme length from time 0 to 10 hours), which we had not previously detected by visual inspection of timelapse movies. However, in the second phase, Mkk7 KD cells displayed an inability to extend their neurites, instead showing a decrease in neurite length (Figure 2, lower right panel, extreme length from time 10 to 20 hours), consistent with what we have previously seen (Feltrin et al. 2012). It is interesting to note that, besides triggering the phosphorylation of MAP1b, JNK also activates another protein called doublecortin (Gdalyahu et al. 2004), which is a MAP that regulates microtubules stabilization (Horesh et al. 1999). Therefore we speculate that the Mkk7-JNK module could act in two distinct phases of neuronal outgrowth, regulating microtubule stabilization during neurite protrusion/retraction via phosphorylation of doublecortin, and microtubule bundling during neurite extension via MAP1b phosphorylation. It is very interesting to note that besides neurite length, other parameters follow exactly the same temporal evolution in the negative control and Mkk7 KD experiments, suggesting the existence of an intrinsic mechanism of regulation that allows the cells to follow a precise program of temporal differentiation during neurite outgrowth.
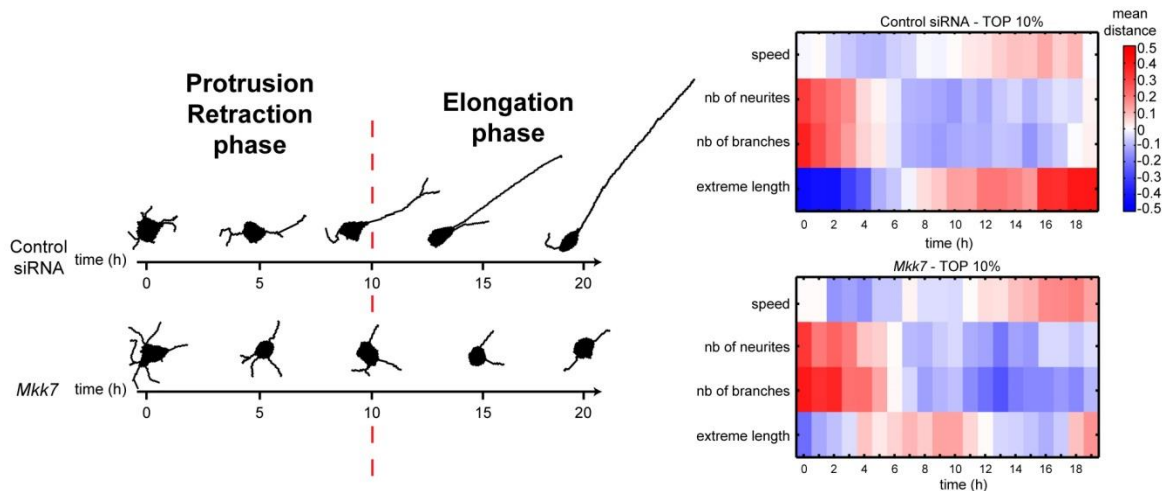
Figure 2. Temporal analysis of neurite outgrowth morphodynamics. 20 hours movies were divided in 1 hour bins to analyze the morphodynamic evolution of specific features. Control siRNA cells analysis shows the existence of two different phases of differentiation termed protrusion/retraction, and elongation. Mkk7 KD, which is known to have a defect in neuronal outgrowth, shows an absence of the elongation phase.

MDS analysis highlights the existence 4 precise phenotypical subgroups.

The high content pipeline was used to analyze movies derived from experiments in which 220 genes of a potential Rho GTPase signaling network were knocked down. As it was not possible to execute temporal analysis due to the limited amount of data acquired, we performed hierarchical clustering to identify sets of gene perturbations leading to a common MDS. As a result, we extracted 24 phenoclusters representing 183 out of the 220 genes. We then grouped these phenoclusters into 4 major subgroups, taking into account the most visually recognizable features, such as neurite length, number of branches, number of neurites and soma speed. These 4 subgroups, which we called: short neurite, multi short neurites, long and unbranched, long and branched, seem to resemble the different phases of neuronal differentiation (Figure 3).

However, in the short neurite subgroup (Figure 3, left panel), we could still identify three different morphodynamic phenotypes which have short neurites and few branches in common, but that can still be easily distinguished by soma speed. These results suggest that in the early stages of differentiation, the cells undergo a phase of protrusion and retraction of small neurites, while progressively polarizing and adopting a migrating shape, therefore increasing the overall speed of the soma. The other subgroup of the short neurites is the most interesting and probably the most challenging to interpret. In this group that we named multi short neurites (Figure 3, central panel), we identified cells with:

127

a large number of short neurites, many branches, and a fast and large migrating soma. This subgroup highlights the existence of an intermediate stage in the differentiation process. In this stage, upon a strong stimulus, polarized cells are able to switch from protruding/retracting to extending one or two very long neurites. In multi neurites, cells can protrude multiple neurites but are unable to undergo the extension phase.

Furthermore, we identified the existence of two subgroups consisting of long neurite phenotypes. These two subgroups can be distinguished from each other by the number of neurite branches (Figure 3. right panels). These subgroups highlight the existence of two different phases of neuronal extension. We speculate that in the first phase, cells undergo a stage of differentiation that allows the extension of one or two neurites. However, these same cells can undergo a supplementary growth phase that allows the formation of multiple branches. With regards to neuronal differentiation in primary neurons, we recognize two phases of extension: axonal differentiation and dendritic arborization (Higgins et al. 1997). Even though our cell system is not programmed to extend axons and dendrites, we speculate that these phases of neuronal differentiation can be compared to the two long neurite phenotype subgroups that we identified in our screen. All together these data suggest that the different subgroups identified through the hierarchical clustering of similar MDSs, resemble different stages of neuronal differentiation, and highlight the possibility of further exploring the molecular mechanisms that regulate these phases by investigating the genes included in each of these subgroups in primary neurons.
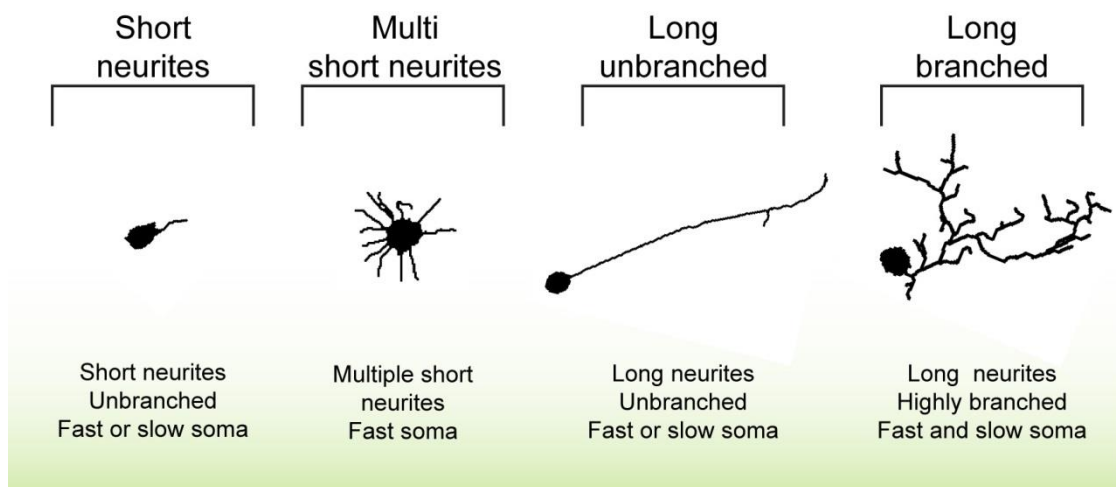
Figure 3. MDS analysis shows 4 phenotypical subgroups. Upon hierarchical clustering, genes with similar a MDS were sorted together. The analysis resulted in the extraction of 24 clusters, which were manually sorted into 4 discrete phenotypical subgroups. Taken together, these subgroups seem to represent the different phases of neuronal differentiation.
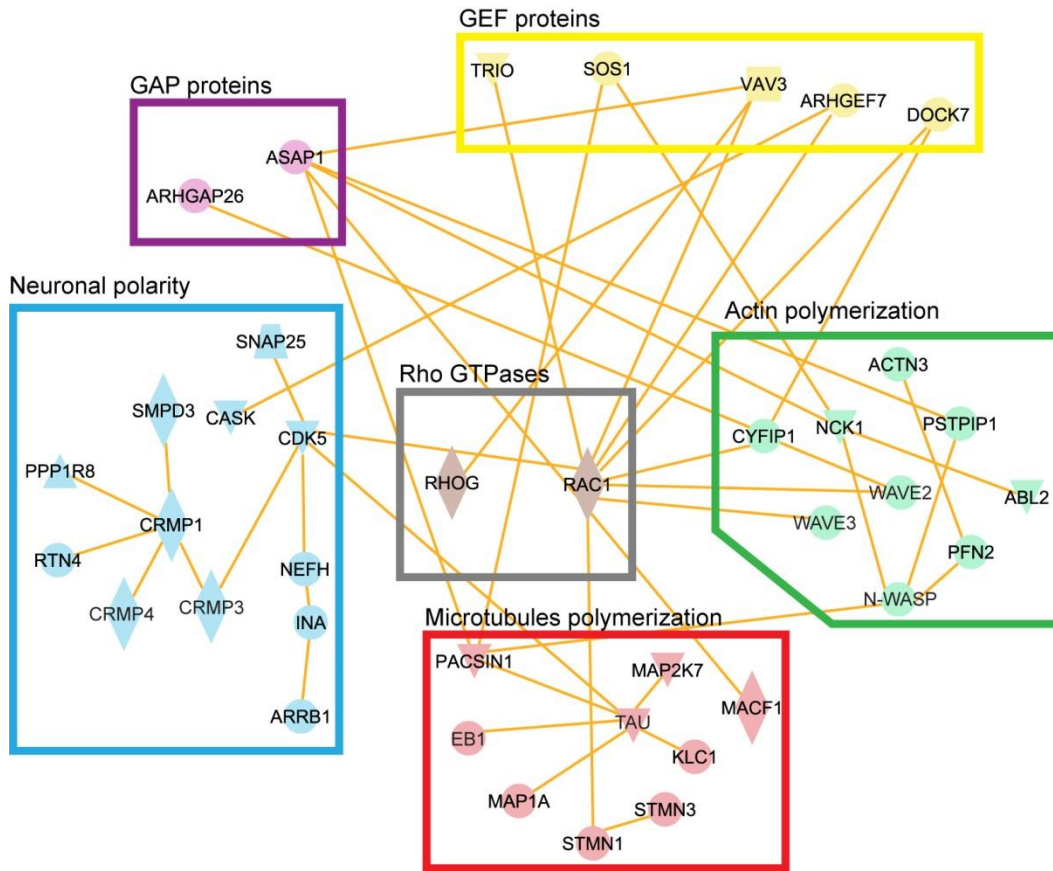
Rac1-mediated signaling modules regulate neurite protrusion and neuronal polarity

Rho GTPases are known to be main controller of the cytoskeleton during neurite outgrowth. Classic experiments, using CA and DN mutants coupled to steady state readouts, have led to a model in which Rac1 and Cdc42 promote neurite extension, while RhoA promotes neurite retraction (Kozma et al. 1997; Sarner et al. 2000). However the milder perturbation (siRNA) and the higher resolution that can be achieved with our imaging platform show important differences in the role of these proteins during neurite outgrowth.

We show that the KD of Rac1 induces a short neurite phenotype. We observed a similar phenotype upon the knock down of several other genes, which seem to be part of specific Rac1-centered signaling modules, involved in fine tuning the different processes of neurite outgrowth. Rac1 is known to control growth cone protrusion by promoting actin polymerisation via activation of the Arp2/3 complex through its effector Wave2 (Machesky et al. 1999). We found a first signaling module comprising several members of the WAVE complex, which promotes actin polymerisation (Figure 4, green box). The WAVE complex includes the adaptor proteins Nck1 and Abi2, as well as the interacting proteins CYFIP1 and CYFIP2. Nck1 is able to interact with activated Rac1 via CYFIP1, inducing the dissociation of the complex and the activation of Arp2/3, via the WAVE family of proteins (Bradley and Koleske 2009). In our screen all these members are clustered together in the same subgroup to which Rac1 belongs, confirming the existence of a signaling module that regulates actin polymerisation during neurite outgrowth. Moreover, we found different members of the WAVE family in the same cluster, such as Wave2 and N-Wasp. While Wave2 is known to be a Rac-1 effector (Tahirovic et al. 2010), it is interesting to note that N-Wasp is known to be a Cdc42 effector, confirming that this protein may also promote actin polymerisation during neurite outgrowth (Banzai et al. 2000).

Another signaling module that is clustered together with Rac1, involves several proteins that are known to be important in the regulation of neuronal polarity, in particular, the Rac1-effector, Cdk5, which is essential for neuronal migration (Nikolic et al. 1998) (Figure 4, blue box). Cdk5 concentrates at the leading edges of axonal growth cones and regulates neurite outgrowth in cultured cortical neurons, via the inhibition of Pak1 and

reorganization of the actin cytoskeleton (Nikolic et al. 1998). It is also interesting to note that together with Cdk5 the signaling module involves several members of the CRMP family of proteins. These proteins are able to bind the microtubules and build a robust bundle that allows the immature neurite to elongate in a mechanism that seems to have an important role during axonal specification (Wang and Strittmatter 1996). It is interesting to note that Cdk5 has been proved to interact with various members of the CRMP family of proteins (Yamashita et al. 2007; Brittain et al. 2012) suggesting that the Rac1-Cdk5 module could have a role in the regulation of neuronal polarity. In the Rac-1 subgroup we also found a signaling module that might regulate microtubule dynamics. Microtubules are important during neuronal development for maintaining elongated neurites and regulating growth speed (Drubin et al. 1985). Our data suggest a possible interaction between Rac1 and stathmin/Op18 in this module (Figure 4, red box). Stathmin/Op18 is a microtubule destabilizing protein that interacts with two molecules of the αβ-tubulin dimer, therefore inhibiting microtubule polymerisation and promoting microtubule catastrophe (Belmont and Mitchison 1996; Lawler 1998). It has been shown that Rac1 can induce stathmin/Op18 phosphorylation, inhibiting its activity and thereby inducing axonal growth (Lawler 1998). In this pathway, Rac1 is activated by a Rac1-specific GEF protein called Dock7, which is also part of the Rac1 subgroup, suggesting that the Dock7/Rac1/stathmin/Op18 module could have an important role in regulating microtubule polymerisation during neurite outgrowth (Lawler 1998).

Figure 4. Rac1-mediated signaling modules. The Rac1-subgroup consists of three different signaling modules regulating actin and microtubule polymerisation during neurite protrusion and neuronal polarity.

RhoA and Cdc42-mediated signaling modules regulate neurite retraction, filopodia formation and axonal guidance

The knock down of RhoA and Cdc42 lead to phenotypes which share a similar MDS, characterized by long and unbranched neurites. It is not surprising to find this phenotype upon RhoA KD, since this protein is known to promote neurite retraction (Borisoff et al. 2003). However, Cdc42, which has been suggested to regulate actin polymerisation via the activation of N-Wasp/Arp2/3, when knocked-down, shows a phenotype that is different from what has been shown before using DN Cdc42 constructs (da Silva and Dotti 2002). We found ROCK2 and MRCK in the same phenotypical subgroup as RhoA and Cdc42 (Figure 5, red box). ROCK2 and MRCK are known to have a role in the regulation of actomyosin contractility (Chen et al. 1999; Borisoff et al. 2003). In colorectal carcinoma, it has been shown that the simultaneous phosphorylation of MLC, induced by RhoA and

131

Cdc42, via ROCK and MRCK, is crucial to promote actomyosin contractility and guarantee proper migration (Wilkinson et al. 2005). However this cooperative mechanism between these two GTPases has never been shown in neuronal cells. Our results show the possibility that RhoA and Cdc42 may cooperate to regulate actomyosin contractility during neuronal differentiation in order to control neurite retraction.

Moreover, our data suggest that in the case of RhoA KD, the activation of ROCK and therefore the collapse of the neurite could be driven by different mechanisms involving two GEF proteins called GEF-H1 and PDZ-RhoGEF. GEF-H1 is a canonical GEF protein for RhoA, known to trigger the RhoA/ROCK/MLC signaling pathway in HeLa cells during tail retraction (Chang et al. 2008). In our screen, GEF-H1 KD leads to long neurites and a large number of branches. Interestingly, GEF-H1 has been shown to associate with microtubules, and it is also known that microtubule depolymerisation releases GEF-H1 to activate RhoA. Therefore, it has been proposed that GEFH1 could act as a mediator between actin polymerisation and microtubule dynamics (Krendel et al. 2002). However the role of this protein during neuronal differentiation has not been completely elucidated.

Receptor plexin B1 and the GEF PDZ-RhoGEF KDs lead to a phenotype with long neurites, similar to the knock down of RhoA, but in contrast to RhoA KD, receptor plexin B1 KD results in a large number of branches. In primary hippocampal neurons, the regulation of PDZ-RhoGEF by receptor plexin b1 leads to RhoA activation, upon semaphorin 4D stimulation. This activation of RhoA leads to MLC phosphorylation via ROCK and therefore induces growth cone retraction and collapse. Moreover, receptor plexin B1 is able to interact with GTP-bound Rac1, inducing Rac1 inhibition (Swiercz et al. 2002). Therefore, we speculate that the branched phenotype shown by receptor plexin b1 KD in our screen, could also be the result of the simultaneous loss of RhoA and activation of Rac1. It has been shown that semaphorins might function as a local repulsive cue, inducing growth cone turning and change in branching (Campbell et al. 2001). Therefore we suggest that, in the context of our cell system, the plexin b1-PDZ RhoGEF complex could act as a local regulator of growth cone repulsion. On the other hand, it has been shown that GEF-H1 leads to RhoA-induced contractility on a global scale (Chang et al. 2008). These data suggest that the plexin b-PDZ-RhoGEF and GEF-H1-mediated modules could function as a global and a local activator of RhoA-induced growth cone collapse. It will be of high interest in the future to elucidate when and where these two mechanisms of RhoA/ROCK/MLC pathway activation are induced during the neurite outgrowth process.

The results of our screen suggest the existence of a second RhoA-related module, which could be implicated in regulating local actin polymerisation (Figure 5, green box). This module is characterized by a specific RhoA effector, called mDIA, a formin protein, which is able to use profilin-bound actin monomers for filament nucleation (Li and Higgs 2003). Therefore, via the activation of this effector, RhoA is able to promote polymerisation of unbranched actin filaments (da Silva and Dotti 2002). In our screen mDIA is part of a module consisting of several molecules which are known to induce actin polymerisation via the Arp2/3 complex. One of these molecules is IRSp53, an adaptor protein that induces filopodia formation via interaction with various actin regulators, such as mDIA and Wave1 (Goh et al. 2012). Therefore we speculate that the activation of mDIA via RhoA could induce formin-driven actin polymerisation in the filopodia. This hypothesis is also supported by FRET experiments, which show a spatio-temporal activation pattern of RhoA at the filopodia tip during growth cone protrusion (Fritz et al. 2013).

It is interesting to note that in the RhoA-Cdc42 long and unbranched neurite subgroup, it is possible to identify a module that controls neuronal polarity and axonal guidance (Figure 5, blue box). This module includes the tuberous sclerosis complex (Tsc1-Tsc2) and the Ras family GTPase, Rheb. Tsc1 and Tsc2 are tumor suppressor proteins that when mutated can lead to the tuberous sclerosis disease. The Tsc1-Tsc2 complex acts as a GAP protein by stimulating GTP hydrolysis, consequently inhibiting Rheb activity. GTP-Rheb acts upstream of mammalian target of rapamycin (mTOR), stimulating the phosphorylation of ribosomal S6 kinase (S6K) and 4E-binding protein 1 (4E-BP1), which function to increase mRNA translation (Inoki et al. 2003; Kwiatkowski and Manning 2005). This pathway seems to be involved in the regulation of neuronal polarity/axon formation. Inactivation of Tsc1-Tsc2 allows the nascent axon to initiate and maintain its growth during mTOR-induced local mRNA translation (Choi et al. 2008). The Tsc1-Tsc2/Rheb pathway is considered to be directly regulated by PI3K/Akt (Kwiatkowski and Manning 2005). Moreover it has been shown that the Tsc complex is able to regulate Cdc42 activity, upon inhibition of PI3K activity, suggesting a possible relationship between the molecular machineries that regulate actin cytoskeleton and neuronal polarity (Larson et al. 2010).
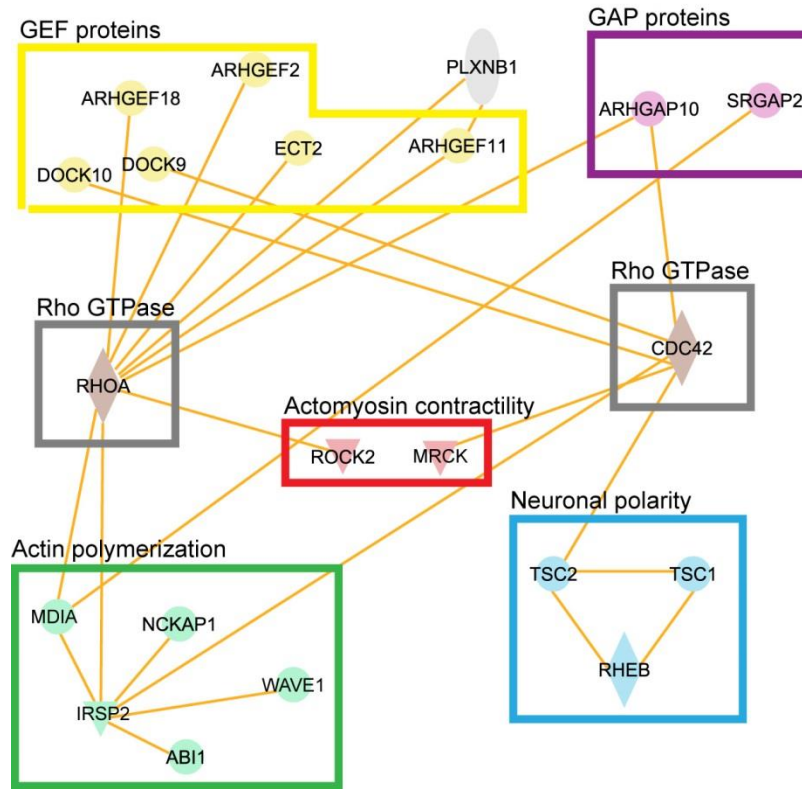
Figure 5. RhoA-Cdc42-mediated signaling modules. RhoA and Cdc42 cooperate to regulate neurite retraction. RhoA appears to be involved in filopodia-related actin polymerisation and Cdc42 cooperates with the Trc1/Trc2/Rheb complex to regulate actin cytoskeleton and neuronal polarity

High resolution morphodynamic signature demonstrates the existence of a Rac1-centered signaling module controlling growth cone veil protrusion.

The results of our screen revealed a strong phenotypical redundancy, which resulted in only 4 phenotypical subgroups among 220 gene MDSs analyzed. The resolution that has been used in the screen (tenth of minutes and tenth of microns) only allows the characterization of global events that occur during neurite outgrowth. However, in the process of growth cone navigation, the dynamics of the actin cytoskeleton in the growth cone and filopodia fluctuate on scales of single seconds and single microns (Jang et al. 2010). Moreover, it is known that Rho GTPases fine tune specific events due to their involvement in spatio-temporal signaling modules. These modules are made up of GEF, GAP and effector proteins, which are localized to a confined subcellular domain, to the order of micrometers of length, and occur in a time shift to the order of tens of seconds (Machacek et al. 2009). Therefore we decided to further investigate a defined subset of

genes, and to quantify the dynamic phenotypes in the growth cones and filopodia of N1E-15 cell. The results revealed that the phenotypical redundancy obtained in the screen could be derived from the perturbation of defined spatio-temporal localized signaling modules, leading to an analogous global effect on the neurite outgrowth process. We decided to use a high resolution (HR), high magnification (HM) imaging approach, together with sophisticated computer vision tools for the analysis of growth cone and filopodia morphodynamics, in order to determine how the localized actin cytoskeleton morphology and dynamics of the growth cone may contribute to neurite outgrowth on a global scale. We started by selecting two smaller subsets of KD genes previously analyzed in our lower resolution (LR) neurite outgrowth screen. We concentrated on the three canonical Rho GTPases, RhoA, Rac1 and Cdc42. We then also studied a potential Rac centered signaling module that contains the Rac1 GEFs, Beta-Pix, Trio, Dock7 (Bellanger et al. 2000; Pinheiro and Gertler 2006; ten Klooster et al. 2006) and the Rac1 GAP protein called SrGAP2 (Guerrier et al. 2009). For each of these genes we obtained an HR MDS, which provides specific information about the morphology and dynamics of the different components within the growth cone, such as the actin veil and the filopodia.
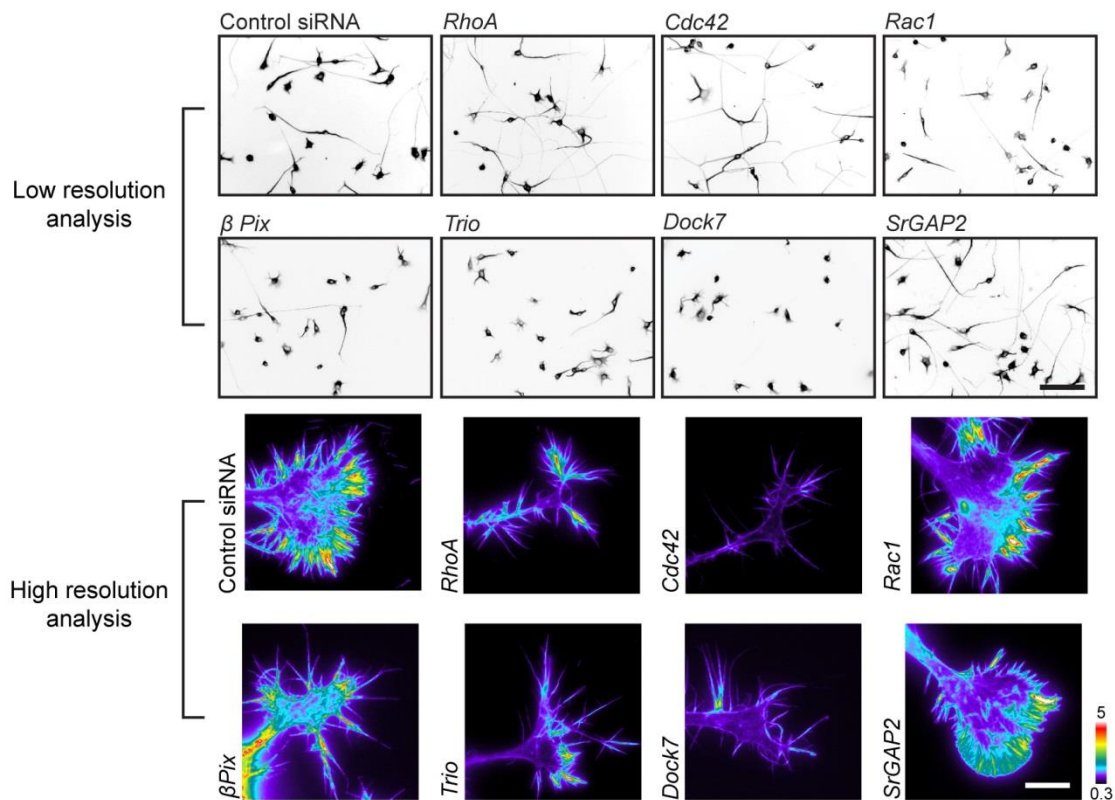
Figure 6. Low resolution vs High resolution phenotypes. HR resolution growth cone analysis allows the characterization of different local phenotypes, in within genes which have redundant phenotypes at LR. Scale bar: Upper panel, 50 µm, Lower panel, 10 µm.

Our results demonstrate that HR analysis of different KD experiments can reveal differences between various conditions that cannot be analyzed at LR. In our LR screen, we demonstrated loss of growth cone collapse and neurite retraction in RhoA and Cdc42 KD cells, resulting in a long unbranched neurite outgrowth phenotype (Figure 6, Upper panel). Using our HR MDS, we were able to demonstrate that RhoA and Cdc42 produce different growth cone morphologies (Figure 6, Lower panel). These dissimilarities hint at the possibility of different mechanisms of regulating neurite retraction. On the other hand, the LR profile of Rac1 KD cells shows a defect in neurite protrusion (Figure 6, Upper panel). However it is interesting to note that HR growth shape doesn't show any particular visual differences compared to control siRNA (Figure 6, Lower panel). In addition the three GEF proteins, Trio, Dock7 and β-Pix KDs, seem to phenocopy Rac1 LR MDS with a short neurite phenotype (Figure 6, Upper panel). However HR resolution images show strong differences in growth cone morphologies resulting from the knock down of these genes. In particular KD of Trio leads to a thin growth cone veil with protruding filopodia outward from the veil, which occasionally can crisscross. β-Pix KD also leads to thin growth cone morphology with protruding filopodia. Dock7 KD shows thin filopodia actin bundles protruding outward from the veil (Figure 6, Lower panel).

It is interesting to note that while these genes phenocopy each other at LR, they show clear morphological differences at HR. Moreover, when we analyzed growth cone and veil dynamics in live cell imaging HR movies, we were able to demonstrate that Rac1, Trio and Dock7 are characterized by a complete immobile veil, which seems to be responsible for their low neurite outgrowth profile. Rac1 is known to participate in neurite protrusion, enhancing Arp2/3-driven actin polymerisation (Machesky et al. 1999; Smith and Li 2004). Therefore, the absence of Rac1 may have an impact on the polymerisation of the actin network that forms the veil and drives robust growth cone advance, and these two GEFs may also regulate this process (Figure 7). Surprisingly, β-Pix KD shows a more dynamic veil, corresponding to higher growth cone dynamics compared to Rac1 and the other two GEF proteins, while still having a global LR short neurite phenotype, suggesting that β-Pix may possibly be involved in a Rac1-dependent mechanism that regulates growth cone and veil dynamics (Figure 7). Moreover, Trio and Dock7 KD, which both share the growth cone and veil dynamic phenotypes of Rac1, are also characterized by morphological differences

in the filopodia, which suggest their possible involvement in the regulation of different filopodia processes (Figure 7). Finally, KD of the Rac-specific GAP protein, SrGAP2 leads to enhanced veil formation (Figure 6, Lower panel). This translates in robust growth cone protrusion characterized by increase in both the velocity and persistence of veil dynamics (Figure 7). These data suggest that SrGAP2 might be the GAP that specifically controls the spatio-temporal Rac1 pool that regulates veil formation. This also suggests that SrGAP2 produces a long and branched phenotype on a global level (Figure 6, Upper panel), simply by stabilizing the growth cone. All together these results highlight the existence of a possible Rac1-centered interactome, involving different GEF and GAP proteins. It will be interesting in the future to investigate the different phenotypes at high resolution in order to gain insight about possible relationships between global and local scales.
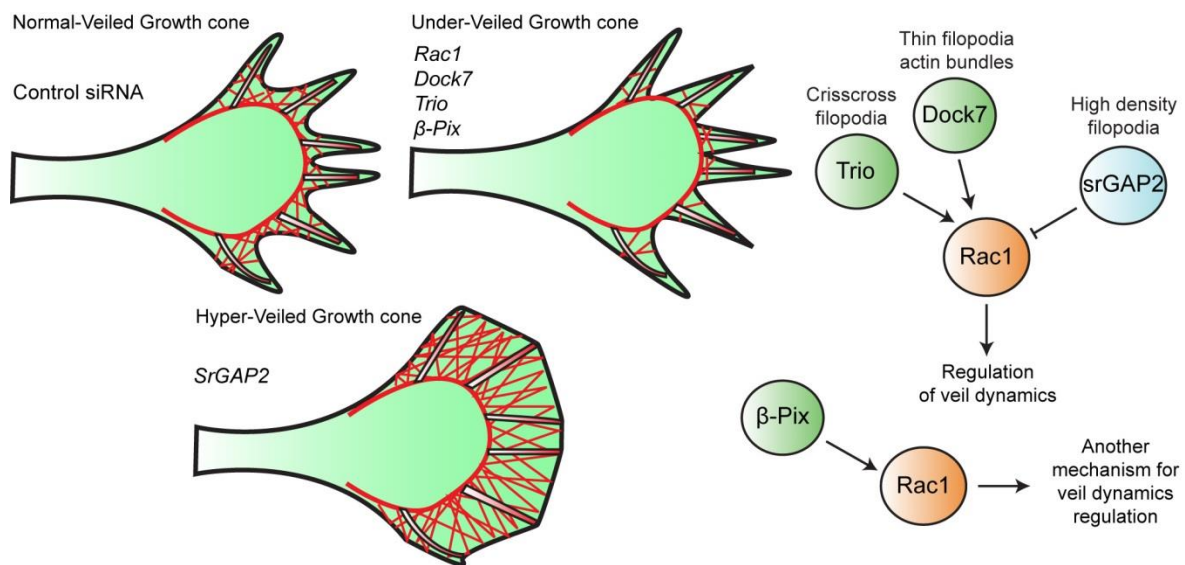
Figure 7. Rac1-centered signaling module controls veil dynamics. Low resolution Rac1 and two GEF proteins, Trio and Dock7, show a decrease in growth cone dynamics, which is also characterized by a veil immobility. On the other hand, SrGAP2, a specific GAP protein for Rac1, shows enhanced growth cone and veil dynamics. Our data suggest that Rac1 could have an important role in the regulation of veil dynamics. In this scenario two GEFs, Trio and Dock, and a GAP, SrGAP2, could participate to this module by modulating Rac1 activity. Moreover the two GEFs show specific filopodia phenotypes that suggest their involvement in the regulation of different filopodia processes.

p190RhoGAP and DLC1 control the spatio-temporal activation of RhoA during neurite retraction and filopodia protrusion.

Another example of how our siRNA screen can shed light on specific Rho GTPase spatio-temporal signaling modules is illustrated by the study of the RhoA specific GAPs: p190RhoGAP and Dlc1 (Arthur and Burridge 2001; Ullmannova-Benson et al. 2009).

The classic dogma proposes that RhoA controls contractility necessary for growth cone collapse (Kozma et al. 1997). Consistently, RhoA KD results in loss of collapse leading to long unbranched neurites. However, recent data from our lab show two distinct spatio-temporal pools of RhoA activity in growth cones, suggesting that 1) RhoA is activated at the tip of filopodia actin bundles during growth cone protrusion, and 2) RhoA is activated globally in the growth cone during collapse (Fritz et al. 2013).

These results clearly show the existence of two different RhoA spatio-temporal signaling modules involved in different cellular processes, which might be regulated by different GEFs and GAPs at specific subcellular localizations. Examination of our siRNA screen revealed that the KD of two RhoA specific GAPs, called p190RhoGAP and DLC1, lead to completely different phenotypes.

KD of p190RhoGAP leads to highly unstable short neurites, while KD of DLC leads to longer, branched neurites. In order to reconcile this observation we performed experiments using the RhoA FRET probe (Fritz et al. 2013) to monitor the activity of this GTPase during the KD of these two GAP proteins. Upon p190RhoGAP KD, RhoA activation increases widely in the filopodia and in the p-domain of the growth cone. It has been shown that RhoA inactivation via p190RhoGAP is crucial for the establishment of polarity, and contributes to both membrane protrusion and cell elongation (Arthur and Burridge 2001). Moreover, p190RhoGAP has been shown to enhance neurite outgrowth via RhoA inactivation in PC12 cells (Jeon et al. 2012). Therefore we suggest that p190RhoGAP could be involved in the regulation of RhoA during neurite retraction in N1E-115 cells (Figure 8, left panel). On the other hand upon Dlc1 KD, RhoA seems to be active specifically along the entire filopodia bundle but not in the p-domain. In addition, our high content screen data suggest that Dlc1 does not affect the ability of RhoA to induce neurite retraction. We therefore speculate that Dlc1 could be the GAP protein controlling RhoA activation at the tip of the filopodia (Figure 8, right panel). These experiments clearly suggest that p190RhoGAP and Dlc1 control distinct spatio-temporal RhoA pools, with distinct functions. Indeed it will be very interesting to confirm the existence of these two separate modes of RhoA activation by characterizing GEFs and effector proteins involved in the regulation of these processes.
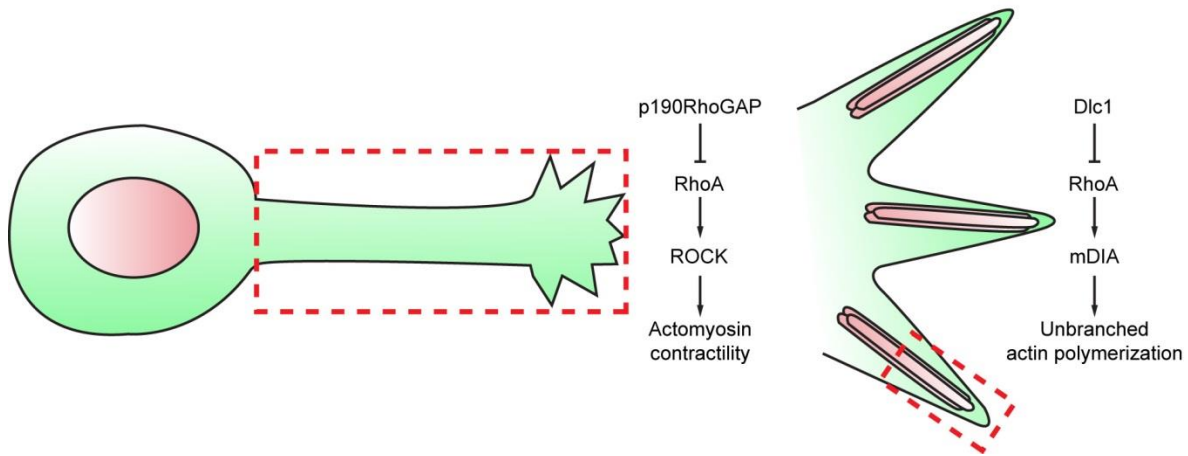
Figure 8. p190RhoGAp and Dlc1 control RhoA-driven neurite retraction and filopodia formation. FRET experiments revealed differences in the pattern of RhoA activation upon p190RhoGAP and Dlc1 KD. Our data suggest that p190RhoGAP could control RhoA-driven neurite retraction via ROCK/MLC phosphorylation, while Dlc1 could regulate RhoA-driven filopodia formation via its effector, mDIA.

Concluding remarks

We developed a platform for high content screening that allowed the analysis of neurite outgrowth morphodynamic signatures (MDSs) of a potential Rho GTPase-centered interactome. We demonstrated the existence of six phenotypical clusters that resemble different stages of neuronal development. Each of these clusters contained specific signaling networks that could fine tune precise events during neurite outgrowth. We investigated some of the phenotypes discovered during the screening process further using a high resolution approach, detecting the existence a local Rac1-centered spatio-temporal signaling module controlling growth cone veil dynamics. All together these results highlight the great complexity of the Rho GTPase signaling network in the regulation of neurite outgrowth, and the existence of specific spatio-temporal signaling modules that regulate different events during this process. This paves the way for further work, in which some of these phenotypes will be analyzed at higher time/length scales, using functional assays such as FRET technology. In the long term, this might provide a comprehensive systems biology view of the spatio-temporal Rho GTPase network regulating neurite outgrowth.

6. References

Abe T, Kato M, Miki H, Takenawa T, Endo T. 2003. Small GTPase Tc10 and its homologue RhoT induce N-WASP-mediated long process formation and neurite outgrowth. *Journal of cell science* **116**: 155-168.

Aebi U, Cohn J, Buhle L, Gerace L. 1986. The nuclear lamina is a meshwork of intermediate-type filaments. *Nature* **323**: 560-564.

Aghazadeh B, Zhu K, Kubiseski TJ, Liu GA, Pawson T, Zheng Y, Rosen MK. 1998. Structure and mutagenesis of the Dbl homology domain. *Nature structural biology* **5**: 1098-1107.

Al-Bassam J, Ozer RS, Safer D, Halpain S, Milligan RA. 2002. MAP2 and tau bind longitudinally along the outer ridges of microtubule protofilaments. *The Journal of cell biology* **157**: 1187-1196.

Alberts AS. 2001. Identification of a carboxyl-terminal diaphanous-related formin homology protein autoregulatory domain. *The Journal of biological chemistry* **276**: 2824-2830.

Allen C, Borisy GG. 1974. Structural polarity and directional growth of microtubules of Chlamydomonas flagella. *Journal of molecular biology* **90**: 381-402.

Amano M, Ito M, Kimura K, Fukata Y, Chihara K, Nakano T, Matsuura Y, Kaibuchi K. 1996. Phosphorylation and activation of myosin by Rho-associated kinase (Rho-kinase). *The Journal of biological chemistry* **271**: 20246-20249.

Aoki J, Katoh H, Mori K, Negishi M. 2000. Rnd1, a novel rho family GTPase, induces the formation of neuritic processes in PC12 cells. *Biochemical and biophysical research communications* **278**: 604-608.

Aoki K, Nakamura T, Matsuda M. 2004. Spatio-temporal regulation of Rac1 and Cdc42 activity during nerve growth factor-induced neurite outgrowth in PC12 cells. *The Journal of biological chemistry* **279**: 713-719.

Arthur WT, Burridge K. 2001. RhoA inactivation by p190RhoGAP regulates cell spreading and migration by promoting membrane protrusion and polarity. *Molecular biology of the cell* **12**: 2711-2720.

Ballestrem C, Wehrle-Haller B, Hinz B, Imhof BA. 2000. Actin-dependent lamellipodia formation and microtubule-dependent tail retraction control-directed cell migration. *Molecular biology of the cell* **11**: 2999-3012.

Banzai Y, Miki H, Yamaguchi H, Takenawa T. 2000. Essential role of neural Wiskott-Aldrich syndrome protein in neurite extension in PC12 cells and rat hippocampal primary culture cells. *The Journal of biological chemistry* **275**: 11987-11992.

Barfod ET, Zheng Y, Kuang WJ, Hart MJ, Evans T, Cerione RA, Ashkenazi A. 1993. Cloning and expression of a human CDC42 GTPase-activating protein reveals a functional SH3-binding domain. *The Journal of biological chemistry* **268**: 26059-26062.

Barry ST, Flinn HM, Humphries MJ, Critchley DR, Ridley AJ. 1997. Requirement for Rho in integrin signalling. *Cell adhesion and communication* **4**: 387-398.

Bellanger JM, Astier C, Sardet C, Ohta Y, Stossel TP, Debant A. 2000. The Rac1- and RhoG-specific GEF domain of Trio targets filamin to remodel cytoskeletal actin. *Nature cell biology* **2**: 888-892.

Belmont LD, Mitchison TJ. 1996. Identification of a protein that interacts with tubulin dimers and increases the catastrophe rate of microtubules. *Cell* **84**: 623-631.

Benink HA, Bement WM. 2005. Concentric zones of active RhoA and Cdc42 around single cell wounds. *The Journal of cell biology* **168**: 429-439.

Bernstein BW, Bamburg JR. 1982. Tropomyosin binding to F-actin protects the F-actin from disassembly by brain actin-depolymerizing factor (ADF). *Cell motility* **2**: 1-8.

Billuart P, Winter CG, Maresh A, Zhao X, Luo L. 2001. Regulating axon branch stability: the role of p190 RhoGAP in repressing a retraction signaling pathway. *Cell* **107**: 195-207.

Boguski MS, McCormick F. 1993. Proteins regulating Ras and its relatives. *Nature* **366**: 643-654.

Borisoff JF, Chan CC, Hiebert GW, Oschipok L, Robertson GS, Zamboni R, Steeves JD, Tetzlaff W. 2003. Suppression of Rho-kinase activity promotes axonal growth on inhibitory CNS substrates. *Molecular and cellular neurosciences* **22**: 405-416.

Bradley WD, Koleske AJ. 2009. Regulation of cell migration and morphogenesis by Abl-family kinases: emerging mechanisms and physiological contexts. *Journal of cell science* **122**: 3441-3454.

Brittain JM, Wang Y, Eruvwetere O, Khanna R. 2012. Cdk5-mediated phosphorylation of CRMP-2 enhances its interaction with CaV2.2. *FEBS letters* **586**: 3813-3818.

Brose K, Tessier-Lavigne M. 2000. Slit proteins: key regulators of axon guidance, axonal branching, and cell migration. *Current opinion in neurobiology* **10**: 95-102.

Brouns MR, Matheson SF, Settleman J. 2001. p190 RhoGAP is the principal Src substrate in brain and regulates axon outgrowth, guidance and fasciculation. *Nature cell biology* **3**: 361-367.

Brugnera E, Haney L, Grimsley C, Lu M, Walk SF, Tosello-Trampont AC, Macara IG, Madhani H, Fink GR, Ravichandran KS. 2002. Unconventional Rac-GEF activity is mediated through the Dock180-ELMO complex. *Nature cell biology* **4**: 574-582.

Buchwald G, Hostinova E, Rudolph MG, Kraemer A, Sickmann A, Meyer HE, Scheffzek K, Wittinghofer A. 2001. Conformational switch and role of phosphorylation in PAK activation. *Molecular and cellular biology* **21**: 5179-5189.

Burns RG. 1991. Alpha-, beta-, and gamma-tubulins: sequence comparisons and structural constraints. *Cell motility and the cytoskeleton* **20**: 181-189.

Burridge K, Fath K, Kelly T, Nuckolls G, Turner C. 1988. Focal adhesions: transmembrane junctions between the extracellular matrix and the cytoskeleton. *Annual review of cell biology* **4**: 487-525.

Calderwood DA, Ginsberg MH. 2003. Talin forges the links between integrins and actin. *Nature cell biology* **5**: 694-697.

Campbell DS, Regan AG, Lopez JS, Tannahill D, Harris WA, Holt CE. 2001. Semaphorin 3A elicits stage-dependent collapse, turning, and branching in Xenopus retinal growth cones. *The Journal of neuroscience : the official journal of the Society for Neuroscience* **21**: 8538-8547.

Carlier MF, Laurent V, Santolini J, Melki R, Didry D, Xia GX, Hong Y, Chua NH, Pantaloni D. 1997. Actin depolymerizing factor (ADF/cofilin) enhances the rate of filament turnover: implication in actin-based motility. *The Journal of cell biology* **136**: 1307-1322.

Chang YC, Nalbant P, Birkenfeld J, Chang ZF, Bokoch GM. 2008. GEF-H1 couples nocodazole-induced microtubule disassembly to cell contractility via RhoA. *Molecular biology of the cell* **19**: 2147-2153.

Chen XQ, Tan I, Leung T, Lim L. 1999. The myotonic dystrophy kinase-related Cdc42-binding kinase is involved in the regulation of neurite outgrowth in PC12 cells. *The Journal of biological chemistry* **274**: 19901-19905.

Cherfils J, Chardin P. 1999. GEFs: structural basis for their activation of small GTP-binding proteins. *Trends in biochemical sciences* **24**: 306-311.

Cherfils J, Zeghouf M. 2013. Regulation of small GTPases by GEFs, GAPs, and GDIs. *Physiological reviews* **93**: 269-309.

Chrzanowska-Wodnicka M, Burridge K. 1996. Rho-stimulated contractility drives the formation of stress fibers and focal adhesions. *The Journal of cell biology* **133**: 1403-1415.

Choi YJ, Di Nardo A, Kramvis I, Meikle L, Kwiatkowski DJ, Sahin M, He X. 2008. Tuberous sclerosis complex proteins control axon formation. *Genes & development* **22**: 2485-2495.

Chong KW, Lee AY, Koay ES, Seet SJ, Cheung NS. 2006. pH dependent high transfection efficiency of mouse neuroblastomas using TransFectin. *Journal of neuroscience methods* **158**: 56-63.

Chuang TH, Xu X, Kaartinen V, Heisterkamp N, Groffen J, Bokoch GM. 1995. Abr and Bcr are multifunctional regulators of the Rho GTP-binding protein family. *Proceedings of the National Academy of Sciences of the United States of America* **92**: 10282-10286.

Clark EA, King WG, Brugge JS, Symons M, Hynes RO. 1998. Integrin-mediated signals regulated by members of the rho family of GTPases. *The Journal of cell biology* **142**: 573-586.

Cohen CM, Tyler JM, Branton D. 1980. Spectrin-actin associations studied by electron microscopy of shadowed preparations. *Cell* **21**: 875-883.

Cooper JA, Buhle EL, Jr., Walker SB, Tsong TY, Pollard TD. 1983. Kinetic evidence for a monomer activation step in actin polymerization. *Biochemistry* **22**: 2193-2202.

Cox AD, Der CJ. 1992. Protein prenylation: more than just glue? *Current opinion in cell biology* **4**: 1008-1016.

Cox EA, Huttenlocher A. 1998. Regulation of integrin-mediated adhesion during cell migration. *Microscopy research and technique* **43**: 412-419.

Craig AM, Banker G. 1994. Neuronal polarity. *Annual review of neuroscience* **17**: 267-310.

Czuchra A, Wu X, Meyer H, van Hengel J, Schroeder T, Geffers R, Rottner K, Brakebusch C. 2005. Cdc42 is not essential for filopodium formation, directed migration, cell polarization, and mitosis in fibroblastoid cells. *Molecular biology of the cell* **16**: 4473-4484.

da Silva JS, Dotti CG. 2002. Breaking the neuronal sphere: regulation of the actin cytoskeleton in neuritogenesis. *Nature reviews Neuroscience* **3**: 694-704.

Da Silva JS, Medina M, Zuliani C, Di Nardo A, Witke W, Dotti CG. 2003. RhoA/ROCK regulation of neuritogenesis via profilin IIa-mediated control of actin stability. *The Journal of cell biology* **162**: 1267-1279.

Dan C, Nath N, Liberto M, Minden A. 2002. PAK5, a new brain-specific kinase, promotes neurite outgrowth in N1E-115 cells. *Molecular and cellular biology* **22**: 567-577.

Daniels RH, Hall PS, Bokoch GM. 1998. Membrane targeting of p21-activated kinase 1 (PAK1) induces neurite outgrowth from PC12 cells. *The EMBO journal* **17**: 754-764.

Daub H, Gevaert K, Vandekerckhove J, Sobel A, Hall A. 2001. Rac/Cdc42 and p65PAK regulate the microtubule-destabilizing protein stathmin through phosphorylation at serine 16. *The Journal of biological chemistry* **276**: 1677-1680.

David-Pfeuty T, Erickson HP, Pantaloni D. 1977. Guanosinetriphosphatase activity of tubulin associated with microtubule assembly. *Proceedings of the National Academy of Sciences of the United States of America* **74**: 5372-5376.

Dehmelt L, Halpain S. 2005. The MAP2/Tau family of microtubule-associated proteins. *Genome biology* **6**: 204.

Dotti CG, Sullivan CA, Banker GA. 1988. The establishment of polarity by hippocampal neurons in culture. *The Journal of neuroscience : the official journal of the Society for Neuroscience* **8**: 1454-1468.

Drewes G, Trinczek B, Illenberger S, Biernat J, Schmitt-Ulms G, Meyer HE, Mandelkow EM, Mandelkow E. 1995. Microtubule-associated protein/microtubule affinity-regulating kinase (p110mark). A novel protein kinase that regulates tau-microtubule interactions and dynamic instability by phosphorylation at the Alzheimer-specific site serine 262. *The Journal of biological chemistry* **270**: 7679-7688.

Drubin DG, Feinstein SC, Shooter EM, Kirschner MW. 1985. Nerve growth factor-induced neurite outgrowth in PC12 cells involves the coordinate induction of microtubule assembly and assembly-promoting factors. *The Journal of cell biology* **101**: 1799-1807.

Echeverri CJ, Beachy PA, Baum B, Boutros M, Buchholz F, Chanda SK, Downward J, Ellenberg J, Fraser AG, Hacohen N et al. 2006. Minimizing the risk of reporting false positives in large-scale RNAi screens. *Nat Methods* **3**: 777-779.

Eden S, Rohatgi R, Podtelejnikov AV, Mann M, Kirschner MW. 2002. Mechanism of regulation of WAVE1-induced actin nucleation by Rac1 and Nck. *Nature* **418**: 790-793.

Edwards DC, Sanders LC, Bokoch GM, Gill GN. 1999. Activation of LIM-kinase by Pak1 couples Rac/Cdc42 GTPase signalling to actin cytoskeletal dynamics. *Nature cell biology* **1**: 253-259.

Erickson HP, O'Brien ET. 1992. Microtubule dynamic instability and GTP hydrolysis. *Annual review of biophysics and biomolecular structure* **21**: 145-166.

Ervasti JM, Campbell KP. 1993. A role for the dystrophin-glycoprotein complex as a transmembrane linker between laminin and actin. *The Journal of cell biology* **122**: 809-823.

Esch T, Lemmon V, Banker G. 1999. Local presentation of substrate molecules directs axon specification by cultured hippocampal neurons. *The Journal of neuroscience : the official journal of the Society for Neuroscience* **19**: 6417-6426.

Estrach S, Schmidt S, Diriong S, Penna A, Blangy A, Fort P, Debant A. 2002. The Human Rho-GEF trio and its target GTPase RhoG are involved in the NGF pathway, leading to neurite outgrowth. *Current biology : CB* **12**: 307-312.

Etienne-Manneville S, Hall A. 2002. Rho GTPases in cell biology. *Nature* **420**: 629-635.

Evans L, Mitchison T, Kirschner M. 1985. Influence of the centrosome on the structure of nucleated microtubules. *The Journal of cell biology* **100**: 1185-1191.

Feltrin D, Fusco L, Witte H, Moretti F, Martin K, Letzelter M, Fluri E, Scheiffele P, Pertz O. 2012. Growth cone MKK7 mRNA targeting regulates MAP1b-dependent microtubule bundling to control neurite elongation. *PLoS biology* **10**: e1001439.

Feltrin D, Pertz O. 2012. Assessment of Rho GTPase signaling during neurite outgrowth. *Methods in molecular biology* **827**: 181-194.

Fink JK, Jones SM, Esposito C, Wilkowski J. 1996. Human microtubule-associated protein 1a (MAP1A) gene: genomic organization, cDNA sequence, and developmental- and tissue-specific expression. *Genomics* **35**: 577-585.

Fritz RD, Letzelter M, Reimann A, Martin K, Fusco L, Ritsma L, Ponsioen B, Fluri E, Schulte-Merker S, van Rheenen J et al. 2013. A versatile toolkit to produce sensitive FRET biosensors to visualize signaling in time and space. *Science signaling* **6**: rs12.

Fuchs E, Cleveland DW. 1998. A structural scaffolding of intermediate filaments in health and disease. *Science* **279**: 514-519.

Fujita A, Hattori Y, Takeuchi T, Kamata Y, Hata F. 2001. NGF induces neurite outgrowth via a decrease in phosphorylation of myosin light chain in PC12 cells. *Neuroreport* **12**: 3599-3602.

Fujita H, Katoh H, Ishikawa Y, Mori K, Negishi M. 2002. Rapostlin is a novel effector of Rnd2 GTPase inducing neurite branching. *The Journal of biological chemistry* **277**: 45428-45434.

Fukuhara S, Murga C, Zohar M, Igishi T, Gutkind JS. 1999. A novel PDZ domain containing guanine nucleotide exchange factor links heterotrimeric G proteins to Rho. *The Journal of biological chemistry* **274**: 5868-5879.

Garcia-Mata R, Boulter E, Burridge K. 2011. The 'invisible hand': regulation of RHO GTPases by RHOGDIs. *Nature reviews Molecular cell biology* **12**: 493-504.

Garcia-Mata R, Burridge K. 2007. Catching a GEF by its tail. *Trends in cell biology* **17**: 36-43.

Gardiner EM, Pestonjamasp KN, Bohl BP, Chamberlain C, Hahn KM, Bokoch GM. 2002. Spatial and temporal analysis of Rac activation during live neutrophil chemotaxis. *Current biology : CB* **12**: 2029-2034.

Gdalyahu A, Ghosh I, Levy T, Sapir T, Sapoznik S, Fishler Y, Azoulai D, Reiner O. 2004. DCX, a new mediator of the JNK pathway. *The EMBO journal* **23**: 823-832.

Geisler N, Kaufmann E, Weber K. 1985. Antiparallel orientation of the two double-stranded coiled-coils in the tetrameric protofilament unit of intermediate filaments. *Journal of molecular biology* **182**: 173-177.

Geisler N, Plessmann U, Weber K. 1982. Related amino acid sequences in neurofilaments and non-neural intermediate filaments. *Nature* **296**: 448-450.

Goh WI, Lim KB, Sudhaharan T, Sem KP, Bu W, Chou AM, Ahmed S. 2012. mDia1 and WAVE2 proteins interact directly with IRSp53 in filopodia and are involved in filopodium formation. *The Journal of biological chemistry* **287**: 4702-4714.

Giancotti FG, Ruoslahti E. 1999. Integrin signaling. *Science* **285**: 1028-1032.

Glenney JR, Jr., Kaulfus P, Matsudaira P, Weber K. 1981. F-actin binding and bundling properties of fimbrin, a major cytoskeletal protein of microvillus core filaments. *The Journal of biological chemistry* **256**: 9283-9288.

Goldberg DJ, Burmeister DW. 1989. Looking into growth cones. *Trends in neurosciences* **12**: 503-506.

Gomez TM, Robles E, Poo M, Spitzer NC. 2001. Filopodial calcium transients promote substrate-dependent growth cone turning. *Science* **291**: 1983-1987.

Guasch RM, Scambler P, Jones GE, Ridley AJ. 1998. RhoE regulates actin cytoskeleton organization and cell migration. *Molecular and cellular biology* **18**: 4761-4771.

Habets GG, Scholtes EH, Zuydgeest D, van der Kammen RA, Stam JC, Berns A, Collard JG. 1994. Identification of an invasion-inducing gene, Tiam-1, that encodes a protein with homology to GDP-GTP exchangers for Rho-like proteins. *Cell* **77**: 537-549.

Hall A. 1990. ras and GAP--who's controlling whom? *Cell* **61**: 921-923.

Hart MJ, Eva A, Evans T, Aaronson SA, Cerione RA. 1991. Catalysis of guanine nucleotide exchange on the CDC42Hs protein by the dbl oncogene product. *Nature* **354**: 311-314.

Hart MJ, Eva A, Zangrilli D, Aaronson SA, Evans T, Cerione RA, Zheng Y. 1994. Cellular transformation and guanine nucleotide exchange activity are catalyzed by a common domain on the dbl oncogene product. *The Journal of biological chemistry* **269**: 62-65.

Hart MJ, Sharma S, elMasry N, Qiu RG, McCabe P, Polakis P, Bollag G. 1996. Identification of a novel guanine nucleotide exchange factor for the Rho GTPase. *The Journal of biological chemistry* **271**: 25452-25458.

Hasegawa H, Kiyokawa E, Tanaka S, Nagashima K, Gotoh N, Shibuya M, Kurata T, Matsuda M. 1996. DOCK180, a major CRK-binding protein, alters cell morphology upon translocation to the cell membrane. *Molecular and cellular biology* **16**: 1770-1776.

Hawkins PT, Eguinoa A, Qiu RG, Stokoe D, Cooke FT, Walters R, Wennstrom S, Claesson-Welsh L, Evans T, Symons M et al. 1995. PDGF stimulates an increase in GTP-Rac via activation of phosphoinositide 3-kinase. *Current biology : CB* **5**: 393-403.

He Z, Wang KC, Koprivica V, Ming G, Song HJ. 2002. Knowing how to navigate: mechanisms of semaphorin signaling in the nervous system. *Science's STKE : signal transduction knowledge environment* **2002**: re1.

Higgins D, Burack M, Lein P, Banker G. 1997. Mechanisms of neuronal polarity. *Current opinion in neurobiology* **7**: 599-604.

Hill KL, Catlett NL, Weisman LS. 1996. Actin and myosin function in directed vacuole movement during cell division in Saccharomyces cerevisiae. *The Journal of cell biology* **135**: 1535-1549.

Hinds JW, Hinds PL. 1978. Early development of amacrine cells in the mouse retina: an electron microscopic, serial section analysis. *The Journal of comparative neurology* **179**: 277-300.

Hiramoto K, Negishi M, Katoh H. 2006. Dock4 is regulated by RhoG and promotes Rac-dependent cell migration. *Experimental cell research* **312**: 4205-4216.

Hirose M, Ishizaki T, Watanabe N, Uehata M, Kranenburg O, Moolenaar WH, Matsumura F, Maekawa M, Bito H, Narumiya S. 1998. Molecular dissection of the Rho-associated protein kinase (p160ROCK)-regulated neurite remodeling in neuroblastoma N1E-115 cells. *The Journal of cell biology* **141**: 1625-1636.

Ho HY, Rohatgi R, Lebensohn AM, Le M, Li J, Gygi SP, Kirschner MW. 2004. Toca-1 mediates Cdc42-dependent actin nucleation by activating the N-WASP-WIP complex. *Cell* **118**: 203-216.

Horesh D, Sapir T, Francis F, Wolf SG, Caspi M, Elbaum M, Chelly J, Reiner O. 1999. Doublecortin, a stabilizer of microtubules. *Human molecular genetics* **8**: 1599-1610.

Hoshino M, Nakamura S. 2003. Small GTPase Rin induces neurite outgrowth through Rac/Cdc42 and calmodulin in PC12 cells. *The Journal of cell biology* **163**: 1067-1076.

Hotulainen P, Lappalainen P. 2006. Stress fibers are generated by two distinct actin assembly mechanisms in motile cells. *The Journal of cell biology* **173**: 383-394.

Huang C, Jacobson K, Schaller MD. 2004. MAP kinases and cell migration. *Journal of cell science* **117**: 4619-4628.

Iden S, Collard JG. 2008. Crosstalk between small GTPases and polarity proteins in cell polarization. *Nature reviews Molecular cell biology* **9**: 846-859.

Inoki K, Li Y, Xu T, Guan KL. 2003. Rheb GTPase is a direct target of TSC2 GAP activity and regulates mTOR signaling. *Genes & development* **17**: 1829-1834.

Ishizaki T, Morishima Y, Okamoto M, Furuyashiki T, Kato T, Narumiya S. 2001. Coordination of microtubules and the actin cytoskeleton by the Rho effector mDia1. *Nature cell biology* **3**: 8-14.

Itoh TJ, Hotani H. 1994. Microtubule-stabilizing activity of microtubule-associated proteins (MAPs) is due to increase in frequency of rescue in dynamic instability: shortening length decreases with binding of MAPs onto microtubules. *Cell structure and function* **19**: 279-290.

Ivins JK, Yurchenco PD, Lander AD. 2000. Regulation of neurite outgrowth by integrin activation. *The Journal of neuroscience : the official journal of the Society for Neuroscience* **20**: 6551-6560.

Jaffer ZM, Chernoff J. 2002. p21-activated kinases: three more join the Pak. *The international journal of biochemistry & cell biology* **34**: 713-717.

Jalink K, van Corven EJ, Hengeveld T, Morii N, Narumiya S, Moolenaar WH. 1994. Inhibition of lysophosphatidate- and thrombin-induced neurite retraction and neuronal cell rounding by ADP ribosylation of the small GTP-binding protein Rho. *The Journal of cell biology* **126**: 801-810.

Jang KJ, Kim MS, Feltrin D, Jeon NL, Suh KY, Pertz O. 2010. Two distinct filopodia populations at the growth cone allow to sense nanotopographical extracellular matrix cues to guide neurite outgrowth. *PloS one* **5**: e15966.

Jeon CY, Moon MY, Kim JH, Kim HJ, Kim JG, Li Y, Jin JK, Kim PH, Kim HC, Meier KE et al. 2012. Control of neurite outgrowth by RhoA inactivation. *Journal of neurochemistry* **120**: 684-698.

Jin Z, Strittmatter SM. 1997. Rac1 mediates collapsin-1-induced growth cone collapse. *The Journal of neuroscience : the official journal of the Society for Neuroscience* **17**: 6256-6263.

Katoh H, Aoki J, Ichikawa A, Negishi M. 1998a. p160 RhoA-binding kinase ROKalpha induces neurite retraction. *The Journal of biological chemistry* **273**: 2489-2492.

Katoh H, Aoki J, Yamaguchi Y, Kitano Y, Ichikawa A, Negishi M. 1998b. Constitutively active Galpha12, Galpha13, and Galphaq induce Rho-dependent neurite retraction through different signaling pathways. *The Journal of biological chemistry* **273**: 28700-28707.

Katoh H, Negishi M. 2003. RhoG activates Rac1 by direct interaction with the Dock180-binding protein Elmo. *Nature* **424**: 461-464.

Katoh H, Negishi M, Ichikawa A. 1996. Prostaglandin E receptor EP3 subtype induces neurite retraction via small GTPase Rho. *The Journal of biological chemistry* **271**: 29780-29784.

Katoh H, Yasui H, Yamaguchi Y, Aoki J, Fujita H, Mori K, Negishi M. 2000. Small GTPase RhoG is a key regulator for neurite outgrowth in PC12 cells. *Molecular and cellular biology* **20**: 7378-7387.

Kaverina I, Krylyshkina O, Small JV. 1999. Microtubule targeting of substrate contacts promotes their relaxation and dissociation. *The Journal of cell biology* **146**: 1033-1044.

Kim AS, Kakalis LT, Abdul-Manan N, Liu GA, Rosen MK. 2000. Autoinhibition and activation mechanisms of the Wiskott-Aldrich syndrome protein. *Nature* **404**: 151-158.

Kirschner MW. 1978. Microtubule assembly and nucleation. *International review of cytology* **54**: 1-71.

Kobayashi K, Kuroda S, Fukata M, Nakamura T, Nagase T, Nomura N, Matsuura Y, Yoshida-Kubomura N, Iwamatsu A, Kaibuchi K. 1998. p140Sra-1 (specifically Rac1-associated protein) is a novel specific target for Rac1 small GTPase. *The Journal of biological chemistry* **273**: 291-295.

Korn ED. 1982. Actin polymerization and its regulation by proteins from nonmuscle cells. *Physiological reviews* **62**: 672-737.

Kovar DR, Harris ES, Mahaffy R, Higgs HN, Pollard TD. 2006. Control of the assembly of ATP- and ADP-actin by formins and profilin. *Cell* **124**: 423-435.

Kozma R, Ahmed S, Best A, Lim L. 1995. The Ras-related protein Cdc42Hs and bradykinin promote formation of peripheral actin microspikes and filopodia in Swiss 3T3 fibroblasts. *Molecular and cellular biology* **15**: 1942-1952.

Kozma R, Sarner S, Ahmed S, Lim L. 1997. Rho family GTPases and neuronal growth cone remodelling: relationship between increased complexity induced by Cdc42Hs, Rac1, and acetylcholine and collapse induced by RhoA and lysophosphatidic acid. *Molecular and cellular biology* **17**: 1201-1211.

Kranenburg O, Poland M, van Horck FP, Drechsel D, Hall A, Moolenaar WH. 1999. Activation of RhoA by lysophosphatidic acid and Galpha12/13 subunits in neuronal cells: induction of neurite retraction. *Molecular biology of the cell* **10**: 1851-1857.

Krawczyk WS. 1971. A pattern of epidermal cell migration during wound healing. *The Journal of cell biology* **49**: 247-263.

Kraynov VS, Chamberlain C, Bokoch GM, Schwartz MA, Slabaugh S, Hahn KM. 2000. Localized Rac activation dynamics visualized in living cells. *Science* **290**: 333-337.

Krendel M, Zenke FT, Bokoch GM. 2002. Nucleotide exchange factor GEF-H1 mediates cross-talk between microtubules and the actin cytoskeleton. *Nature cell biology* **4**: 294-301.

Krugmann S, Jordens I, Gevaert K, Driessens M, Vandekerckhove J, Hall A. 2001. Cdc42 induces filopodia by promoting the formation of an IRSp53:Mena complex. *Current biology : CB* **11**: 1645-1655.

Kutschera W, Zauner W, Wiche G, Propst F. 1998. The mouse and rat MAP1B genes: genomic organization and alternative transcription. *Genomics* **49**: 430-436.

Kwiatkowski DJ, Manning BD. 2005. Tuberous sclerosis: a GAP at the crossroads of multiple signaling pathways. *Human molecular genetics* **14 Spec No. 2**: R251-258.

Lamalice L, Le Boeuf F, Huot J. 2007. Endothelial cell migration during angiogenesis. *Circulation research* **100**: 782-794.

Lancaster CA, Taylor-Harris PM, Self AJ, Brill S, van Erp HE, Hall A. 1994. Characterization of rhoGAP. A GTPase-activating protein for rho-related small GTPases. *The Journal of biological chemistry* **269**: 1137-1142.

Larson Y, Liu J, Stevens PD, Li X, Li J, Evers BM, Gao T. 2010. Tuberous sclerosis complex 2 (TSC2) regulates cell migration and polarity through activation of CDC42 and RAC1. *The Journal of biological chemistry* **285**: 24987-24998.

Lawler S. 1998. Microtubule dynamics: if you need a shrink try stathmin/Op18. *Current biology : CB* **8**: R212-214.

Lauffenburger DA, Horwitz AF. 1996. Cell migration: a physically integrated molecular process. *Cell* **84**: 359-369.

Laurin M, Cote JF. 2014. Insights into the biological functions of Dock family guanine nucleotide exchange factors. *Genes & development* **28**: 533-547.

Lazarides E. 1982. Intermediate filaments: a chemically heterogeneous, developmentally regulated class of proteins. *Annual review of biochemistry* **51**: 219-250.

Lee CH, Della NG, Chew CE, Zack DJ. 1996. Rin, a neuron-specific and calmodulin-binding small G-protein, and Rit define a novel subfamily of ras proteins. *The Journal of neuroscience : the official journal of the Society for Neuroscience* **16**: 6784-6794.

Leeuwen FN, Kain HE, Kammen RA, Michiels F, Kranenburg OW, Collard JG. 1997. The guanine nucleotide exchange factor Tiam1 affects neuronal morphology; opposing roles for the small GTPases Rac and Rho. *The Journal of cell biology* **139**: 797-807.

Letourneau PC. 1983. Differences in the organization of actin in the growth cones compared with the neurites of cultured neurons from chick embryos. *The Journal of cell biology* **97**: 963-973.

Leung T, Chen XQ, Tan I, Manser E, Lim L. 1998. Myotonic dystrophy kinase-related Cdc42-binding kinase acts as a Cdc42 effector in promoting cytoskeletal reorganization. *Molecular and cellular biology* **18**: 130-140.

Leung T, Manser E, Tan L, Lim L. 1995. A novel serine/threonine kinase binding the Ras-related RhoA GTPase which translocates the kinase to peripheral membranes. *The Journal of biological chemistry* **270**: 29051-29054.

Li F, Higgs HN. 2003. The mouse Formin mDia1 is a potent actin nucleation factor regulated by autoinhibition. *Current biology : CB* **13**: 1335-1340.

Li Z, Hannigan M, Mo Z, Liu B, Lu W, Wu Y, Smrcka AV, Wu G, Li L, Liu M et al. 2003. Directional sensing requires G beta gamma-mediated PAK1 and PIX alpha-dependent activation of Cdc42. *Cell* **114**: 215-227.

Lin Q, Yang W, Baird D, Feng Q, Cerione RA. 2006. Identification of a DOCK180-related guanine nucleotide exchange factor that is capable of mediating a positive feedback activation of Cdc42. *The Journal of biological chemistry* **281**: 35253-35262.

Liu BP, Burridge K. 2000. Vav2 activates Rac1, Cdc42, and RhoA downstream from growth factor receptors but not beta1 integrins. *Molecular and cellular biology* **20**: 7160-7169.

Lo SH, Janmey PA, Hartwig JH, Chen LB. 1994. Interactions of tensin with actin and identification of its three distinct actin-binding domains. *The Journal of cell biology* **125**: 1067-1075.

Louvet E, Percipalle P. 2009. Transcriptional control of gene expression by actin and myosin. *International review of cell and molecular biology* **272**: 107-147.

Luo L. 2000. Rho GTPases in neuronal morphogenesis. *Nature reviews Neuroscience* **1**: 173-180.

Maccioni RB, Cambiazo V. 1995. Role of microtubule-associated proteins in the control of microtubule assembly. *Physiological reviews* **75**: 835-864.

Machacek M, Hodgson L, Welch C, Elliott H, Pertz O, Nalbant P, Abell A, Johnson GL, Hahn KM, Danuser G. 2009. Coordination of Rho GTPase activities during cell protrusion. *Nature* **461**: 99-103.

Machesky LM, Mullins RD, Higgs HN, Kaiser DA, Blanchoin L, May RC, Hall ME, Pollard TD. 1999. Scar, a WASp-related protein, activates nucleation of actin filaments by the Arp2/3 complex. *Proceedings of the National Academy of Sciences of the United States of America* **96**: 3739-3744.

Maekawa M, Ishizaki T, Boku S, Watanabe N, Fujita A, Iwamatsu A, Obinata T, Ohashi K, Mizuno K, Narumiya S. 1999. Signaling from Rho to the actin cytoskeleton through protein kinases ROCK and LIM-kinase. *Science* **285**: 895-898.

Marin O, Rubenstein JL. 2003. Cell migration in the forebrain. *Annual review of neuroscience* **26**: 441-483.

Matsuo N, Hoshino M, Yoshizawa M, Nabeshima Y. 2002. Characterization of STEF, a guanine nucleotide exchange factor for Rac1, required for neurite growth. *The Journal of biological chemistry* **277**: 2860-2868.

Meller N, Merlot S, Guda C. 2005. CZH proteins: a new family of Rho-GEFs. *Journal of cell science* **118**: 4937-4946.

Miki H, Yamaguchi H, Suetsugu S, Takenawa T. 2000. IRSp53 is an essential intermediate between Rac and WAVE in the regulation of membrane ruffling. *Nature* **408**: 732-735.

Millard TH, Sharp SJ, Machesky LM. 2004. Signalling to actin assembly via the WASP (Wiskott-Aldrich syndrome protein)-family proteins and the Arp2/3 complex. *The Biochemical journal* **380**: 1-17.

Mitchison T, Kirschner M. 1984. Microtubule assembly nucleated by isolated centrosomes. *Nature* **312**: 232-237.

Mitchison TJ, Cramer LP. 1996. Actin-based cell motility and cell locomotion. *Cell* **84**: 371-379.

Miyashita M, Ohnishi H, Okazawa H, Tomonaga H, Hayashi A, Fujimoto TT, Furuya N, Matozaki T. 2004. Promotion of neurite and filopodium formation by CD47: roles of integrins, Rac, and Cdc42. *Molecular biology of the cell* **15**: 3950-3963.

Moll R, Franke WW, Schiller DL, Geiger B, Krepler R. 1982. The catalog of human cytokeratins: patterns of expression in normal epithelia, tumors and cultured cells. *Cell* **31**: 11-24.

Moon MS, Gomez TM. 2010. Balanced Vav2 GEF activity regulates neurite outgrowth and branching in vitro and in vivo. *Molecular and cellular neurosciences* **44**: 118-128.

Mullins RD, Heuser JA, Pollard TD. 1998. The interaction of Arp2/3 complex with actin: nucleation, high affinity pointed end capping, and formation of branching networks of filaments. *Proceedings of the National Academy of Sciences of the United States of America* **95**: 6181-6186.

Nadarajah B, Parnavelas JG. 2002. Modes of neuronal migration in the developing cerebral cortex. *Nature reviews Neuroscience* **3**: 423-432.

Nakamura T, Komiya M, Sone K, Hirose E, Gotoh N, Morii H, Ohta Y, Mori N. 2002. Grit, a GTPase-activating protein for the Rho family, regulates neurite extension through association with the TrkA receptor and N-Shc and CrkL/Crk adapter molecules. *Molecular and cellular biology* **22**: 8721-8734.

Neal SE, Eccleston JF, Hall A, Webb MR. 1988. Kinetic analysis of the hydrolysis of GTP by p21N-ras. The basal GTPase mechanism. *The Journal of biological chemistry* **263**: 19718-19722.

Negishi M, Katoh H. 2002. Rho family GTPases as key regulators for neuronal network formation. *Journal of biochemistry* **132**: 157-166.

Neuhaus JM, Wanger M, Keiser T, Wegner A. 1983. Treadmilling of actin. *Journal of muscle research and cell motility* **4**: 507-527.

Nikolic M, Chou MM, Lu W, Mayer BJ, Tsai LH. 1998. The p35/Cdk5 kinase is a neuron-specific Rac effector that inhibits Pak1 activity. *Nature* **395**: 194-198.

Nishimura T, Kato K, Yamaguchi T, Fukata Y, Ohno S, Kaibuchi K. 2004. Role of the PAR-3-KIF3 complex in the establishment of neuronal polarity. *Nature cell biology* **6**: 328-334.

Nishimura T, Yamaguchi T, Kato K, Yoshizawa M, Nabeshima Y, Ohno S, Hoshino M, Kaibuchi K. 2005. PAR-6-PAR-3 mediates Cdc42-induced Rac activation through the Rac GEFs STEF/Tiam1. *Nature cell biology* **7**: 270-277.

Nobes CD, Hawkins P, Stephens L, Hall A. 1995. Activation of the small GTP-binding proteins rho and rac by growth factor receptors. *Journal of cell science* **108 (Pt 1)**: 225-233.

Nobes CD, Lauritzen I, Mattei MG, Paris S, Hall A, Chardin P. 1998. A new member of the Rho family, Rnd1, promotes disassembly of actin filament structures and loss of cell adhesion. *The Journal of cell biology* **141**: 187-197.

Nusser N, Gosmanova E, Zheng Y, Tigyi G. 2002. Nerve growth factor signals through TrkA, phosphatidylinositol 3-kinase, and Rac1 to inactivate RhoA during the initiation of neuronal differentiation of PC12 cells. *The Journal of biological chemistry* **277**: 35840-35846.

O'Connor TP, Bentley D. 1993. Accumulation of actin in subsets of pioneer growth cone filopodia in response to neural and epithelial guidance cues in situ. *The Journal of cell biology* **123**: 935-948.

Oleksy A, Opalinski L, Derewenda U, Derewenda ZS, Otlewski J. 2006. The molecular basis of RhoA specificity in the guanine nucleotide exchange factor PDZ-RhoGEF. *The Journal of biological chemistry* **281**: 32891-32897.

Olson MF, Pasteris NG, Gorski JL, Hall A. 1996. Faciogenital dysplasia protein (FGD1) and Vav, two related proteins required for normal embryonic development, are upstream regulators of Rho GTPases. *Current biology : CB* **6**: 1628-1633.

Ong LL, Lim AP, Er CP, Kuznetsov SA, Yu H. 2000. Kinectin-kinesin binding domains and their effects on organelle motility. *The Journal of biological chemistry* **275**: 32854-32860.

Palecek SP, Huttenlocher A, Horwitz AF, Lauffenburger DA. 1998. Physical and biochemical regulation of integrin release during rear detachment of migrating cells. *Journal of cell science* **111 (Pt 7)**: 929-940.

Panda D, Samuel JC, Massie M, Feinstein SC, Wilson L. 2003. Differential regulation of microtubule dynamics by three- and four-repeat tau: implications for the onset of neurodegenerative disease. *Proceedings of the National Academy of Sciences of the United States of America* **100**: 9548-9553.

Peck J, Douglas Gt, Wu CH, Burbelo PD. 2002. Human RhoGAP domain-containing proteins: structure, function and evolutionary relationships. *FEBS letters* **528**: 27-34.

Pelham RJ, Chang F. 2002. Actin dynamics in the contractile ring during cytokinesis in fission yeast. *Nature* **419**: 82-86.

Pelletier O, Pokidysheva E, Hirst LS, Bouxsein N, Li Y, Safinya CR. 2003. Structure of actin cross-linked with alpha-actinin: a network of bundles. *Physical review letters* **91**: 148102.

Pertz O. 2010. Spatio-temporal Rho GTPase signaling - where are we now? *Journal of cell science* **123**: 1841-1850.

Pertz O, Hodgson L, Klemke RL, Hahn KM. 2006. Spatiotemporal dynamics of RhoA activity in migrating cells. *Nature* **440**: 1069-1072.

Pertz OC, Wang Y, Yang F, Wang W, Gay LJ, Gristenko MA, Clauss TR, Anderson DJ, Liu T, Auberry KJ et al. 2008. Spatial mapping of the neurite and soma proteomes reveals a functional Cdc42/Rac regulatory network. *Proceedings of the National Academy of Sciences of the United States of America* **105**: 1931-1936.

Pinheiro EM, Gertler FB. 2006. Nervous Rac: DOCK7 regulation of axon formation. *Neuron* **51**: 674-676.

Pollard TD, Blanchoin L, Mullins RD. 2000. Molecular mechanisms controlling actin filament dynamics in nonmuscle cells. *Annual review of biophysics and biomolecular structure* **29**: 545-576.

Pollard TD, Cooper JA. 1986. Actin and actin-binding proteins. A critical evaluation of mechanisms and functions. *Annual review of biochemistry* **55**: 987-1035.

Pollard TD, Mooseker MS. 1981. Direct measurement of actin polymerization rate constants by electron microscopy of actin filaments nucleated by isolated microvillus cores. *The Journal of cell biology* **88**: 654-659.

Postma FR, Jalink K, Hengeveld T, Moolenaar WH. 1996. Sphingosine-1-phosphate rapidly induces Rho-dependent neurite retraction: action through a specific cell surface receptor. *The EMBO journal* **15**: 2388-2392.

Prakash SK, Paylor R, Jenna S, Lamarche-Vane N, Armstrong DL, Xu B, Mancini MA, Zoghbi HY. 2000. Functional analysis of ARHGAP6, a novel GTPase-activating protein for RhoA. *Human molecular genetics* **9**: 477-488.

Pruyne D, Evangelista M, Yang C, Bi E, Zigmond S, Bretscher A, Boone C. 2002. Role of formins in actin assembly: nucleation and barbed-end association. *Science* **297**: 612-615.

Rayment I, Holden HM, Whittaker M, Yohn CB, Lorenz M, Holmes KC, Milligan RA. 1993. Structure of the actin-myosin complex and its implications for muscle contraction. *Science* **261**: 58-65.

Rebecchi MJ, Scarlata S. 1998. Pleckstrin homology domains: a common fold with diverse functions. *Annual review of biophysics and biomolecular structure* **27**: 503-528.

Read DE, Gorman AM. 2009. Involvement of Akt in neurite outgrowth. *Cellular and molecular life sciences : CMLS* **66**: 2975-2984.

Reif K, Nobes CD, Thomas G, Hall A, Cantrell DA. 1996. Phosphatidylinositol 3-kinase signals activate a selective subset of Rac/Rho-dependent effector pathways. *Current biology : CB* **6**: 1445-1455.

Rensland H, Lautwein A, Wittinghofer A, Goody RS. 1991. Is there a rate-limiting step before GTP cleavage by H-ras p21? *Biochemistry* **30**: 11181-11185.

Ridley AJ. 2001. Rho GTPases and cell migration. *Journal of cell science* **114**: 2713-2722.

Ridley AJ, Hall A. 1992. The small GTP-binding protein rho regulates the assembly of focal adhesions and actin stress fibers in response to growth factors. *Cell* **70**: 389-399.

Ridley AJ, Paterson HF, Johnston CL, Diekmann D, Hall A. 1992. The small GTP-binding protein rac regulates growth factor-induced membrane ruffling. *Cell* **70**: 401-410.

Ridley AJ, Schwartz MA, Burridge K, Firtel RA, Ginsberg MH, Borisy G, Parsons JT, Horwitz AR. 2003. Cell migration: integrating signals from front to back. *Science* **302**: 1704-1709.

Riedl J, Crevenna AH, Kessenbrock K, Yu JH, Neukirchen D, Bista M, Bradke F, Jenne D, Holak TA, Werb Z et al. 2008. Lifeact: a versatile marker to visualize F-actin. *Nat Methods* **5**: 605-607.

Riento K, Ridley AJ. 2003. Rocks: multifunctional kinases in cell behaviour. *Nature reviews Molecular cell biology* **4**: 446-456.

Rohatgi R, Ma L, Miki H, Lopez M, Kirchhausen T, Takenawa T, Kirschner MW. 1999. The interaction between N-WASP and the Arp2/3 complex links Cdc42-dependent signals to actin assembly. *Cell* **97**: 221-231.

Rossman KL, Der CJ, Sondek J. 2005. GEF means go: turning on RHO GTPases with guanine nucleotide-exchange factors. *Nature reviews Molecular cell biology* **6**: 167-180.

Roy R, Hohng S, Ha T. 2008. A practical guide to single-molecule FRET. *Nature methods* **5**: 507-516.

Sanchez S, Jimenez C, Carrera AC, Diaz-Nido J, Avila J, Wandosell F. 2004. A cAMP-activated pathway, including PKA and PI3K, regulates neuronal differentiation. *Neurochemistry international* **44**: 231-242.

Sanchez-Madrid F, del Pozo MA. 1999. Leukocyte polarization in cell migration and immune interactions. *The EMBO journal* **18**: 501-511.

Sanders LC, Matsumura F, Bokoch GM, de Lanerolle P. 1999. Inhibition of myosin light chain kinase by p21-activated kinase. *Science* **283**: 2083-2085.

Sanes JR. 1983. Roles of extracellular matrix in neural development. *Annual review of physiology* **45**: 581-600.

Sanz-Moreno V, Gadea G, Ahn J, Paterson H, Marra P, Pinner S, Sahai E, Marshall CJ. 2008. Rac activation and inactivation control plasticity of tumor cell movement. *Cell* **135**: 510-523.

Sarner S, Kozma R, Ahmed S, Lim L. 2000. Phosphatidylinositol 3-kinase, Cdc42, and Rac1 act downstream of Ras in integrin-dependent neurite outgrowth in N1E-115 neuroblastoma cells. *Molecular and cellular biology* **20**: 158-172.

Scheffzek K, Ahmadian MR. 2005. GTPase activating proteins: structural and functional insights 18 years after discovery. *Cellular and molecular life sciences : CMLS* **62**: 3014-3038.

Schmidt A, Hall A. 2002. Guanine nucleotide exchange factors for Rho GTPases: turning on the switch. *Genes & development* **16**: 1587-1609.

Seoh ML, Ng CH, Yong J, Lim L, Leung T. 2003. ArhGAP15, a novel human RacGAP protein with GTPase binding property. *FEBS letters* **539**: 131-137.

Sheetz MP, Felsenfeld DP, Galbraith CG. 1998. Cell migration: regulation of force on extracellular-matrix-integrin complexes. *Trends in cell biology* **8**: 51-54.

Small JV. 1981. Organization of actin in the leading edge of cultured cells: influence of osmium tetroxide and dehydration on the ultrastructure of actin meshworks. *The Journal of cell biology* **91**: 695-705.

Smith LG, Li R. 2004. Actin polymerization: riding the wave. *Current biology : CB* **14**: R109-111.

Stanyon CA, Bernard O. 1999. LIM-kinase1. *The international journal of biochemistry & cell biology* **31**: 389-394.

Steffen A, Rottner K, Ehinger J, Innocenti M, Scita G, Wehland J, Stradal TE. 2004. Sra-1 and Nap1 link Rac to actin assembly driving lamellipodia formation. *The EMBO journal* **23**: 749-759.

Steinert PM, Jones JC, Goldman RD. 1984. Intermediate filaments. *The Journal of cell biology* **99**: 22s-27s.

Sun HQ, Yamamoto M, Mejillano M, Yin HL. 1999. Gelsolin, a multifunctional actin regulatory protein. *The Journal of biological chemistry* **274**: 33179-33182.

Swiercz JM, Kuner R, Behrens J, Offermanns S. 2002. Plexin-B1 directly interacts with PDZ-RhoGEF/LARG to regulate RhoA and growth cone morphology. *Neuron* **35**: 51-63.

Tahirovic S, Hellal F, Neukirchen D, Hindges R, Garvalov BK, Flynn KC, Stradal TE, Chrostek-Grashoff A, Brakebusch C, Bradke F. 2010. Rac1 regulates neuronal polarization through the WAVE complex. *The Journal of neuroscience : the official journal of the Society for Neuroscience* **30**: 6930-6943.

ten Klooster JP, Jaffer ZM, Chernoff J, Hordijk PL. 2006. Targeting and activation of Rac1 are mediated by the exchange factor beta-Pix. *The Journal of cell biology* **172**: 759-769.

Tigyi G, Fischer DJ, Sebok A, Marshall F, Dyer DL, Miledi R. 1996. Lysophosphatidic acid-induced neurite retraction in PC12 cells: neurite-protective effects of cyclic AMP signaling. *Journal of neurochemistry* **66**: 549-558.

Tojkander S, Gateva G, Lappalainen P. 2012. Actin stress fibers--assembly, dynamics and biological roles. *Journal of cell science* **125**: 1855-1864.

Tucker KL, Meyer M, Barde YA. 2001. Neurotrophins are required for nerve growth during development. *Nature neuroscience* **4**: 29-37.

Ueda T, Kikuchi A, Ohga N, Yamamoto J, Takai Y. 1990. Purification and characterization from bovine brain cytosol of a novel regulatory protein inhibiting the dissociation of GDP from and the subsequent binding of GTP to rhoB p20, a ras p21-like GTP-binding protein. *The Journal of biological chemistry* **265**: 9373-9380.

Ullmannova-Benson V, Guan M, Zhou X, Tripathi V, Yang XY, Zimonjic DB, Popescu NC. 2009. DLC1 tumor suppressor gene inhibits migration and invasion of multiple myeloma cells through RhoA GTPase pathway. *Leukemia* **23**: 383-390.

Van Aelst L, D'Souza-Schorey C. 1997. Rho GTPases and signaling networks. *Genes & development* **11**: 2295-2322.

Vandecandelaere A, Pedrotti B, Utton MA, Calvert RA, Bayley PM. 1996. Differences in the regulation of microtubule dynamics by microtubule-associated proteins MAP1B and MAP2. *Cell motility and the cytoskeleton* **35**: 134-146.

Vignal E, Blangy A, Martin M, Gauthier-Rouviere C, Fort P. 2001. Kinectin is a key effector of RhoG microtubule-dependent cellular activity. *Molecular and cellular biology* **21**: 8022-8034.

Wallar BJ, Alberts AS. 2003. The formins: active scaffolds that remodel the cytoskeleton. *Trends in cell biology* **13**: 435-446.

Wang K, Singer SJ. 1977. Interaction of filamin with f-actin in solution. *Proceedings of the National Academy of Sciences of the United States of America* **74**: 2021-2025.

Wang LH, Strittmatter SM. 1996. A family of rat CRMP genes is differentially expressed in the nervous system. *The Journal of neuroscience : the official journal of the Society for Neuroscience* **16**: 6197-6207.

Waterman-Storer CM, Salmon ED. 1997. Microtubule dynamics: treadmilling comes around again. *Current biology : CB* **7**: R369-372.

Weisenberg RC, Deery WJ, Dickinson PJ. 1976. Tubulin-nucleotide interactions during the polymerization and depolymerization of microtubules. *Biochemistry* **15**: 4248-4254.

Welch MD, Mullins RD. 2002. Cellular control of actin nucleation. *Annual review of cell and developmental biology* **18**: 247-288.

Wheeler AP, Wells CM, Smith SD, Vega FM, Henderson RB, Tybulewicz VL, Ridley AJ. 2006. Rac1 and Rac2 regulate macrophage morphology but are not essential for migration. *Journal of cell science* **119**: 2749-2757.

Wilkinson S, Paterson HF, Marshall CJ. 2005. Cdc42-MRCK and Rho-ROCK signalling cooperate in myosin phosphorylation and cell invasion. *Nature cell biology* **7**: 255-261.

Winder SJ, Hemmings L, Maciver SK, Bolton SJ, Tinsley JM, Davies KE, Critchley DR, Kendrick-Jones J. 1995. Utrophin actin binding domain: analysis of actin binding and cellular targeting. *Journal of cell science* **108 (Pt 1)**: 63-71.

Witke W, Podtelejnikov AV, Di Nardo A, Sutherland JD, Gurniak CB, Dotti C, Mann M. 1998. In mouse brain profilin I and profilin II associate with regulators of the endocytic pathway and actin assembly. *The EMBO journal* **17**: 967-976.

Xiao Y, Peng Y, Wan J, Tang G, Chen Y, Tang J, Ye WC, Ip NY, Shi L. 2013. The atypical guanine nucleotide exchange factor Dock4 regulates neurite differentiation through modulation of Rac1 GTPase and actin dynamics. *The Journal of biological chemistry* **288**: 20034-20045.

Yamaguchi Y, Katoh H, Yasui H, Mori K, Negishi M. 2001. RhoA inhibits the nerve growth factor-induced Rac1 activation through Rho-associated kinase-dependent pathway. *The Journal of biological chemistry* **276**: 18977-18983.

Yamashita N, Morita A, Uchida Y, Nakamura F, Usui H, Ohshima T, Taniguchi M, Honnorat J, Thomasset N, Takei K et al. 2007. Regulation of spine development by semaphorin3A through cyclin-dependent kinase 5 phosphorylation of collapsin response mediator protein 1. *The Journal of neuroscience : the official journal of the Society for Neuroscience* **27**: 12546-12554.

Yang N, Higuchi O, Ohashi K, Nagata K, Wada A, Kangawa K, Nishida E, Mizuno K. 1998. Cofilin phosphorylation by LIM-kinase 1 and its role in Rac-mediated actin reorganization. *Nature* **393**: 809-812.

Zheng Y, Fischer DJ, Santos MF, Tigyi G, Pasteris NG, Gorski JL, Xu Y. 1996. The faciogenital dysplasia gene product FGD1 functions as a Cdc42Hs-specific guanine-nucleotide exchange factor. *The Journal of biological chemistry* **271**: 33169-33172.

Zheng Y. 2001. Dbl family guanine nucleotide exchange factors. *Trends in biochemical sciences* **26**: 724-732.

7. Acknowledgements

8. Curriculum vitae

Ludovico Maria Fusco

Date of birth: Naples, Italy, 19 August 1986

Eimeldingerweg 39. 4057. Basel Switzerland

Phone: +41-789110960 E-Mail: ludovico.fuscom@gmail.com

Education

Doctoral Thesis in Neurobiology/Cell biology　　　　　**[January 2010 - today]**

Development of a doctoral thesis entitled: Morphodynamic profiling to explore spatio-temporal signaling networks regulating neurite outgrowth

- Dynamic profiling of genes involved in neurite outgrowth using an siRNA screen.
- Established an advanced high-throughput microscopy platform for siRNA screening.
- Generated a timelapse video library using advanced high-throughput microscopy techniques detailing the specific defects resulting from knocking down various genes involved in neurite outgrowth.
- Developed image analysis tools to analyze the morphodynamic profile of each siRNA knock down phenotype.
- Characterization of different groups of genes regulating the neurite outgrowth process.

Master Thesis in Medical biotechnology　　　　**[January 2008 - November 2009]**

Development of a master thesis entitled: Regulation of the expression of the gene Klf5 in mouse embryonic stem cells.

- Studied the involvement of the transcription factor Klf5 in the maintenance of stemness.
- Explored the interaction of the Klf5 gene with other transcriptional factors expressed in mouse embryonic stem cells

- Execution of molecular biology and biochemical techniques which allowed the identification of a new regulator of the stemness

Professional Courses

Biological Image Processing Summer School, ETHZ, Zurich, Switzerland   [August 2010]

- Basics of ImageJ/MATLAB programming
- Introduction to Image Processing
- Image Analysis (Segmentation, Classification, Tracking)
- Image Enhancement (Histogram operations, Filtering, Morphology)
- Image Restoration (Deconvolution)
- Image Synthesis (Stitching, Registration, Visualization)
- High-Content Screening

Light Microscopy and Imaging Course University of Geneva, Geneva, Switzerland [April 2010]

- Basic and advanced light microscopy techniques
- Principles of live cell imaging
- Usage of confocal and wide field light microscopes

IT proficiency

- Professional proficiency with Microsoft Word, Excel, Power Point, Adobe Illustrator and Graph Pad Prism
- Professional proficiency in image analysis using ImageJ, Methamorph and NIS-Elements software
- Professional proficiency in high content image acquisition using Metamorph

Publication and Conferences

Paper in preparation **[July 2014]**

Ludovico Fusco, Maria Bagonis, Gaudenz Danuser, Olivier Pertz. Analysis of a Rho GTPase centered interactome reveals complex regulation of neurite outgrowth

Paper in preparation **[October 2014]**

Ludovico Fusco, Kevin Smith, Fethallah Benmansour, Riwal Lefort, Francois Fleuret, Pascal Fua, and Olivier Pertz. Morphodynamic profiling to explore spatio-temporal signaling networks regulating neurite outgrowth

Paper published in Science Signaling **[April 2013]**

Rafael D. Fritz, Michel Letzelter1, Andreas Reimann, Katrin Martin, **Ludovico Fusco**, Laila Ritsma, Bas Ponsioen, Erika Fluri, Stefan Schulte-Merker, Jacco van Rheenen and Olivier Pertz. A versatile toolkit to produce sensitive FRET biosensors to visualize signaling in time and space.

Paper published in Plos Biology **[December 2012]**

Daniel Feltrin, **Ludovico Fusco**, Harald Witte, Francesca Moretti, Katrin Martin, Michel Letzelter, Erika Fluri, Peter Scheiffele and Olivier Pertz. Growth cone MKK7 mRNA targeting regulates MAP1b-dependent.

Paper published in Journal of Biological Chemistry **[March 2010]**

Luigi Aloia, Silvia Parisi, **Ludovico Fusco**, Lucio Pastore, Tommaso Russo. Dies1 is a component of BMP4 signaling pathway required for proper differentiation of mouse embryonic stem cells.

Poster presentation at the 2012 Annual Meeting of the American Society for Cell Biology. San Francisco, CA, United States of America   [December 2012]

Analysis of a Rho GTPase centered interactome reveals complex regulation of neurite outgrowth. **Ludovico Fusco**, Maria Bagonis, Gaudenz Danuser, Olivier Pertz

Poster presentation at the EuroMEMBRANE International Conference 2012, Basel, Switzerland   [June 2012]

Morphodynamic profiling to explore spatio-temporal signaling networks regulating neurite outgrowth. **Ludovico Fusco**, Kevin Smith, Fethallah Benmansour, Riwal Lefort, Francois Fleuret, Pascal Fua, and Olivier Pertz

Poster presentation at the 1st International SystemsX.ch Conference on Systems Biology Basel, Switzerland   [October 2011]

Morphodynamic profiling to explore spatio-temporal signaling networks regulating neurite outgrowth. **Ludovico Fusco**, Kevin Smith, Fethallah Benmansour, Riwal Lefort, Francois Fleuret, Pascal Fua, and Olivier Pertz

Language proficiency

Italian (native), English (fluent), Spanish (fluent), French (intermediate), German (basic)

Membership in professional organizations

Predoctoral student membership in the American Society for Cell Biology Bethesda, MD, United States of America   **[since August 2012]**